

# Overview of Plasma-Based Accelerator Concepts

Eric Esarey, Phillip Sprangle, *Senior Member, IEEE*, Jonathan Krall, and Antonio Ting

(Invited Review)

**Abstract**—An overview is given of the physics issues relevant to the plasma wakefield accelerator, the plasma beat-wave accelerator, the laser wakefield accelerator, including the self-modulated regime, and wakefield accelerators driven by multiple electron or laser pulses. Basic properties of linear and nonlinear plasma waves are discussed, as well as the trapping and acceleration of electrons in the plasma wave. Formulas are presented for the accelerating field and the energy gain in the various accelerator configurations. The propagation of the drive electron or laser beams is discussed, including limitations imposed by key instabilities and methods for optically guiding laser pulses. Recent experimental results are summarized.

## I. INTRODUCTION

IT HAS BEEN over 16 years since Tajima and Dawson [1] proposed using laser beams to excite plasma waves for electron acceleration. Since that time there have been numerous workshops on plasma-based accelerators [2]–[9]: the first was in Los Alamos in 1982 and the most recent was in Kardamyl, Greece, in June 1995. There has been tremendous progress in recent years, both theoretically and experimentally. This is partly due to advances in technology, particularly the development of compact terawatt laser systems based on the technique of chirped-pulse amplification [10]–[17]. Electron acceleration has been observed in several experiments world-wide [18]–[35], demonstrating the basic mechanisms of the plasma wakefield accelerator, the plasma beat-wave accelerator, and the laser wakefield accelerator. Accelerated electrons with energy gains as high as 44 MeV have been detected [33].

Plasma-based accelerators are of great interest because of their ability to sustain extremely large acceleration gradients. The accelerating gradients in conventional radio frequency linear accelerators (RF linacs) are presently limited to roughly 100 MV/m, partly due to breakdown which occurs on the walls of the structure. Ionized plasmas, however, can sustain electron plasma waves with electric fields on the order of the nonrelativistic wavebreaking field [36], [37],  $E_0 = cm_e\omega_p/e$ , or

$$E_0 [\text{V/cm}] \simeq 0.96n_0^{1/2}[\text{cm}^{-3}] \quad (1)$$

where  $\omega_p = (4\pi n_0 e^2/m_e)^{1/2}$  is the electron plasma frequency and  $n_0$  is the ambient electron density. For example,  $n_0 =$

Manuscript received January 1, 1996; revised February 20, 1996. This work was supported by the U.S. Department of Energy and the Office of Naval Research.

The authors are with the Beam Physics Branch, Plasma Physics Division, Naval Research Laboratory, Washington, D.C. 20375-5346 USA (e-mail: esarey@ppd.nrl.navy.mil).

Publisher Item Identifier S 0093-3813(96)04223-3.

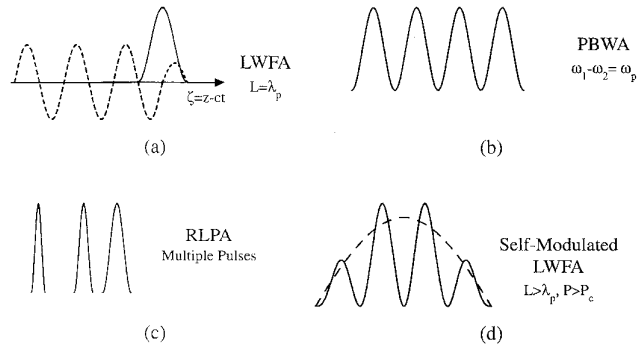


Fig. 1. Schematic of the plasma-based accelerators: (a) LWFA (or PWFA), in which a short  $L \simeq \lambda_p$  laser pulse (or electron beam) drives a plasma wave (dashed curve), (b) PBWA, in which two long pulse ( $L > \lambda_p$ ) lasers with frequencies  $\omega_1 - \omega_2 \simeq \omega_p$  resonantly drive a plasma wave, (c) RLPA, in which a train of short laser pulses resonantly drives a plasma wave, and (d) self-modulated LWFA, in which an initially long pulse (dashed curve) breaks up into a series of short pulses and resonantly drives a plasma wave. The laser pulses are moving to the right.

$10^{18} \text{ cm}^{-3}$  gives  $E_0 \simeq 100 \text{ GV/m}$ , which is approximately three orders of magnitude greater than that obtained in conventional RF linacs. Accelerating gradients on the order of 100 GV/m have been inferred in recent experiments [33].

This paper is intended to give an overview of some of the concepts and issues relevant to plasma-based accelerators. This discussion will be limited to only the most widely investigated plasma-based accelerators, namely the plasma wakefield accelerator (PWFA) [19]–[24], [38]–[51], the plasma beat-wave accelerator (PBWA) [1], [25]–[29], [52]–[79], the laser wakefield accelerator (LWFA) [1], [30], [80]–[107], including the self-modulated regime [31]–[35], [96], [97], [108]–[117], and wakefield accelerators driven by multiple electron or laser pulses [22]–[24], [38]–[40], [91], [118]–[122]. These configurations are shown schematically in Fig. 1. The remainder of this Introduction gives a brief overview of each of these accelerator configurations. Some of the more relevant theoretical and experimental results will be highlighted. Tables I and II summarize the parameters of plasma-based accelerator experiments which have observed accelerated electrons. Section II discusses the basic models used to describe plasma wave generation in the cold fluid limit. Included is a discussion of the ponderomotive force and the quasi-static approximation. Section III describes the properties of nonlinear plasma waves (wavebreaking, period lengthening, and phase velocity) as well as the trapping and acceleration of electrons and photons by the plasma wave. The basic properties of the PWFA are described in Section IV, including a discussion of the stability

TABLE I  
ELECTRON BEAM DRIVEN ACCELERATION

$V_{\text{drive}}$ (MeV)	$Q_{\text{drive}}$ (nC)	$L_{\text{drive}}$ (mm)	$r_{\text{drive}}$ (mm)	$n_p$ ( $\text{cm}^{-3}$ )	$\Delta E$ (MeV)	$E_{\text{acc}}$ (MV/m)
USA (ANL)[20]	21	4.0	2.1	$10^{12}$	0.2	5.0
Japan (KEK)[23]	500	10	3.0	$10^{12}$	30	30 <sup>(a)</sup>
Ukraine (KhFTI)[24]	2	0.4	17	$10^{11}$	0.5	0.25

(a) result from the third of six bunches in a resonant pulse train

TABLE II  
LASER-DRIVEN ACCELERATION OF ELECTRONS

	$P$ (TW) <sup>(a)</sup>	$I$ (W/cm <sup>2</sup> ) <sup>(a)</sup>	$\tau_L$ (ps)	$\lambda_1$ ( $\mu\text{m}$ )	$\lambda_2$ ( $\mu\text{m}$ )	$n_p$ ( $\text{cm}^{-3}$ )	$\Delta E$ (MeV)	$E_{\text{acc}}$ (GV/m)
<b>PBWA</b>								
Japan (ILE)[25]	0.3	$10^{13}$	1000	9.6	10.6	$10^{17}$	$10^{(b)}$	1.5
USA (UCLA)[27]	0.2 <sup>(c)</sup>	$10^{14}$	300	10.3	10.6	$10^{16}$	28	2.8
Canada (CRL)[28]	0.1	$10^{14}$	500	10.3	10.6	$10^{16}$	17	1.7
France (LULI)[29]	0.2 <sup>(d)</sup>	$10^{17(d)}$	90 <sup>(d)</sup>	1.05	1.06	$10^{17}$	1.4	0.6
<b>LWFA</b>								
Japan (KEK)[30]	8	$10^{17}$	1.0	1.05	—	$10^{15}$	5	0.7
<b>SM-LWFA</b>								
USA (LANL)[18]	0.4	$10^{15}$	700	10.6	—	—	$1.4^{(b)}$	—
Japan (KEK)[31]	3	$10^{17}$	1.0	1.05	—	$10^{19}$	17	30
USA (LLNL)[32]	5	$10^{18}$	0.6	1.05	—	$10^{19}$	$2^{(b)}$	—
UK (RAL)[33]	25	$10^{19}$	0.8	1.05	—	$10^{19}$	$44^{(b)}$	100
USA (CUOS)[34]	2.5	$10^{19}$	0.4	1.05	—	$10^{19}$	$>1^{(b)}$	—
USA (NRL)[35]	2.5	$10^{19}$	0.5	1.05	—	$10^{19}$	$>1^{(b)}$	—

(a) for PBWA  $P \equiv P_1 \simeq P_2$  and  $I \equiv I_1 \simeq I_2$

(b) accelerated electrons come from the background plasma

(c)  $P_2 \simeq 0.05$  TW

(d)  $P_2 \simeq 0.02$  TW,  $I_2 \simeq 10^{16}$  W/cm<sup>2</sup>,  $\tau_L = 160$  ps

and propagation of the primary electron beam. Section V describes the various laser-driven plasma-based acceleration configurations, specifically, the LWFA, the PBWA, the self-modulated LWFA, and wakefields driven by multiple pulses. Included is a brief discussion of diffraction, detuning, and pump depletion, which can limit the single-stage energy gain. Methods for optically guiding laser pulses in plasmas are discussed in Section VI, including relativistic self-focusing, preformed density channels, ponderomotive self-channeling, plasma wave effects, and self-modulation. Recent experimental results on optical guiding are mentioned. Section VII describes a few of the more relevant laser-plasma instabilities, including backward and forward Raman scattering, self-modulation, and laser-hosing. A conclusion is presented in Section VIII. This paper also includes an Appendix which briefly discusses compact terawatt lasers.

#### A. Plasma Wakefield Accelerator

Plasma-based accelerators in which the plasma wave is driven by one or more electron beams are referred to as plasma wakefield accelerators (PWFA's) [19]–[24], [38]–[51]. In the PWFA, plasma wakefields can be excited by a relativistic

electron beam provided that the electron beam terminates in a time shorter than the plasma period,  $\omega_p^{-1}$ . The concept of using electron beam driven plasma waves to accelerate charge particles was apparently first proposed by Fainberg in 1956 [38]. More recently, the basic mechanism of the PWFA in the linear regime was proposed and analyzed by Chen *et al.* in 1985 [39]. Ruth *et al.* [40] showed that the transformer ratio  $R_t$  (the ratio of energy gain to the drive beam energy) is limited to  $R_t \leq 2$  for a symmetric driving beam in the linear regime. Chen *et al.* [41] showed that the transformer ratio could be increased by using an asymmetric drive beam, e.g., a triangular drive beam (a long linear rise followed by a rapid termination) of length  $L_b$  gives  $R_t \simeq \pi L_b / \lambda_p$ , where  $\lambda_p = 2\pi c / \omega_p$  is the plasma wavelength and  $L_b > \lambda_p$  is assumed. Rosenzweig [46] proposed operation in the nonlinear regime and showed that a long symmetric drive beam can produce  $R_t > 2$ . Rosenzweig *et al.* [48] later described beneficial features of operating in a two-dimensional (2-D) nonlinear “blowout” regime of the PWFA. Various authors have examined other aspects of the PWFA [42]–[51]. For example, the idea of enhancing the wakefield amplitude by using multiple electron drive bunches spaced at the plasma period was noted in the original work on the PWFA [38]–[40].

Experiments on the PWFA process were apparently first carried out by Berezin and co-workers [24] in the early 1970's. More recently, the PWFA mechanism was demonstrated in a set of experiments by Rosenzweig *et al.* [19]–[21]. In these experiments, the wakefield amplitude was mapped out by measuring the energy of a “witness” electron beam which trailed the drive beam by an adjustable delay. Wakefields were driven by a single electron bunch with an energy of 21 MeV, a duration of 7 ps, and a total charge of 4 nC, in a plasma of density  $(0.4\text{--}7) \times 10^{12} \text{ cm}^{-3}$  and of length 33 cm. Linear [19] and nonlinear [20] wakefields were observed, with a maximum energy gain of 0.2 MeV, and a maximum accelerating gradient of 5 MV/m. In Japan [22], [23], PWFA experiments were carried out using a train of electron bunches from a high-energy RF accelerator (electron bunch parameters: energy 500 MeV, length 10 ps, charge 10 nC) in a plasma of density  $(2\text{--}8) \times 10^{12} \text{ cm}^{-3}$  and of length 1 m. A maximum energy gain of 30 MeV (30 MV/m) was observed. Experiments in the Ukraine [24] were carried out using multiple bunches, each of energy 2 MeV, duration 60 ps, and total charge 0.4 nC, in a plasma of density  $10^{11} \text{ cm}^{-3}$  and of length 20–100 cm. A maximum energy gain of 0.5 MeV and a maximum accelerating gradient of 0.25 MV/m were observed.

### B. Plasma Beat-Wave Accelerator

In the PBWA [1], [25]–[29], [52]–[79], two long pulse laser beams of frequencies  $\omega_1$  and  $\omega_2$  are used to resonantly excite a plasma wave. This is done by appropriately adjusting the laser frequencies and plasma density such that the resonance condition  $\omega_1 - \omega_2 \simeq \omega_p$  is satisfied. The PBWA was first proposed by Tajima and Dawson [1] as an alternative to the laser wakefield accelerator, since compact ultrashort pulse, ultrahigh power laser technology (see Appendix) was not available in 1979. The PBWA was subsequently analyzed by various researchers [52]–[69]. (Resonant excitation of a plasma wave using two laser beams had been previously analyzed by Rosenbluth and Liu [53] for plasma heating applications.) To overcome the problem of phase detuning between the accelerated electrons and the plasma wave, Katsouleas and Dawson [54] proposed the use of a transverse magnetic field. Tang *et al.* [55] described how the plasma wave amplitude could be increased by operating at an optimal frequency mismatch  $\delta\omega_{\text{opt}}$ , such that  $\omega_1 - \omega_2 = \omega_p - \delta\omega_{\text{opt}}$ . Since this early work, various aspects of the PBWA have been analyzed and simulated, such as the self-focusing of the laser beams by relativistic, plasma wave, and cascading effects [65]–[69].

The observation of plasma wave generation in the PBWA via Thomson scattering was first demonstrated by Clayton *et al.* [70] and later observed by several groups [25]–[29], [71]–[74]. Acceleration of background plasma electrons in the PBWA was first observed by Kitagawa *et al.* [25] using two lines of a CO<sub>2</sub> laser in a plasma of density  $10^{17} \text{ cm}^{-3}$ . Plasma electrons were trapped and accelerated to an energy in excess of 10 MeV. A plasma wave amplitude of  $\delta n/n_0 = 5\%$  was observed and an acceleration gradient of 1.5 GV/m was estimated. Clayton *et al.* [26], [27] observed electron acceleration in a series of PBWA experiments using

two lines of a CO<sub>2</sub> laser in a plasma of density  $9 \times 10^{15} \text{ cm}^{-3}$ . A 28 MeV energy gain was observed using a 2 MeV injected electron beam, corresponding to a gradient of 2.8 GV/m and a plasma wave amplitude of  $\delta n/n_0 = 28\%$ . The UCLA experiments were particularly well diagnosed and various laser-plasma interaction phenomena and instabilities have been observed [75]–[79]. Electron acceleration was also observed in the PBWA experiments of Ebrahim [28] using two CO<sub>2</sub> laser lines in a plasma of density  $10^{16} \text{ cm}^{-3}$ . A 12.5 MeV injected electron beam was accelerated to 29 MeV over a plasma length of approximately 1 cm ( $\approx 1.7 \text{ GV/m}$ ). More recently, Amiranoff *et al.* [29] observed acceleration in a PBWA experiment using two Nd laser lines in a plasma of density  $10^{17} \text{ cm}^{-3}$ . A 3.4 MeV injected electron beam was observed to increase by 1.4 MeV. A plasma wave amplitude of 2% and a gradient of 0.6 GV/m were observed. Plasma wave saturation and parametric coupling to ion waves were also observed in these experiments [73], [74].

### C. Laser Wakefield Accelerator

In the laser wakefield accelerator (LWFA) [1], [30], [80]–[107], a single short ( $\lesssim 1 \text{ ps}$ ) ultrahigh intensity ( $\gtrsim 10^{18} \text{ W/cm}^2$ ) laser pulse drives a plasma wave. The wakefield is driven most efficiently when the laser pulse length  $L = c\tau_L$  is approximately the plasma wavelength  $\lambda_p = 2\pi c/\omega_p$ , i.e.,  $L \simeq \lambda_p$ . The LWFA was first proposed by Tajima and Dawson [1] and simulated (one-dimensional (1-D) particle-in-cell) by Sullivan and Godfrey [80] and by Mori [81]. Prior to 1988, the technology for generating ultra-intense picosecond laser pulses did not exist and only the PBWA concept appeared feasible (which relied on long pulses of modest intensity). The LWFA was later reinvented independently by Gorbunov and Kirsanov [82] and by Sprangle *et al.* [83], [84]. This roughly coincides with the time when chirped-pulse amplification was applied to compact solid-state lasers and a table-top terawatt laser system was first demonstrated by Mourou and co-workers [11] (see Appendix). The nonlinear theory of the LWFA in one dimension was developed by Bulanov *et al.* [87], Sprangle *et al.* [88], [89], and Berezhiani and Murusidze [90]. The nonlinear theory of the LWFA in two dimensions, including the self-consistent evolution of the laser pulse, was analyzed by Sprangle *et al.* [96], [97].

Perhaps the first experimental evidence for plasma wave generation by the LWFA mechanism was obtained by Hamster *et al.* [105]. In these experiments, the emission of terahertz radiation at the plasma frequency was observed when the plasma was driven by a laser pulse of length  $L \simeq \lambda_p$ . Specifically,  $\omega_p/2\pi = 4.6 \text{ THz}$  radiation was observed for a 0.1 ps laser pulse propagating in a plasma of density  $2 \times 10^{17} \text{ cm}^{-3}$ . This radiation is emitted by the 2-D electron plasma currents of the laser-induced wakefield. Recently, the measurement of plasma wave generation in the LWFA has been reported by researchers at Ecole Polytechnique [106] and at the University of Texas at Austin (UTA) [107] by using probe pulses and optical interferometry techniques. In the French experiments [106], a 120 fs duration, 800 nm wavelength laser pulse with a maximum energy of 40 mJ

was focused to a maximum intensity of  $3 \times 10^{17} \text{ W/cm}^2$  in a plasma of density  $10^{17} \text{ cm}^{-3}$ . A pair of probe pulses, separated from each other by 1.5 times the plasma wavelength, were used to map out the wakefield by adjusting the delay between the pump and probe pulses. A plasma wave with a perturbed density of 30% to 100% was measured over several plasma periods behind the probe pulse. At UTA [107], three probe pulses were used to measure the density perturbation at a fixed delay behind the pump pulse. By varying the ambient plasma density, the plasma wave amplitude was observed to vary in good agreement with theory.

Nakajima *et al.* [30] have reported electron acceleration in LWFA experiments. Electrons from a synchronous laser-solid interaction were injected with energies near 1 MeV and accelerated to energies  $>5$  MeV by an 8-TW 1-ps laser pulse in a plasma of density  $3.5 \times 10^{15} \text{ cm}^{-3}$ . Estimates based on simulations imply an acceleration gradient of 0.7 GV/m.

#### D. Self-Modulated LWFA

The self-modulated LWFA [31]–[35], [96], [97], [108]–[117] uses a single short ( $\lesssim 1$  ps) ultrahigh intensity ( $\gtrsim 10^{18} \text{ W/cm}^2$ ) laser pulse, as in the standard LWFA. The self-modulated LWFA, however, operates at higher densities than the standard LWFA, such that the laser pulse length is long compared to the plasma wavelength,  $L > \lambda_p$ , and the laser power  $P$  is somewhat larger than the critical power  $P_c$  for relativistic guiding,  $P \geq P_c$ . In this high-density regime, the laser pulse undergoes a self-modulation instability [108]–[113] which causes the pulse to become axially modulated at the plasma period. Associated with the modulated pulse structure is a large amplitude, resonantly driven plasma wave. The self-modulation instability resembles a highly 2-D version of a forward Raman instability. Forward Raman scattering occurs simultaneously, adding to the modulation, and in the 1-D limit, pulse modulation can occur via forward Raman scattering alone [114].

The process by which a plasma wave can modulate a laser pulse by producing periodic regions of enhanced focusing and diffraction was first described and analyzed by Esarey *et al.* [69]. The self-modulation of relativistically guided laser pulses was observed in the simulations of Andreev *et al.* [108], Sprangle *et al.* [96], and Antonsen and Mora [109]. Krall *et al.* [110] simulated a self-modulated LWFA, including the acceleration of an injected electron beam, and showed that this configuration can have certain advantages over the standard LWFA. The self-modulation instability was subsequently analyzed by Esarey *et al.* [111] and Andreev *et al.* [112], [113], and, in the 1-D limit, forward Raman scattering (FRS) was analyzed by Mori *et al.* [114]. Extensive particle-in-cell simulations of short intense pulses propagating in the high-density regime have been carried out by Decker *et al.* [115] and Bulanov *et al.* [116].

Evidence for plasma wave generation in the high-density self-modulated regime was first detected by Coverdale *et al.* [32]. The presence of a plasma wave leads to the generation of Stokes and anti-Stokes lines in the frequency spectrum of the pump laser pulse. The first two anti-Stokes lines were observed

by Coverdale *et al.*, the appearance of which were correlated with production of fast electrons, as discussed below. Subsequently, multiple anti-Stokes lines in the forward spectrum of the pump laser have been observed by several other groups [33]–[35], [117]. At the Naval Research Laboratory (NRL) [117], plasma wave generation in the self-modulated regime was measured via coherent Thomson scattering with a frequency-doubled probe pulse. The evolution of the plasma wave was observed by varying the time delay between the pump and probe pulses.

Joshi *et al.* [18] detected fast electrons in an early experiment via forward Raman scattering. A single long pulse (700 ps) CO<sub>2</sub> laser pulse of modest intensity ( $10^{15} \text{ W/cm}^2$ ) interacting with a thin Carbon foil was observed to produce 1.4 MeV electrons. Electron acceleration in the high-density self-modulated regime has been observed recently using ultra-short pulses ( $\lesssim 1$  ps). Nakajima *et al.* [31] observed electron acceleration to energies  $\gtrsim 17$  MeV using a 3-TW 1-ps  $10^{17} \text{ W/cm}^2$  laser pulse in a plasma of density near  $10^{19} \text{ cm}^{-3}$ . A laser-solid interaction was used to produce a source of injected electrons with energies near 1 MeV. Particle simulations in 1-D suggest acceleration gradients on the order of 30 GV/m. Coverdale *et al.* [32] observed 2 MeV electrons, which were trapped and accelerated from the background plasma, when a 600-fs 5-TW  $8 \times 10^{17} \text{ W/cm}^2$  laser pulse propagated in a plasma of density  $2 \times 10^{19} \text{ cm}^{-3}$ . The generation of electrons was also correlated with the occurrence of anti-Stokes lines in the laser pulse spectrum, which indicates the presence of a plasma wave. Modena *et al.* [33] demonstrated the acceleration of self-trapped electrons to energies  $\gtrsim 44$  MeV (limit of the detector) using a 1-ps 25-TW  $5 \times 10^{18} \text{ W/cm}^2$  laser pulse in a plasma of density  $1.5 \times 10^{19} \text{ cm}^{-3}$ . A large flux of electrons was observed ( $10^6$  electrons/MeV at 44 MeV) and the electron signal was correlated to the appearance of up to five anti-Stokes lines in the laser spectrum. Estimates based on the electron phase detuning length imply an acceleration gradient  $>100$  GV/m. Acceleration of self-trapped electrons has also been observed by Wagner *et al.* [34]. The electrons were emitted in a well-collimated beam in the forward direction (a divergence angle  $\simeq 8^\circ$ ) and the cross section of the beam resembled the shape of the cross section of the laser at focus. By varying the laser pulse energy, a threshold for electron acceleration was observed near  $P \simeq P_c$ . More recently, accelerated plasma electrons were observed at NRL [35] using a 2.5-TW 0.5-ps  $6 \times 10^{18} \text{ W/cm}^2$  laser pulse in a plasma of density  $10^{19} \text{ cm}^{-3}$ .

#### E. Multiple Pulses

By using multiple laser pulses (in the LWFA) or electron bunches (in the PWFA), the wakefield amplitude can be enhanced [22]–[24], [38]–[40], [91], [118]–[122]. In the linear regime,  $N$  identical pulses will increase the wakefield by a factor of  $N$  when the front of the pulses are separated by an integer number of plasma wavelengths. In the nonlinear regime, greater enhancements may be possible. The idea of using multiple electron pulses in the PWFA was put forth in the first papers on the PWFA [38]–[40]. In fact, experiments

on the PWFA in Ukraine [24] and in Japan [22], [23] utilized multiple bunches. Several groups have suggested and analyzed the possibility of using multiple laser pulses to enhance the wakefield in the LWFA [91], [118]–[122]. Recently, Umstadter *et al.* [119], [120] calculated the conditions for an optimized laser pulse train which corresponds to maximizing the plasma wave amplitude in the 1-D nonlinear regime. In particular, they showed that for realistic laser pulse profiles, the spacing between pulses increases whereas the width of each subsequent pulse decreases as the plasma wave becomes more nonlinear. Preliminary experiments on the production of multiple pulse trains using chirped-pulse amplification (CPA) laser systems have been reported [123].

## II. PLASMA WAVE GENERATION

Calculation of the plasma wakefields generated by nonevolving drive beams is straightforward. Analytical solutions exist in the three-dimensional (3-D) linear regime and in the 1-D nonlinear regime. In the 3-D nonlinear regime, the use of numerical codes is usually required. The full problem, which includes the self-consistent evolution of the drive beams, is sufficiently complicated to require simulation. Various aspects of the propagation and transport of the drive beams will be discussed in subsequent sections. Before discussing specific plasma-based accelerator configurations (e.g., PWFA, PBWA, LWFA, etc.), the physical forces which drive wakefields (i.e., space-charge and ponderomotive forces) and the mathematical models used to describe wakefield generation will be briefly discussed. In the following, it is convenient to use the normalized electrostatic potential  $\phi = e\Phi/m_ec^2$  and vector  $\mathbf{a} = e\mathbf{A}/m_ec^2$  potentials.

An important parameter in the discussion of ultra-intense laser-plasma interactions is the laser strength parameter  $a_0$ , defined as the peak amplitude of the normalized vector potential of the laser field. The laser strength parameter is related to the peak intensity  $I$  and power  $P$  of a linearly polarized Gaussian laser pulse by

$$\begin{aligned} a_0 &= (2e^2\lambda^2 I/\pi m_e^2 c^5)^{1/2} \\ &\simeq 8.6 \times 10^{-10} \lambda [\mu\text{m}] I^{1/2} [\text{W/cm}^2] \end{aligned} \quad (2)$$

and  $P[\text{GW}] \simeq 21.5(a_0 r_0/\lambda)^2$ , where  $r_0$  is the laser spot size at focus,  $\lambda = 2\pi/k$  is the laser wavelength,  $\omega = ck$  is the laser frequency,  $I = 2P/\pi r_0^2$ , and a vector potential of the form  $\mathbf{a} = a_0 \exp(-r^2/r_0^2) \cos(kz - \omega t) \mathbf{e}_x$  is assumed. Furthermore, the peak laser electric field amplitude  $E_L$  is given by  $E_L [\text{TV/m}] \simeq 3.2a_0/\lambda [\mu\text{m}]$ . Physically,  $\mathbf{a} = \mathbf{p}_\perp/m_ec$  is the normalized transverse “quiver” momentum of the electrons in the laser field, as indicated by conservation of transverse canonical momentum in the 1-D limit ( $r_0 \gg \lambda$ ). Highly relativistic electron motion ( $a_0 \gtrsim 1$ ) requires laser intensities  $I \gtrsim 10^{18} \text{ W/cm}^2$  for wavelengths of  $\lambda \simeq 1 \mu\text{m}$ . Such intensities are now available from compact CPA laser systems [15], [16].

### A. Space-Charge and Ponderomotive Forces

The physical origin of the plasma wave in the PWFA is the space-charge force associated with the drive electron beam.

When the electron beam propagates into a uniform plasma,  $n = n_0$ , where  $n$  is the plasma electron density, the beam density  $n_b$  generates a space-charge potential via Poisson's equation,  $\nabla^2\phi = k_p^2(n/n_0 + n_b/n_0 - 1)$ , where  $k_p = \omega_p/c$ . The resulting space-charge force  $\mathbf{F}_{sc} = -m_ec^2\nabla\phi$  can drive a plasma wakefield. Consider a long uniform relativistic electron beam of density  $n_b \ll n_0$  and radius  $r_b \gg \lambda_p$ . The space-charge potential within the beam,  $r < r_b$ , is  $\phi_{sc} = r^2 k_b^2/4$ , where  $k_b^2 = 4\pi e^2 n_b/m_ec^2$ . The plasma electrons will respond so as to cancel the space-charge potential of the beam, i.e., the perturbed plasma density is  $\delta n = -n_b$ . If the electron beam terminates in a time short compared to  $\omega_p^{-1}$ , a plasma wakefield of the form  $\delta n = n_b \sin k_p(z - ct)$  is generated. The axial electric field of the wake behind the beam is given by  $\partial E_z/\partial z = -4\pi e\delta n$ , i.e.,  $E_z = 4\pi e(n_b/k_p) \cos k_p(z - ct)$ . The peak amplitude of the wake is  $E_{max} = (n_b/n_0)E_0$ .

In laser-driven plasma-based accelerators, wakefields are driven via the ponderomotive force. The ponderomotive force [124] can be derived by considering the electron momentum equation in the cold fluid limit,  $d\mathbf{p}/dt = -e[\mathbf{E} + (\mathbf{v} \times \mathbf{B})/c]$ , where  $d/dt = \partial/\partial t + \mathbf{v} \cdot \nabla$ . The electric and magnetic fields of the laser can be written as  $\mathbf{E} = -\partial\mathbf{A}/\partial ct$  and  $\mathbf{B} = \nabla \times \mathbf{A}$ , where the vector potential of the laser is polarized predominately in the transverse direction, e.g.,  $\mathbf{A} = A_0 \cos(kz - \omega t) \mathbf{e}_\perp$ . In the linear limit  $|a| = e|A|/m_ec^2 \ll 1$ , the leading order electron motion is the quiver velocity  $\mathbf{v}_q = ca$ , as indicated by  $m_e \partial \mathbf{v}_q / \partial t = -e\mathbf{E}$ . Letting  $\mathbf{v} = \mathbf{v}_q + \delta\mathbf{v}$ , the second-order motion is given by

$$\begin{aligned} d\delta\mathbf{p}/dt &= -m_e[(\mathbf{v}_q \cdot \nabla)\mathbf{v}_q + c\mathbf{v}_q \times (\nabla \times \mathbf{a})] \\ &= -m_ec^2\nabla(a^2/2). \end{aligned} \quad (3)$$

Hence,  $\mathbf{F}_p = -m_ec^2\nabla(a^2/2)$  is the 3-D ponderomotive force in the linear limit ( $a^2 \ll 1$ ). The ponderomotive force can also be viewed as the gradient of the radiation pressure.

In the 1-D nonlinear regime, conservation of canonical momentum implies  $\mathbf{u}_\perp = \mathbf{a}_\perp$ , where  $\mathbf{u}_\perp = \mathbf{p}_\perp/m_ec$ , i.e.,  $\mathbf{a}_\perp$  is the normalized quiver momentum. Hence, in one dimension, the nonlinear ponderomotive force is given by  $F_{pz} = -(m_ec^2/2\gamma)\partial a_\perp^2/\partial z$ . In the 3-D nonlinear regime, the leading order transverse motion of the electron is still the quiver motion,  $\mathbf{u}_\perp = \mathbf{a}_\perp$ , provided that the laser pulse has a sufficiently broad spot size,  $r_0 > \lambda_p \gg \lambda$ . Assuming that the laser pulse is a function of only the variables  $r$  and  $\zeta = z - ct$ , as in the quasi-static approximation [88], [89], it can be shown [96], [97] that the momentum equation can be written as

$$\partial(\mathbf{u} - \mathbf{a})/\partial\zeta = \nabla(\gamma - \phi). \quad (4)$$

Here,  $\nabla\phi$  is the space-charge force and  $\nabla\gamma$  represents an effective nonlinear ponderomotive force,  $\mathbf{F}_{pN} = -m_ec^2\nabla\gamma$ . Since the axial component of (4) implies  $\gamma - u_z = 1 + \phi - a_z$ , it can be shown that [96], [97]

$$\gamma = \frac{1 + (u_{\perp s})^2 + |a_{\perp s}|^2 + (1 + \Psi_s)^2}{2(1 + \Psi_s)} \quad (5)$$

where  $\Psi_s = \phi_s - a_{zs}$  and the subscript  $s$  denotes the slow component, which is obtained by averaging over the fast laser period.

### B. Linear Regime

In the linear 3-D regime, wakefield generation can be examined using the cold fluid equations, i.e., Poisson's equation, the continuity equation, and the momentum equation. For example, the plasma wave generated in an initially uniform plasma, by either a laser or electron beam, is described by [39], [40], [58], [82]–[84]

$$\left( \frac{\partial^2}{\partial t^2} + \omega_p^2 \right) \frac{\delta n}{n_0} = -\omega_p^2 \frac{n_b}{n_0} + c^2 \nabla^2 \frac{a^2}{2} \quad (6)$$

where  $n_b/n_0 \ll 1$  is the normalized density of the driving electron beam,  $a^2 \ll 1$  is the normalized intensity of the driving laser beam, and  $\delta n/n_0 \ll 1$  is the perturbed density of the plasma wave. The solution to (6) is

$$\delta n/n_0 = \omega_p^{-1} \int_0^t dt' \sin \omega_p(t-t') F(t') \quad (7)$$

where  $F(t)$  is the right side of (6). Equations (6) and (7) describe plasma waves generated at the frequency  $\omega_p$  and are valid far from wavebreaking,  $E \ll E_0$ . Solutions to (7) indicate that wakefields will be generated most efficiently when the envelope scale length, which characterizes the axial gradient in the profile of the beam density  $n_b$  or the normalized laser intensity  $a^2$ , is on the order of the plasma wavelength  $\lambda_p = 2\pi c/\omega_p$ .

For the plasma wakefield accelerator [ $a^2 = 0$  in (6)], the electric field of the wake can be calculated from  $\nabla^2 \phi = k_p^2(\delta n + n_b)/n_0$ . For a highly relativistic,  $v_b \simeq c$ , axisymmetric drive beam, the axial electric field of the wake behind the beam is given by [43], [44], [125], [126]

$$E_z(r, \zeta) = 4\pi e k_p^2 \int_{\infty}^{\zeta} d\zeta' \int_0^{\infty} dr' r' \cos k_p(\zeta - \zeta') I_0(k_p r_{<}) K_0(k_p r_{>}) n_b(\zeta', r') \quad (8)$$

where  $\zeta = z - ct$ ,  $I_0$  and  $K_0$  are zeroth-order modified Bessel functions, and  $r_{<}$  and  $r_{>}$  denote the smaller and larger of  $r$  and  $r'$ , respectively.

For laser-driven accelerators,  $n_b = 0$ , and (6) implies  $(\partial^2/\partial t^2 + \omega_p^2)\phi = \omega_p^2 a^2/2$ . Hence

$$\mathbf{E}(\mathbf{r}, t) = -(m_e c^2 \omega_p / e) \int_0^t dt' \sin \omega_p(t-t') \nabla a^2(\mathbf{r}, t') / 2. \quad (9)$$

For laser-driven wakefields, (9) implies that the radial extent of the wake is on the order of the laser spot size  $r_s$ . For electron beam-driven wakefields, however, the radial extent of the wake is given approximately by the larger of the beam radius  $r_b$  and the plasma skin depth  $k_p^{-1} = c/\omega_p$ , due to the factor  $I_0(k_p r_{<}) K_0(k_p r_{>})$  in (8).

As an example, consider an LWFA driven by a circularly polarized laser pulse with a normalized intensity profile given by  $a^2 = a_0^2 \exp(-2r^2/r_s^2) \sin^2(\pi\zeta/L)$  for  $0 < \zeta < L$ , where  $\zeta = z - ct$ . Solutions to (9) indicate that the wakefield amplitude is maximum for pulse lengths  $L \simeq \lambda_p$ . Behind the pulse,  $\zeta < 0$ , the axial electric field and density perturbation of the wake are given by [83], [84]

$$\frac{E_z}{E_0} = -\frac{\pi}{4} a_0^2 \exp\left(-\frac{2r^2}{r_s^2}\right) \cos k_p \zeta \quad (10)$$

$$\frac{\delta n}{n_0} = -\frac{\pi}{4} a_0^2 \left[ 1 + \frac{8}{k_p^2 r_s^2} \left( 1 - \frac{2r^2}{r_s^2} \right) \right] \exp\left(-\frac{2r^2}{r_s^2}\right) \sin k_p \zeta \quad (11)$$

for the case  $L = \lambda_p$ . For linear polarization, replace  $a_0^2$  with  $a_0^2/2$ .

In addition to the axial wakefield  $E_z$ , transverse wakefields  $E_r$  and  $B_\theta$  will be generated. The transverse wakefields are related to the axial wakefield by the Panofsky–Wenzel theorem [40], [43], [44], [125]–[127],  $\partial E_z/\partial r = \partial(E_r - B_\theta)/\partial\zeta$ . A relativistic particle with  $v_z \simeq c$  which is being accelerated by a wakefield with  $v_p \simeq c$  will experience a radial force proportional to  $E_r - B_\theta$ . Notice that if  $E_z \sim \exp(-2r^2/r_s^2)$ , then  $E_r - B_\theta \sim (4r/k_p r_s^2) \exp(-2r^2/r_s^2)$  and the radial force is zero along the axis. Typically, for an electron displaced from the axis, there is a phase region of the wake with an axial length of  $|\Delta\zeta| = \pi/4k_p$  within which a relativistic electron will experience simultaneous axial accelerating and radial focusing forces [40].

### C. Nonlinear Regime

Wakefield generation in the nonlinear 1-D regime can be examined by assuming that the drive beam is nonevolving, i.e., the drive beam is a function of only the coordinate  $\zeta = z - v_p t$ , where  $v_p \leq c$  is the phase velocity of the plasma wave. For electron beam drivers,  $v_p \simeq v_b$  is the drive beam velocity, and for laser drivers,  $v_p \simeq v_g$  is the laser pulse group velocity. The 1-D limit applies to broad drivers,  $k_p r_\perp \gg 1$ , where  $r_\perp$  is the characteristic radial dimension of the drive beam. Using the momentum and continuity equations, Poisson's equation,  $\partial^2 \phi / \partial \zeta^2 = k_p^2(n/n_0 + n_b/n_0 - 1)$ , can be written as [91], [101], [119]–[121], [128], [129]

$$k_p^{-2} \frac{\partial^2 \phi}{\partial \zeta^2} = \frac{n_b}{n_0} + \gamma_p^2 \left\{ \beta_p \left[ 1 - \frac{(1+a^2)}{\gamma_p^2(1+\phi)^2} \right]^{-1/2} - 1 \right\} \quad (12)$$

where  $\gamma_p = (1 - \beta_p^2)^{-1/2}$  and  $\beta_p = v_p/c$ . The axial electric field of the wake is given by  $E_z = -E_0 \partial \phi / \partial \zeta$ . In the limit  $\gamma_p^2 \gg 1$ , (12) simplifies to [46], [87]–[90]

$$k_p^{-2} \frac{\partial^2 \phi}{\partial \zeta^2} = \frac{n_b}{n_0} + \frac{(1+a^2)}{2(1+\phi)^2} - \frac{1}{2}. \quad (13)$$

(Similar expressions were used by Noble [57] to study the PBWA.) Solutions can be found analytically for square electron beam [46] or laser pulse profiles [87]–[90]. Numerical solutions to (12) and (13) indicate that the general features of the wakefield generated by a more realistically shaped pulse, e.g., Gaussian, do not differ dramatically from those of a square pulse. As the plasma wave amplitude becomes nonlinear, (12) and (13) indicate that the plasma wave steepens and its period lengthens, as is discussed in Section III-B. Notice that in the linear limit,  $|\phi| \ll 1$ , (13) reduces to

$$(\partial^2/\partial \zeta^2 + k_p^2)\phi = k_p^2(n_b/n_0 + a^2/2) \quad (14)$$

which is implied by the 1-D limit of (6).

In the 2-D nonlinear regime, simulations are usually required. One possible approach is to use a nonlinear quasi-static fluid model [96], [97], which is briefly discussed in the

following section. An alternative approach is to use 2-D particle-in-cell simulations [115], [116].

#### D. Quasi-Static Approximation

A useful approximation in the study of short pulse interactions with plasmas is the quasi-static approximation (QSA), which was first applied to nonlinear laser-plasma interactions by Sprangle *et al.* [88], [89]. In the QSA, the plasma fluid equations are written in terms of the independent variables  $\zeta = z - v_g t$  and  $\tau = t$ , where  $v_g$  is the velocity of the driver (e.g., laser pulse). The QSA assumes that in the time it takes the laser pulse to transit a plasma electron, the laser pulse does not significantly evolve. In other words,  $\tau_L \ll \tau_E$ , where  $\tau_L = L/c$  is the laser pulse duration and  $\tau_E$  is the laser pulse evolution time, which is typically on the order of a Rayleigh (diffraction) time. Thus, the plasma electrons experience a static (independent of  $\tau$ ) laser field. In the QSA, the  $\partial/\partial\tau$  derivatives are neglected in the plasma fluid equations which determine the plasma response to the laser pulse. The  $\partial/\partial\tau$  derivatives, however, are retained in the wave equation which describes the evolution of the laser pulse. The QSA allows the laser-plasma interaction to be calculated in an iterative fashion. For a fixed  $\tau$ , the plasma response to the laser field is determined as a function of  $\zeta$  by solving the QSA fluid equations (e.g., (12) in the 1-D limit). Using this fluid response, the wave equation is then solved to update the laser pulse in  $\tau$ .

For example, the wave equation describing the evolution of the laser field can be written as [96], [97], [128]

$$\left( \nabla_{\perp}^2 + \frac{2v_g}{c^2} \frac{\partial^2}{\partial\zeta\partial\tau} + \frac{1}{\gamma_g^2} \frac{\partial^2}{\partial\zeta^2} - \frac{1}{c^2} \frac{\partial^2}{\partial\tau^2} \right) a \simeq k_p^2 \rho a \quad (15)$$

where  $\rho = n/\gamma n_0$ ,  $n$  is the electron plasma density, and  $\gamma$  is the relativistic factor associated with the electron fluid velocity, e.g., (5). Typically, the third and fourth terms on the left side of (15) can be neglected. In addition, if the approximation  $\partial^2/\partial\zeta\partial\tau \simeq ik\partial/\partial\tau$  is made to the second term of the left side of (15), then the resulting equation is referred to as the paraxial wave equation. The paraxial approximation assumes that the laser field can be written as  $a = \hat{a}(r, \zeta, \tau) \exp(ik\zeta)$ , where  $|\partial\hat{a}/\partial\zeta| \ll |k\hat{a}|$ , i.e., the laser envelope  $\hat{a}$  is slowly varying compared to the laser wavelength. The fluid quantity  $\rho = n/\gamma n_0$  is determined from the quasi-static fluid equations. For example, in the 1-D limit, it can be shown [128] that  $\rho = (1+\phi)^{-1}(1+k_p^{-2}\gamma_g^{-2}\partial^2\phi/\partial\zeta^2)$ , where  $\partial^2\phi/\partial\zeta^2$  satisfies (12). In 2-D and assuming  $v_g \simeq c$ , it can be shown [96], [97], [130] that  $\rho = (1+\Psi)^{-1}(\rho_0 + k_p^{-2}\nabla_{\perp}^2\Psi)$ , where  $\rho_0$  is the initial value of  $\rho$  (prior to the laser pulse) and the quantity  $\Psi = \phi - a_z$  satisfies a quasi-static equation of the form  $\partial^2\Psi/\partial\zeta^2 = G_f(\Psi, a^2)$  with  $G_f$  an involved function [130].

### III. NONLINEAR PLASMA WAVES AND ACCELERATION

#### A. Wavebreaking

Plasmas are capable of supporting large amplitude electrostatic waves with phase velocities near the speed of light. Such waves can be used to accelerate electrons. In the linear regime, the electric field of a plasma wave in a plasma-based

accelerator has the form  $E_z = E_{\max} \sin \omega_p(z/v_p - t)$ , where  $v_p \simeq c$  is the phase velocity. The peak field amplitude  $E_{\max}$  of the plasma wave can be very high and can be estimated from Poisson's equation,  $\nabla \cdot E = 4\pi e(n_0 - n_e)$ . A simple estimate for the maximum field amplitude is given by assuming all of the plasma electrons are oscillating with a wavenumber  $k_p = \omega_p/c$ . This gives  $(\omega_p/c)E_{\max} = 4\pi e n_0$ , or  $E_{\max} = E_0$ , where  $E_0$  is the nonrelativistic wavebreaking field [36] given by (1).

It is possible for the maximum amplitude of a nonlinear plasma wave to exceed the value  $E_0$ . Using the nonlinear relativistic cold fluid equations in 1-D, it is possible to show that the maximum amplitude of a plasma wave is given by

$$E_{WB} = \sqrt{2}(\gamma_p - 1)^{1/2} E_0 \quad (16)$$

where  $\gamma_p = (1 - v_p^2/c^2)^{-1/2}$  is the relativistic factor associated with the phase velocity of the plasma wave, assuming  $v_p < c$ . The quantity  $E_{WB}$  is often referred to as the relativistic wavebreaking field and was first derived by Akhiezer and Polovin [37]. As an example, consider a laser-driven accelerator with a plasma density of  $n_0 \simeq 10^{16} \text{ cm}^{-3}$ . The plasma wave phase velocity is approximately the group velocity of the laser,  $\gamma_p \simeq \omega/\omega_p$ , where  $\omega$  is the frequency of the laser. For a laser wavelength of 1  $\mu\text{m}$ ,  $\gamma_p \simeq 330$  and  $E_{WB} \simeq 26E_0 \simeq 250 \text{ GV}$ .

Fluid equations can be used to describe a coherent plasma wave as long as the electron fluid velocity  $v_e$  is less than the phase velocity of the wave,  $v_e < v_p$ . In the 1-D cold fluid limit, the nonlinear plasma wave is described by (12). As the wave amplitude increases,  $v_e$  increases. The wave is said to "break" when  $v_e \rightarrow v_p$ , at which point the plasma density becomes singular,  $n \rightarrow \infty$ . Mathematically, wavebreaking occurs in a cold 1-D plasma when  $E_{\max} \rightarrow E_{WB}$ , where  $E_{WB}$  is given by (16).

The above value for the wavebreaking field was based on cold fluid theory. Thermal electron effects, however, can lead to a reduction in the wavebreaking field. In a warm plasma, the electron distribution has a thermal spread about its mean fluid velocity  $v_e$ . Roughly speaking, a large fraction of the electron distribution will become trapped in the plasma wave when  $|v_e + v_{th,eff}| \rightarrow v_p$ , where  $v_{th,eff}$  is an effective thermal velocity spread. This leads to wavebreaking. Using warm relativistic fluid theories, expressions for the thermal wavebreaking field amplitude  $E_{th}$  have been derived [47], [131] of the form

$$E_{th} = (m_e c^2 / 3T)^{1/4} f_{th}(\gamma_p, T) E_0 \quad (17)$$

where  $f_{th}(\gamma_p, T)$  is a slowly varying function of  $\gamma_p$  and the electron temperature  $T$  with a typical magnitude on the order of unity,  $f_{th}(\gamma_p, T) \sim 1$ . Katsouleas and Mori [131] give  $f_{th}^2 = \ln(2\gamma_p^{1/2}\beta_{th}^{1/4})$  for  $\gamma_p\beta_{th}^{1/2} \gg 1$ , where  $\beta_{th} = 3T/m_e c^2$ . Thermal effects will limit the wave amplitude if the warm wavebreaking field is less than the cold wavebreaking field,  $E_{th} < E_{WB}$ . As an example,  $\gamma_p \simeq 330$  and  $T = 10 \text{ eV}$  give a thermal wavebreaking limit of  $E_{th} \simeq 12 E_0$ , which is approximately one-half that of the cold wavebreaking result,  $E_{WB}$ .

The above expressions for the wavebreaking field were based on 1-D theories. Wavebreaking in 3-D has not been thoroughly investigated and general expressions for the maximum

field amplitude are not known. Two-dimensional particle-in-cell simulations [115], [116] have demonstrated the generation of plasma waves with amplitudes on the order of  $E_0$ . Simulations [96], [97], [110] based on nonlinear 2-D axisymmetric fluid equations have shown wave amplitudes in excess of  $E_0$ .

### B. Nonlinear Plasma Waves

In the linear regime,  $E_{\max} \ll E_0$ , the plasma wave is a simple sinusoidal oscillation with frequency  $\omega_p$  and an arbitrary phase velocity  $v_p$  (the phase velocity is determined by the driver), e.g.,  $\phi = \phi_0 \cos \omega_p(z/v_p - t)$ . When  $E_{\max} \gtrsim E_0$ , the plasma wave becomes highly nonlinear. In the 1-D cold fluid limit, the nonlinear plasma wave is described by (12). In the region behind the drive beam,  $n_b = a^2 = 0$ , an analysis of (12) indicates that the electrostatic potential oscillates between  $\phi_{\min} \leq \phi \leq \phi_{\max}$  and the axial electric field oscillates between  $-E_{\max} \leq E \leq E_{\max}$ . The values  $\phi_{\min}$  and  $\phi_{\max}$ , denoted by  $\phi_m$ , are given by [129]

$$\phi_m = \hat{E}_{\max}^2/2 \pm \beta_p \left[ (1 + \hat{E}_{\max}^2/2)^2 - 1 \right]^{1/2} \quad (18)$$

where  $\hat{E}_{\max} = E_{\max}/E_0$  and the  $\pm$  give  $\phi_{\max}$  and  $\phi_{\min}$ , respectively. Wavebreaking occurs when the density becomes singular. From (12), this occurs when  $(1 + \phi) \rightarrow 1/\gamma_p$ . At wavebreaking,  $\phi_{\min} = 1/\gamma_p - 1$ , and (18) implies  $E_{\max} = \sqrt{2}(\gamma_p - 1)^{1/2}E_0 \equiv E_{WB}$ .

As  $E_{\max}/E_0 \gtrsim 1$ , (12) indicates that the electric field departs from a simple sinusoidal form [37], [46], [87]–[90]. In particular, the electric field exhibits the characteristic “sawtooth” profile associated with wave steepening and the density oscillations become highly peaked. Furthermore, the period of the nonlinear plasma wave increases as the amplitude increases. The nonlinear plasma wavelength in the limit  $\gamma_p \gg 1$  is given by [87]–[90]

$$\lambda_{Np} = \lambda_p \begin{cases} 1, & E_{\max}/E_0 \ll 1 \\ (2/\pi)E_{\max}/E_0, & E_{\max}/E_0 \gg 1 \end{cases} \quad (19)$$

where  $E_{\max}$  is the peak electric field of the plasma wave and  $\lambda_p = 2\pi/k_p = 2\pi c/\omega_p$ .

As an example of nonlinear plasma wave behavior, (13) has been solved numerically [88], [89] for a linearly polarized laser of the form  $a^2 = a_0^2 \sin^2(\pi\zeta/L) \cos^2 k\zeta$  for  $0 < |\zeta| < L$ , where  $L = \lambda_p$ , as in the LWFA. A mildly relativistic case  $a_0 = 0.5$  is shown in Fig. 2(a) and a highly relativistic case  $a_0 = 2$  is shown in Fig. 2(b). Here,  $E_z$  is given by the solid curve,  $\delta n/n_0$  is given by the dashed curve, the density is  $n_0 \simeq 10^{16} \text{ cm}^{-3}$ , and the laser pulse exists in the region  $-0.03 \text{ cm} = -L \leq \zeta \leq 0$ . Note that the rapid oscillations in the plasma density at one-half the laser wavelength are due to a fast component of the ponderomotive force, i.e.,  $a^2 \sim 1 + \cos 2k\zeta$ . The nonlinear effects of wave steepening and period lengthening are clearly evident in Fig. 2(b).

The lengthening of the plasma wave period can have an important role in plasma-based accelerators. For example, in the PBWA, the plasma wave is driven at a constant beat frequency  $\Delta\omega = \omega_1 - \omega_2 \simeq \omega_p$ . As the wave grows, however, the effective plasma frequency decreases,  $\omega_{p,\text{eff}} = 2\pi c/\lambda_{Np}$ .

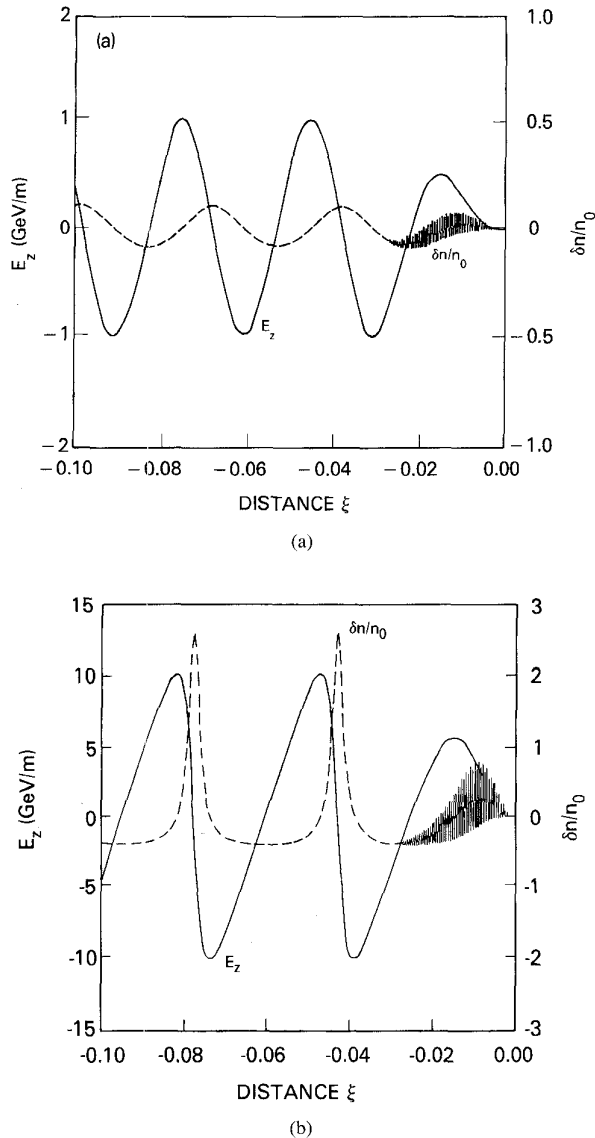


Fig. 2. Density variation  $\delta n/n_0 = n/n_0 - 1$  and axial electric field  $E_z$  in an LWFA driven by a laser pulse located in the region  $-L \leq \zeta \leq 0$  (the pulse is moving to the right), where  $L = \lambda_p = 0.03 \text{ cm}$ , for (a)  $a_0 = 0.5$  and (b)  $a_0 = 2.0$  (from [88]).

Hence, the driver (i.e., the laser beat wave) becomes out of phase with the nonlinear plasma wave. This leads to saturation of the plasma wave amplitude in the PBWA [53], [55], [62], [63]. Alternatively, if the plasma wave is to be driven to large amplitudes a series of individual pulses (laser pulses or electron bunches), the change in the nonlinear plasma period can affect the optimal spacing between pulses as well as the optimal duration of the pulses [119], [120].

The increase in the plasma wavelength with increasing wave amplitude has an additional effect on nonlinear plasma waves in two dimensions. Consider a plasma wave which is driven more strongly on axis than it is off axis. This would be the case in a laser-driven accelerator, where the laser intensity peaks on axis and typically has a Gaussian radial profile. On axis, the plasma wave amplitude is maximum and, in the

nonlinear regime, the plasma wavelength on axis is larger than it is off-axis. Thus, the plasma wavelength varies as a function of radius  $\lambda_{Np}(r)$ . This causes the wavefronts of the plasma wave to become curved and take on a "horseshoe" shape [52], [63]. For a plasma wave of fixed amplitude, the farther back within the plasma wave train, the more curved the plasma wave front, i.e., after  $\ell$  periods, the phase front at large radii is located at  $\ell\lambda_p$ , whereas on axis, the phase front is located at  $\ell\lambda_{Np}(r=0)$ . The plasma wave fronts can also become distorted due to distortions which develop in the laser intensity profile [115]. These effects have been observed in 2-D nonlinear fluid simulations [96], [97], [110], and 2-D particle simulations [115], [116].

### C. Electron Acceleration and Detuning

An electron can be accelerated along the  $z$ -axis by an electrostatic plasma wave of the form  $E_z = E_{\max} \sin \omega_p(z/v_p - t)$ . As the electron is accelerated, its velocity  $v_z$  will increase and approach the speed of light,  $v_z \rightarrow c$ . If the phase velocity of the plasma wave is constant with  $v_p < c$ , the electrons will eventually outrun the plasma wave and move into a phase region of the plasma wave which is decelerating. This limits the energy gain of the electron in the plasma wave and is commonly referred to as electron phase detuning. The detuning length  $L_d$  is defined as the length the electron must travel before it phase slips by one-half of a period with respect to the plasma wave. For a highly relativistic electron,  $v_e \simeq c$ , the detuning time  $t_d$  is given by  $\omega_p(c/v_p - 1)t_d = \pi$ , i.e.,  $L_d = ct_d \simeq \gamma_p^2 \lambda_p$ , assuming  $\gamma_p \gg 1$ . The maximum energy gain after a detuning length [1], [52], [58] is given approximately by  $W_{\max} \simeq eE_{\max}L_d \simeq 2\pi\gamma_p^2(E_{\max}/E_0)m_ec^2$ .

In a 1-D plasma wave, electron trapping, acceleration, and detuning can be studied by examining the electron orbits in phase space  $(\gamma, \psi)$ , where  $\gamma = (1 - v_z^2/c^2)^{1/2}$  is the electron energy. In the linear regime, the plasma wave is described by a sinusoidal electrostatic potential  $\phi = \phi_0 \cos \psi$ , where  $\phi_0 = \hat{E}_{\max}/k_p$  is the amplitude and  $\psi = k_p(z - v_p t)$  is the phase. The phase region  $-\pi < \psi < 0$  is accelerating. Consider an electron injected into the plasma wave with  $v_z < v_p$  at  $\psi = 0$ . Initially, the electron is slipping backward with respect to the plasma wave. If the initial electron velocity is too low, the electron does not gain sufficient energy and  $v_z < v_p$  at  $\psi = -\pi$ . Hence, the electron would be untrapped and would continue to slip backward through the plasma wave. If, however, the electron has a sufficiently high initial velocity such that  $v_z > v_p$  as the electron approaches  $\psi \rightarrow -\pi$ , the electron will be trapped and execute closed orbits in the  $-\pi < \psi < \pi$  phase region.

An important characteristic of phase space is the separatrix, which is the orbit that separates the region of trapped and untrapped electrons in phase space, as shown schematically in Fig. 3 for a small amplitude, sinusoidal plasma wave. The separatrix corresponds to the orbit of an electron injected at  $\psi = 0$  with the precise initial velocity  $v_z = v_{\min} < v_p$  to give  $v_z = v_p$  at  $\psi = -\pi$ . The minimum energy necessary to trap an electron  $\gamma_{\min}$  (sometimes referred to as the minimum injection energy) and the maximum energy of a trapped electron  $\gamma_{\max}$

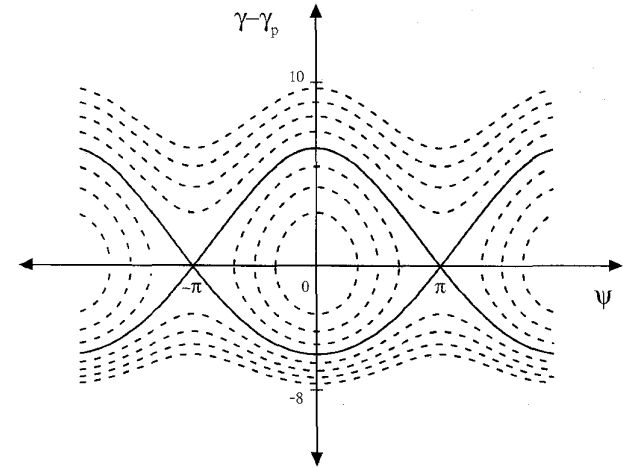


Fig. 3. Single particle orbits in phase space  $(\gamma, \psi)$  for an electron in a small amplitude, sinusoidal plasma wave with a normalized potential given by  $\phi = \phi_0 \cos \psi$  with  $\gamma_p = 20$  and  $\phi_0 = 10^{-3}$ . Within the separatrix (solid curve) the orbits are closed and the particles trapped.

occur at the phase  $\psi = 0$  for an electron which lies on a trapped orbit just inside the separatrix.

The motion of a test electron in a 1-D nonlinear plasma wave can be studied by solving the equations  $d\gamma/d\hat{z} = \partial\phi/\partial\psi$  and  $d\psi/d\hat{z} = 1 - \beta_p/\beta$  along with the nonlinear Poisson equation, (12). Here,  $\gamma = (1 - \beta^2)^{-1/2}$  is the relativistic factor of the electron,  $\beta = v_z/c$ ,  $\beta_p = v_p/c$ ,  $\hat{z} = k_p z$ , and  $\psi = k_p \zeta = k_p(z - v_p t)$  is the phase of the electron relative to that of the plasma wave. The test electron motion in the plasma wave is described by the Hamiltonian [129]

$$H(\gamma, \psi) = \gamma(1 - \beta\beta_p) - \phi(\psi) \quad (20)$$

where  $H(\gamma, \psi) = \text{constant}$  along a given electron orbit and  $\phi = \phi(\psi)$  is the solution to (12), which oscillates between  $\phi_{\min} \leq \phi \leq \phi_{\max}$ . In particular, the separatrix  $\gamma_s(\psi)$  characterizing the test electron orbits in  $(\gamma, \psi)$  phase space is given by  $H(\gamma_s, \psi) = H(\gamma_p, \psi_{\min})$ , where  $\phi(\psi_{\min}) = \phi_{\min}$ .

Fig. 4 shows several separatrices for  $\gamma_p = 20$  and for different values of the plasma wave amplitude, characterized by the parameter  $\epsilon$ , where  $\phi_{\max} = (2\gamma_p^2 - 1)\epsilon/\gamma_p - 1$ , for  $\epsilon = 0.03, 0.04, 0.1, 0.3$ , and  $0.9$  ( $\epsilon = 1$  corresponds to wavebreaking). This corresponds to values of the peak electric field  $E_{\max}$  given by  $E_{\max}/E_0 = 0.18, 0.47, 1.5, 3.2$ , and  $5.8$ , respectively (at wavebreaking,  $E_{WB}/E_0 = 6.2$ ). The value  $\epsilon = 0.03$  corresponds to the innermost curve and  $\epsilon = 0.9$  corresponds to the outermost curve. These curves were obtained [129] by plotting  $H(\gamma_s, \psi) = H(\gamma_p, \psi_{\min})$  after numerically solving (12) for  $\phi = \phi(\psi)$  with the initial conditions  $\partial\phi/\partial\zeta = 0$  and  $\phi = \phi_{\max}$  at  $\psi = 0$ . The width of the separatrix  $\Delta\psi_s$  corresponds to the nonlinear plasma wavelength,  $\lambda_{Np} = \Delta\psi_s/k_p$ , given by (19). As the plasma wave amplitude increases, the nonlinear wavelength increases.

For small wave amplitudes, e.g.,  $\epsilon = 0.03$ , the separatrix is nearly symmetric (as would be the case for a linear sinusoidal plasma wave). Notice that for  $\epsilon = 0.03$ ,  $\gamma_{\min} > 1$ , indicating that an electron injected with  $v = v_{\min} > 0$  at  $\psi = 0$  would be trapped, where  $v_{\min} = c(1 - \gamma_{\min}^{-2})^{1/2}$ . As the wave amplitude

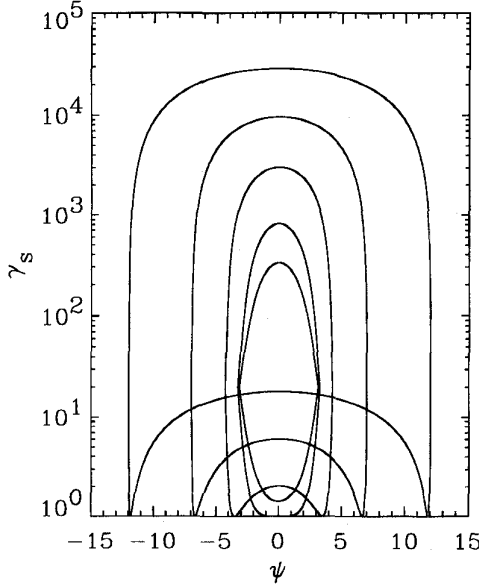


Fig. 4. The separatrix  $\gamma_s(\psi)$  plotted for several values of the plasma wave amplitude,  $\epsilon = 0.03, 0.04, 0.1, 0.3$ , and  $0.9$  ( $\epsilon = 1$  corresponds to wavebreaking), where  $\phi_{\max} = \epsilon(2\gamma_p^2 - 1)/\gamma_p - 1$ , with  $\gamma_p = 20$ . The value  $\epsilon = 0.03$  corresponds to the innermost curve and  $\epsilon = 0.9$  corresponds to the outermost curve (from [129]).

increases,  $\gamma_{\min}$  decreases to the point  $\gamma_{\min} = 1$ , corresponding approximately to the curve  $\epsilon = 0.04$  in Fig. 4. Hence, a test electron which is at rest at  $\psi = 0$  would be trapped. This does not mean that the background plasma electrons will be trapped. The background electrons are undergoing a plasma wave fluid oscillation and, at the phase  $\psi = 0$ , are flowing backward (opposite to  $v_p$ ) with the maximum fluid velocity. Increasing  $\epsilon$  further causes  $\gamma_{\min}$  (at  $\psi = 0$ ) to increase. This implies that a test electron at  $\psi = 0$  with  $v = -|v_{\min}|$  would be trapped. Further increasing  $\epsilon$  causes  $v_{\min}$  to become more negative. Wavebreaking occurs when  $\epsilon = 1$ , at which point  $\gamma_{\min} = \gamma_p$ ,  $v_{\min} = -v_p$  and, hence, all of the plasma electrons become trapped in the wave.

The maximum energy  $\gamma_{\max}$  and minimum energy  $\gamma_{\min}$ , denoted by  $\gamma_m$ , for an electron on the separatrix are given by [129]

$$\gamma_m = \gamma_p(1 + \gamma_p \Delta\phi) \pm \gamma_p \beta_p [(1 + \gamma_p \Delta\phi)^2 - 1]^{1/2} \quad (21)$$

where  $\Delta\phi = \phi_{\max} - \phi_{\min}$ , i.e.,  $\Delta\phi = 2\beta_p[(1 + \hat{E}_{\max}^2/2)^2 - 1]^{1/2}$ , as indicated by (18). In the limits  $\gamma_p \Delta\phi \gg 1$  and  $\gamma_p^2 \gg 1$ ,  $\gamma_{\max} \simeq 2\Delta\phi\gamma_p^2$  and  $\gamma_{\min} \simeq \Delta\phi/2 + 1/2\Delta\phi$ . In particular, the maximum energy of a trapped electron is given by [129]

$$\gamma_{\max} \simeq 2\gamma_p^2 \begin{cases} 2\hat{E}_{\max}, & \text{for } 2 \gg \hat{E}_{\max}^2 \gg 1/4\gamma_p^2 \\ \hat{E}_{\max}^2, & \text{for } \hat{E}_{\max}^2 \gg 2 \end{cases} \quad (22)$$

where  $\hat{E}_{\max} = E_{\max}/E_0$ . The limit  $\hat{E}_{\max}^2 \ll 2$  corresponds to the well-known limit for linear sinusoidal plasma waves [1], [52], [58], [132]–[134]. When  $\hat{E}_{\max}^2 \gg 2$ , however,  $\gamma_{\max} \simeq 2\gamma_p^2 \hat{E}_{\max}^2$ , which implies that higher electron energies can be obtained for electrons trapped in nonlinear plasma waves. The nonlinear regime where  $\hat{E}_{\max} > 1$  has been observed in simulations of the nonlinear plasma wakefield accelerator

[46]–[49], the self-modulated LWFA [110], [115], [116], and laser wakefields driven by multiple pulses [118]–[122]. At wavebreaking ( $\epsilon = 1$ ,  $E_{\max} = E_{\text{WB}}$ ), (21) indicates that [129]  $\gamma_{\max} = 4\gamma_p^3 - 3\gamma_p$ .

A rough estimate for the detuning length is given by  $W_{\max} = m_e c^2 \gamma_{\max} = e E_{\max} L_d$ . This gives

$$L_d = \gamma_p^2 \lambda_{Np} \begin{cases} 2/\pi, & \hat{E}_{\max} \ll 1 \\ 1/2, & \hat{E}_{\max} \gg 1 \end{cases} \quad (23)$$

where  $\lambda_{Np}$  is given by (19). Determination of the actual detuning length [132] requires a simultaneous solution of the equations of motion and (12).

As an example, consider an LWFA with  $n_0 = 2.8 \times 10^{18} \text{ cm}^{-3}$ ,  $\gamma_g \simeq 20$ , and  $E_0 \simeq 160 \text{ GV/m}$ . In the limit  $\hat{E}_{\max}^2 \gg 2$ , (22) gives  $\gamma_{\max} \simeq 800 \hat{E}_{\max}^2$ . At wavebreaking,  $E_{\text{WB}} \simeq 6.2 E_0$  and  $W_{\max} \simeq 16 \text{ GeV}$ . Furthermore, notice that (16) and (22) imply  $\gamma_{\max} \simeq 4\gamma_p^3 (E_{\max}/E_{\text{WB}})^2$ , where  $\gamma_p^2 \gg 1$  and  $\gamma_p (E_{\max}/E_{\text{WB}})^2 \gg 1$  have been assumed. Hence, for a fixed value of  $E_{\max}/E_{\text{WB}}$ ,  $\gamma_{\max} \sim \gamma_p^3 \sim n_0^{-3/2}$  and the single-stage energy gain can be enhanced by operating at lower densities.

It should be noted that the above results are obtained from 1-D theory and assume a constant amplitude plasma wave. An evolving plasma wave amplitude and 2-D effects could alter these results [133], [134]. For example, Mora [134] has shown that the effects of laser diffraction can lead to a more restrictive trapping condition for linear plasma waves.

#### D. Plasma Wave Phase Velocity

The phase velocity of the plasma wave is important for determining the minimum injection energy, the maximum energy gain, and the detuning length. Neglecting the evolution of the drive beam as it propagates, the phase velocity of the plasma wave is equal to the phase velocity of the drive beam. For the plasma wakefield accelerator, the phase velocity is equal to the velocity of the drive electron beam,  $v_p = v_b$ . For laser-driven wakefields, the phase velocity is equal to the group velocity of the laser,  $v_p = v_g$ .

In the linear regime, the group velocity of a laser pulse in a plasma can be determined from the 1-D dispersion relation,  $\omega^2 = c^2 k^2 + \omega_p^2$ . This gives  $v_g = c(1 - \omega_p^2/c^2)^{1/2}$  and  $\gamma_g = (1 - v_g^2/c^2)^{-1/2} = \omega/\omega_p$ . Nonlinear corrections to the group velocity in 1-D have recently been analyzed by Decker and Mori [135]. In the limit  $\omega_p/\omega \ll 1$ , the leading order correction is found by replacing  $\omega_p^2$  with its relativistic value,  $\omega_p^2/\gamma_{\perp}$ , where  $\gamma_{\perp} = (1 + a_0^2/2)^{1/2}$  is the relativistic factor associated with the quiver motion of the electrons in the laser field.

The group velocity of a laser pulse is also reduced by 3-D effects. For example, consider a laser pulse in vacuum undergoing Rayleigh diffraction. The evolution of the spot size (or radius) of a Gaussian laser beam evolves according to  $r_s = r_0(1 + z^2/Z_R^2)^{1/2}$ , where  $r_0$  is the minimum spot size at the focal point  $z = 0$  and  $Z_R = kr_0^2/2$  is the Rayleigh length. In effect, the photons are traveling at approximately a diffraction angle  $\theta_d = r_0/Z_R$  with respect to the  $z$ -axis. Hence, the axial group velocity is reduced by  $v_g \simeq c \cos \theta_d \simeq c(1 - \theta_d^2/2)$ . A more detailed calculation indicates that, in the linear regime,

the 3-D group velocity is given by [136]

$$\gamma_g \simeq (\omega_p^2/\omega^2 + 2c^2/\omega^2 r_0^2)^{-1/2}. \quad (24)$$

In effect, the linear 3-D dispersion relation is given by  $\omega^2 - c^2 k^2 = \omega_p^2 + 2c^2/r_0^2$ . For tightly focused laser pulses, this 3-D correction can significantly limit the group velocity. As an example, consider a laser pulse with a  $\lambda = 1 \mu\text{m}$  wavelength, a  $r_0 = 10 \mu\text{m}$  spot size, propagating in a plasma of density  $n = 10^{16} \text{ cm}^{-3}$ . In 1-D,  $\gamma_g \simeq 330$ , however, the finite spot size reduces the group velocity such that  $\gamma_g \simeq 44$ .

Distortions of the pulse driving the plasma wave can also affect the plasma wave phase velocity. In the LWFA in the 1-D limit, it has been shown that the wake phase velocity is approximately equal to the group velocity associated with the position of the peak of intensity profile [135], [137]. Furthermore, the plasma wave can lead to locally enhanced diffraction and focusing, which distorts the pulse profile and reduces the plasma wave phase velocity [138], [139].

#### E. Photon Acceleration

In addition to accelerating electrons, a plasma wave can be used to upshift the frequency of a properly phased low-intensity short laser pulse (often referred to as photon acceleration) [140]–[142], as shown schematically in Fig. 5. Consider a plasma wave with an electron density perturbation of the form  $\delta n = -\delta n_0 \sin k_p \zeta$ , where  $\zeta = z - ct$ , and a low intensity, “witness” laser pulse centered about  $\zeta = 0$  with a pulse length  $L \ll \lambda_p$ . The local density at the front of the pulse,  $n(\zeta = L/2)$ , will be less than that at the back of the pulse,  $n(\zeta = -L/2)$ . Since the local phase velocity is given by  $\beta_p = v_p/c \simeq 1 + \omega_p^2(\zeta)/2\omega^2$ , where  $\omega_p^2(\zeta) \sim n(\zeta)$ , the phase velocity at the pulse front is less than that at the back of the pulse, i.e.,  $v_p(L/2) < v_p(-L/2)$ . Hence, the phase peaks at the back move faster than those at the front and the pulse wavelength decreases (the pulse frequency increases). For small shifts, the laser wavelength will evolve according to  $\lambda \simeq \lambda_0 + z\Delta\beta_p$ , where  $\Delta\beta_p = \lambda_0 d\beta_p/d\zeta < 0$  is the difference in phase velocity between adjacent phase peaks,  $z$  is the propagation distance, and  $\lambda_0 = 2\pi c/\omega_0$  is the initial laser wavelength. Hence, the frequency shift is given by  $\omega/\omega_0 \simeq 1 - zd\beta_p/d\zeta$ , where  $d\beta_p/d\zeta \simeq (\omega_p^2/2\omega_0^2)d(\delta n/n_0)/d\zeta$ . A more detailed calculation indicates that the frequency will be upshifted according to [141]

$$\frac{\omega}{\omega_0} \simeq \left( 1 + \frac{\omega_p^2}{\omega_0^2} \frac{\delta n_0}{n_0} k_p z \cos k_p \zeta \right)^{1/2} \quad (25)$$

where nonlinear effects and phase slippage between the laser pulse and plasma wave (i.e., detuning) [142] have been neglected.

Typically, the plasma wave induced frequency shifts are small. For example, consider a laser with  $\lambda = 1 \mu\text{m}$  and  $r_0 = 30 \mu\text{m}$ , propagating in a plasma of density  $n_0 = 10^{18} \text{ cm}^{-3}$  ( $\lambda_p = 30 \mu\text{m}$ ). After propagating one Rayleigh length,  $z = Z_R$ ,  $\omega/\omega_0 \simeq 1 + \delta n_0/3n_0$ . Small frequency shifts, however, can be detected and this process can be useful for diagnosing the wakefield [106], [107], [143]. Large frequency

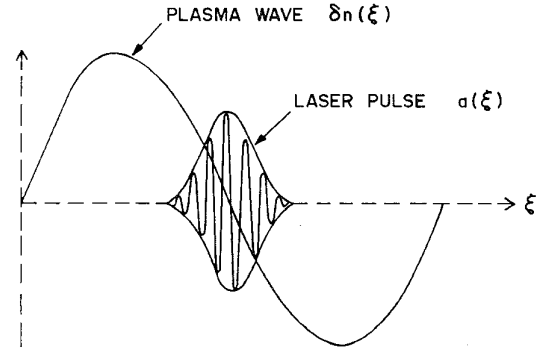


Fig. 5. Schematic of laser pulse frequency upshifting by a plasma wave with  $v_p \simeq v_g \simeq c$  (the pulse is moving to the right). Positive shifts require the laser pulse to be centered about regions of the wave with a decreasing density (from [141]).

shifts require long propagation distances and large plasma wave amplitudes. For example, after one electron detuning length  $L_d = \lambda_p \omega^2/\omega_p^2$ ,  $\omega/\omega_0 = (1 + 2\pi\delta n_0/n_0)^{1/2}$ .

#### IV. PLASMA WAKEFIELD ACCELERATOR

In the plasma wakefield accelerator (PWFA), plasma waves are excited by the space-charge force of the drive electron beam [19]–[24], [38]–[51]. An electron beam propagating into a plasma will displace plasma electrons. Provided that the electron beam terminates in a time  $\tau_f$  short compared to the plasma period,  $\tau_f \omega_p < 1$ , the electron beam will excite a plasma wave. Electron acceleration in the PWFA has been observed in several experiments [19]–[24], as mentioned in Section I. In addition, PWFA experiments are being pursued at several laboratories [144]–[146].

##### A. Linear Regime

In the linear regime, the amplitude of the plasma wave can be estimated from Poisson's equation  $\nabla \cdot \mathbf{E} = -4\pi e n_b$ , along with the assumptions that the electron beam radius  $r_b$  is large compared to a plasma wavelength  $r_b k_p \gg 1$ , the beam is relativistic  $v_z \simeq c$ , and  $E_z \sim \exp ik_p(z - ct)$ . This gives a maximum wakefield amplitude of  $k_p E_{\max} = 4\pi e n_b$ , or

$$E_{\max}/E_0 = n_b/n_0. \quad (26)$$

More rigorously, this result can be derived from 3-D linear fluid theory ( $n_b/n_0 \ll 1$ ) via (8) assuming  $\tau_f \omega_p < 1$  and  $k_p r_b \gg 1$ . The transverse profile of the wake can be calculated for various transverse beam profiles. For a flat transverse beam profile out to a radius  $r_b$ , the amplitude of the axial wakefield is given by  $E_z/E_0 = (n_b/n_0) F_R(r)$ , where the radial profile function is given by [43], [44], [125], [126]

$$F_R(r) = \begin{cases} 1 - k_p r_b K_1(k_p r_b) I_0(k_p r), & \text{for } r < r_b \\ k_p r_b I_1(k_p r_b) K_0(k_p r), & \text{for } r > r_b \end{cases} \quad (27)$$

where  $K_{0,1}$  and  $I_{0,1}$  are modified Bessel functions. Along the axis,  $F_R(0) \simeq 1$  for  $k_p r_b \gg 1$ , which is the 1-D limit. For a narrow beam,  $k_p r_b \ll 1$ , the axial electric field at  $r = 0$  will be reduced by the amount  $F_R(0) \simeq k_p^2 r_b^2 [\gamma_e + \ln(k_p r_b/2)]$ , where  $\gamma_e \simeq 0.577$  is Euler's constant.

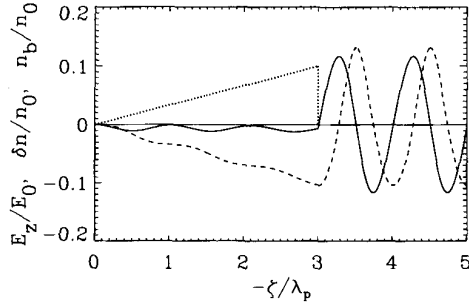


Fig. 6. Electron beam density  $n_b$  (dotted line), plasma electron density response  $\delta n$  (dashed line), and electric field  $E_z$  (solid line) plotted versus  $\zeta$ , from numerical solution of (13). In the plot, the beam is moving to the left and  $E_z > 0$  is accelerating. The plot shows  $R = 9.7$  in good agreement with linear theory:  $R = \pi N_b \simeq 9.4$ .

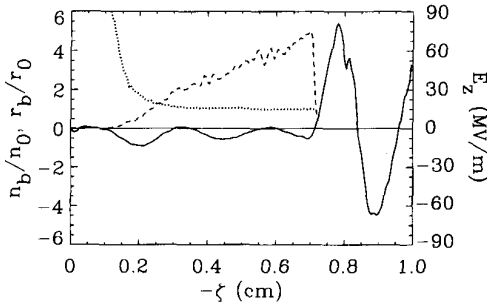


Fig. 7. Beam density on axis  $n_b$  (dashed line), beam radius  $r_b$  (dotted line), and electric field on axis  $E_z$  (solid line) plotted versus  $\zeta$  at  $c\tau = 5$  cm. The portion of the beam where  $n_b > n_0$  is in an equilibrium state with  $r_b = 41 \mu\text{m}$ , in agreement with (29). The plot shows  $R = 5.8$  (from [51]).

One limitation to the wakefield amplitude is the density of the drive beam. Typically,  $n_b < 10^{14} \text{ cm}^{-3}$ . For example, an electron beam with a peak current  $I_b = 100 \text{ A}$  and a radius of  $r_b = 100 \mu\text{m}$  has a density  $n_b \simeq 7 \times 10^{13} \text{ cm}^{-3}$ . Hence, assuming  $n_b = 10^{14} \text{ cm}^{-3}$  and  $n_b \lesssim n_0$  implies  $E_z \lesssim 1 \text{ GV/m}$ .

The energy gain in the PWFA is also limited by the transformer ratio  $R_t$ , which is the ratio of the electron energy gained in the wakefield to the initial drive beam energy,  $R_t = \Delta\gamma/\gamma_b$ . As the drive beam propagates through the plasma, it will experience a decelerating electric field  $E_-$  due to the wake induced within the drive beam. This implies that the drive beam will lose all of its energy after propagating a depletion length given roughly by  $L_{dp} \simeq \gamma_b m_e c^2/eE_-$ . After propagating a distance  $L_{dp}$ , the energy gain of an electron in the wakefield is given by  $\Delta\gamma m_e c^2 \simeq eE_+ L_{dp}$ , where  $E_+$  denotes the accelerating field of the wake behind the drive beam. Hence, the transformer ratio is defined as  $R_t = E_+/E_-$ . For an axially symmetric drive beam, Ruth *et al.* [40] have shown that  $R_t \leq 2$ , i.e., the maximum energy gain for a symmetric drive beam is twice the energy of the drive beam.

One possible method for increasing the wakefield amplitude is to use multiple electron bunches to drive the wake [22]–[24], [38]–[40]. For a series of  $M_b$  short bunches separated by a distance  $\lambda_p$ , linear theory predicts that wakefield amplitude will be enhanced by the factor  $M_b$ , i.e.,  $E_z/E_0 = M_b n_b/n_0$ , assuming  $E_z/E_0 \ll 1$ . Ruth *et al.* [40], however, have shown

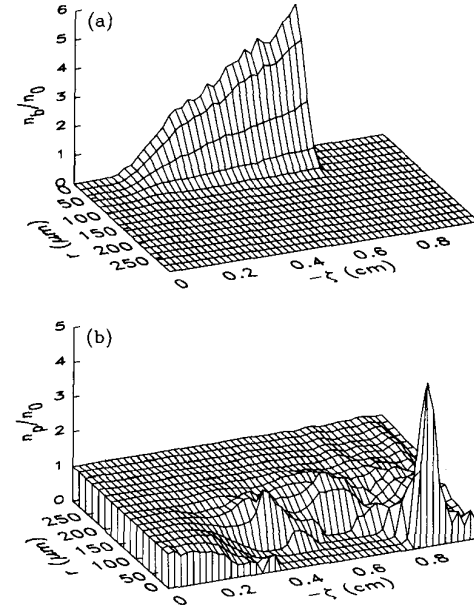


Fig. 8. (a) Beam density  $n_b$  and (b) plasma electron density  $n_p$  plotted at  $c\tau = 5$  cm for the simulation of Fig. 7. In (b) the radial direction is reversed relative to (a). The plot shows a region of complete evacuation (blowout) of the plasma electrons (from [51]).

that, under idealized conditions, the transformer ratio is at best enhanced by the square root of this factor,  $R_t \leq 2\sqrt{M_b}$ .

The transformer ratio can also be increased by properly tailoring the axial profile of a single driving electron beam, as suggested by Chen *et al.* [41]. For example, consider a triangular-shaped beam which has a linear rise over a length  $L_b = N_b \lambda_p$  with  $N_b > 1$  followed by a rapid termination over a length  $L_f \ll \lambda_p$ . In this case the transformer ratio is  $R_t \simeq \pi N_b$ . An example is shown in Fig. 6, where the beam density, plasma density, and electric field are plotted for a 1-D triangular-shaped electron beam with  $n_{b,\text{peak}} = 0.1 n_0$  and  $N_b = 3$ . Fig. 6 was obtained by numerically solving (13) (with  $a^2 = 0$ ) and indicates a transformer ratio  $R_t = 9.7$ , in good agreement with linear theory.

Recently, 2-D axisymmetric particle simulations were used [51] to demonstrate that  $R_t \simeq \pi N_b$  can hold in a regime where  $n_b > n_0$  (but with  $E_z/E_0 \ll 1$ ), as shown in Figs. 7 and 8. In this example, a triangular-shaped electron beam was injected into a plasma of density  $n_0 = 2.0 \times 10^{14} \text{ cm}^{-3}$  ( $\lambda_p = 0.24 \text{ cm}$ ). Initially, the beam has energy 20 MeV ( $\gamma_b = 40$ ), charge  $Q = 3.0 \text{ nC}$  (peak current  $I_{b0} = 2Q\beta c/L_b = 250 \text{ A}$ ), and peak density  $n_{b,\text{peak}}/n_0 = 5$ .

Fig. 7 shows the beam density on axis  $n_b$  and electric field on axis  $E_z$  plotted versus  $\zeta$  after  $c\tau = 5$  cm of propagation. A transformer ratio  $R_t = 5.8 < \pi N_b \simeq 7.2$  is observable. The reduced value of  $R_t$  can be attributed to the fact that, after 5 cm of propagation, the beam no longer has a precise triangular shape (details of the propagation in this case will be discussed below). Fig. 8 shows surface plots of  $n_b$  and plasma electron density  $n_p$  at  $c\tau = 5$  cm (as in Fig. 7). In this nonlinear case, generation of the wakefield is dominated by the radial motion of the plasma electrons, which are completely evacuated from the axis within the beam.

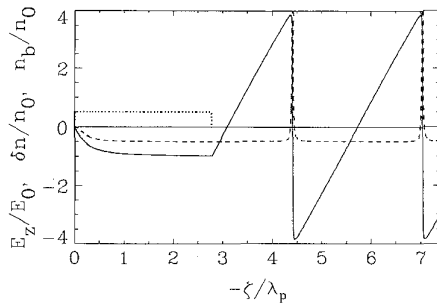


Fig. 9. Beam density  $n_b$  (dotted line), plasma electron density response  $\delta n$  (dashed line), and electric field  $E_z$  (solid line) plotted versus  $\zeta$ , from a numerical solution of (13). The plot shows  $R = 4.0$  in excellent agreement with nonlinear theory (see [46, Fig. 1]) and 1-D simulation (see [49, Fig. 6]).

Note that, with a more precisely chosen pulse shape, such as the “door-step” pulse of [41], the transformer ratio can be increased to  $R_t \simeq 2\pi N_b$ . In either case, large energy gains can be achieved when  $N_b \gg 1$ . Specifically, in the absence of electron detuning, the energy gain is  $\Delta\gamma = R_t\gamma_b$ . Katsouleas [42] showed that detuning can reduce the energy gain, i.e.,  $\Delta\gamma/\gamma_b \lesssim R_t/(1 + R_t n_0/\pi\gamma_b n_b)$ . In practice, the energy gain can also be limited by electron beam–plasma instabilities, such as the two-stream and electron–hose instabilities [147]–[150].

### B. Nonlinear Regime

The wakefield amplitude and transformer ratio in the PWFA can be enhanced by operating in the nonlinear regime  $n_b \sim n_0$ . In the 1-D nonlinear regime, analytical solutions exist to (12) for drive beams with square axial profiles. Rosenzweig [46] described an “optimal” 1-D nonlinear PWFA in which  $n_b = n_0/2$ . For this case, a square drive beam of length  $N_b = L_b/\lambda_p$  would generate a nonlinear plasma wave of amplitude  $E_+ = \sqrt{2\pi N_b} E_0$  with a corresponding transform ratio  $R_t \simeq \sqrt{2\pi N_b}$ , assuming  $2\pi N_b \gg 1$ . An example is shown in Fig. 9, where a 1-D square pulse with  $n_b = n_0/2$  and length  $L_b = 2.79\lambda_p$  produces a wake with  $R_t = 4$ . This is in agreement with theory [46] and 1-D simulations [49]. In the simulation, however, the wave breaks after the first oscillation.

Rosenzweig *et al.* [48] also described a 2-D nonlinear “blowout” or “ion-focused” regime [151] of the PWFA. In this regime  $r_b k_p < 1$ ,  $n_b/n_0 > 1$ , and the wakefield is dominated by highly nonlinear transverse plasma motion. Since  $n_b/n_0 > 1$ , essentially all of the plasma electrons can be blown out of the region of the drive beam. (A similar regime can be obtained in the LWFA by using a tightly focused ultra-intense laser pulse [96], [115].) Immediately behind the drive beam, the wake is characterized by an accelerating field which is constant as a function of radius and varies linearly as a function of  $\zeta$ , and an electrostatic focusing field which is linear as a function of radius. Because the focusing forces in the wakefield are linear, the emittance of a short electron bunch will be preserved as it is transported and accelerated by the wakefield. Due to the highly nonlinear nature of the wake, however, the wake may be destroyed (i.e., break) after a single oscillation. An example [51] of this regime is provided by Figs. 7 and 8. In Fig. 7, the linear variation in  $E_z(\zeta)$  is observable at  $-\zeta =$

0.72 cm. In this example, ion focusing is also used to focus and transport the primary beam, as discussed in the following section.

### C. Primary Beam Propagation

Issues of particular importance in the PWFA are the equilibrium state and the stability of the primary beam as it propagates through the plasma. Typically, the secondary beam has lower current and higher energy, relative to the primary beam, resulting in lower growth for most beam–plasma instabilities. In addition, the secondary beam is strongly focused by the plasma wave. The primary beam, however, is subject to a number of instabilities, particularly the Weibel instability [147], the transverse two-stream (TTS) instability [42], [148], and the electron–hose (EH) instability [149]. The longitudinal two-stream instability has also been considered [41], [42], [45], but is of less interest because it grows more slowly than TTS.

The equilibrium state of the driving beam is characterized by a balance between the spreading of the beam due to its emittance (transverse temperature) and the focusing of the beam by the plasma. Without the plasma, the beam self-electric and magnetic fields cancel for  $\gamma_b \gg 1$ , and the emittance of the beam causes it to spread. For  $n_b < n_0$ , the plasma electrons neutralize the space–charge field of the beam. In this case, the focusing force is provided by the self-magnetic field of the beam. For  $r_b < c/\omega_p$ , the equilibrium radius  $R_{eq}$  is given implicitly by [51]

$$R_{eq}^2 = \frac{4m_e c^3 \epsilon_{n,rms}^2}{\beta \gamma_b e I_b} \left\{ 1 - 2R_{eq}^2 k_p^2 \left[ 1 - \exp(-k_p^{-2} R_{eq}^{-2}) \right] \right\}^{-1} \quad (28)$$

where  $I_b$  is the beam current,  $\beta$  is the normalized beam velocity, and  $\epsilon_{n,rms}$  is the normalized rms emittance [152]. For  $n_b > n_0$ , the plasma electrons are expelled from the region of the beam and the focusing force is provided by the plasma ions. For  $r_b < c/\omega_p$  and  $\gamma_b \gg 1$  [51]

$$R_{eq} = \left( 8 \frac{\epsilon_{n,rms}^2}{\gamma_b k_p^2} \right)^{1/4}. \quad (29)$$

A number of simulations, each of which were initialized with a cold beam (emittance = 0) in a nonequilibrium state with  $n_b < n_0$  and  $r_b < c/\omega_p$ , showed pinching of the beam and evolution toward an equilibrium as the beam emittance grew via phase-mixing [42], [44], [45]. More recently [51], (28) and (29) were verified in 2-D axisymmetric particle simulations, including the example given in Figs. 7 and 8 above. In that case, the beam is radially matched with initial radius  $r_b = R_{eq} = 41 \mu\text{m}$ , as determined from (29). Fig. 7 shows the beam radius  $r_b$  plotted versus  $\zeta$  after  $c\tau = 5 \text{ cm}$  of propagation. The beam remains in an equilibrium state with  $r_b = R_{eq}$  over most of the beam, where  $n_b > n_0$ . The head of the beam, where  $n_b < n_0$ , is not focused.

The Weibel instability [147], which causes filamentation of the beam in the regime where  $n_b < n_0$  and  $r_b > c/\omega_p$ , has been observed in simulations by Keinigs and Jones [44] and Su *et al.* [45]. Operating in the Weibel-unstable regime has the advantage that, by having a very broad pulse, it may be

possible to obtain a wakefield with linear transverse focusing, which preserves the emittance of the accelerated electron beam [45]. In this regime, it may also be possible to maintain stability in the primary beam with a sufficiently large emittance [45].

The TTS and EH instabilities can occur for  $L_b > \lambda_p$ , where  $L_b$  is the beam length. In the PWFA, a typical case where  $L_b > \lambda_p$  is a triangular-shaped electron beam with  $N_b > 1$ , as discussed in Section III-A. Theoretical estimates for TTS suggest that it may be a severe limitation on the propagation distance [41], [42], [148]. Because the TTS wavelength is a function of the beam density, however, it can be stabilized by a sufficiently strong ramp-up in the beam density. Based on this approach, limits on the useful beam length and transformer ratio can be estimated [42].

Simulations using 2-D Cartesian geometry [42] did not clearly show TTS. These simulations, however, were initialized with a cold beam, which developed emittance and evolved toward an equilibrium state throughout the simulation. In a later study, using a 3-D particle code, the beam was initialized in an approximate equilibrium state and the growth of TTS was observed, with results that were consistent with theory [51].

The EH instability [149] occurs in the regime where the plasma electrons have been expelled from the region of the beam by the beam space charge, leaving a bare ion column. In this equilibrium state, the ion column is surrounded by a “wall” of plasma at the charge-neutralization radius  $r_n = (n_b/n_0)^{1/2}r_b$ . When the beam suffers a small transverse displacement, the plasma electrons at  $r = r_n$  are also displaced in such a way that the interaction is unstable. Note that the PWFA corresponds to the “short pulse limit” of [149], where asymptotic expressions are given for the growth of the EH instability for several plasma density profiles versus radius. For the PWFA, where the plasma density is uniform, the number of  $e$ -foldings at a position  $-\zeta = ct - z$  within the beam and as a function of the propagation distance  $z$  is given by [149]

$$N_e = \pi(3/2)^{3/2}\gamma_b^{-1/6}\lambda_p^{-1}z^{1/3}|\zeta|^{2/3} \quad (30)$$

where  $\gamma_b \gg 1$  was assumed. As discussed in Section III-B above, the  $n_b > n_0$  regime has the advantage of linearly focusing transverse wakefields [48].

It is important to note that the EH growth rate and frequencies are independent of the beam density such that the variation in beam density along the length of the beam does not affect the growth of the instability. Also, the instability is absolute, with exponential growth within the beam at any fixed position relative to the head of the beam. This is a result of the linear focusing force of the ion channel, which does not allow phase mixing of the beam electron trajectories. Thus, EH imposes a more severe restriction on beam propagation than TTS. The growth of the EH instability is illustrated in Fig. 10, which shows the results of a 3-D simulation [51] with parameters identical to those of Figs. 7 and 8. In Fig. 10, the simulation particles are projected onto the  $(x, \zeta)$  plane at  $c\tau = 0, 5$ , and  $10$  cm. The variation in the density of beam particles versus  $\zeta$  reflects the linearly ramped beam current. At  $c\tau = 5$  cm, a small deflection at the tail of the beam is apparent. The axisymmetric expansion of the beam head (see Fig. 7) is also

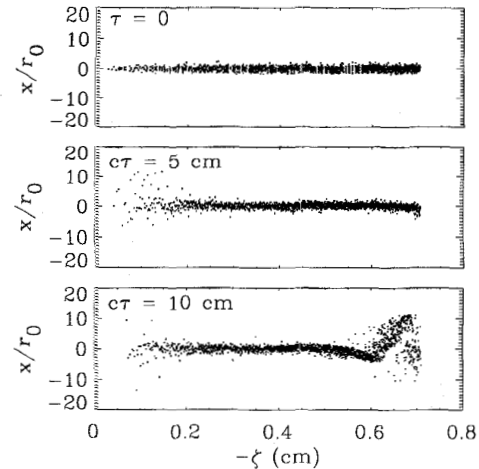


Fig. 10. Simulation particles, projected onto the  $(x, \zeta)$  plane at  $\tau = 0$ ,  $c\tau = 5$  cm, and  $c\tau = 10$  cm, show the severity of the electron-hose instability in this case. The initial beam radius is  $r_b(\tau = 0) = 41 \mu\text{m}$  (from [51]).

apparent. At  $c\tau = 10$  cm, the beam is severely disrupted. Plots of the beam centroid versus  $\zeta$  (not shown) indicate that the instability grows from the initial centroid perturbation rather than from particle noise.

Additional simulations [51] showed that, by adjusting the beam emittance to obtain a sufficiently large equilibrium beam radius, the EH regime can be avoided and the lower growth-rate associated with the TTS instability can be obtained. For these parameters, however, the TTS instability is also severely restrictive. Alternatively, 3-D simulations have shown that EH and TTS can be avoided entirely by abandoning the shaped-pulse approach and using a sufficiently short pulse [150]. Beam equilibrium and dynamics in this limit have also been studied by Barov and Rosenzweig [50].

## V. LASER-PLASMA ACCELERATORS

### A. Laser Wakefield Accelerator

As an intense laser pulse propagates through an underdense plasma,  $\lambda^2/\lambda_p^2 \ll 1$ , the ponderomotive force associated with the laser pulse envelope,  $F_p \sim \nabla a^2$ , expels electrons from the region of the laser pulse. If the length scale  $L_z$  of the axial gradient in the pulse profile is approximately equal to the plasma wavelength,  $L_z \sim \lambda_p$ , the ponderomotive force excites a large amplitude plasma wave (wakefield) with a phase velocity approximately equal to the laser pulse group velocity (see Fig. 1) [1], [30], [80]–[107]. For a typical axially symmetric laser pulse (e.g., a Gaussian profile), the wakefield amplitude will be maximum when  $L \simeq \lambda_p/2$ , where  $L = c\tau_L$  is laser pulse length. The precise value of  $L$  which maximizes the wake amplitude will depend on the shape of the axial pulse profile. For example, consider a circularly polarized laser pulse with a square axial profile in the 1-D limit  $r_0^2 \gg \lambda_p^2$ . The wakefield amplitude is maximum when  $L \simeq \lambda_{NP}/2$ , where  $\lambda_{NP}$  is the nonlinear plasma wavelength, (19), and is given by [87]–[90]

$$E_{\max}/E_0 = a_0^2(1 + a_0^2)^{-1/2} \quad (31)$$

where  $a_0^2 = 3.6 \times 10^{-19} \lambda^2 [\mu\text{m}] I [\text{W/cm}^2]$  (for linear polarization, replace  $a_0^2$  with  $a_0^2/2$ ). Notice that  $E_{\max} \sim \lambda_p^{-1} \sim L^{-1}$ . Hence, the wakefield amplitude can be increased by operating at high densities and shorter pulse lengths. At high densities, however, the laser pulse group velocity is reduced and electron phase detuning can limit the energy gain, as discussed in Section V-E.

Numerical examples [88], [89] of wakefield generation in an LWFA are shown in Fig. 2(a) and (b), where the axial electric field  $E_z$  (solid curve) and perturbed plasma density  $\delta n$  (dashed curve) are plotted versus  $\zeta$ . These plots are obtained by solving the 1-D nonlinear Poisson equation, (13), with  $n_b = 0$ . The laser is linearly polarized with  $\lambda = 1 \mu\text{m}$  and a normalized intensity profile  $a^2 = a_0^2 \sin^2(\pi\zeta/L) \sin^2(k\zeta)$  for  $-L < \zeta < 0$  and zero otherwise (referred to as a sine pulse profile). The ambient plasma density is  $n_0 = 1.2 \times 10^{16} \text{ cm}^{-3}$  and the pulse length is set to  $L = \lambda_p = 300 \mu\text{m}$  ( $\tau_L = L/c = 1 \text{ ps}$ ). In Fig. 2(a),  $a_0 = 0.5$  ( $I = 3.5 \times 10^{17} \text{ W/cm}^2$ ) and the maximum accelerating gradient is  $E_{\max} \simeq 1 \text{ GV/m}$ ; whereas in Fig. 2(b),  $a_0 = 2$  ( $I = 5.6 \times 10^{18} \text{ W/cm}^2$ ) and  $E_{\max} \simeq 10 \text{ GV/m}$ . The high-frequency density fluctuation inside the laser pulse envelope is due to the fast component of the ponderomotive force at twice the laser frequency, i.e.,  $a^2 \sim \sin^2 k\zeta = (1 - \cos 2k\zeta)/2$ . In the limit  $a^2 \ll 1$ , the radial profile of the wake is determined by the radial profile of the intensity [82]–[84], as indicated by (9)–(11), e.g., if  $a^2 \sim \exp(-2r^2/r_0^2)$ , then  $E_z \sim \exp(-2r^2/r_0^2)$ .

Because the plasma wave is driven by a single laser pulse with  $L \simeq \lambda_p$ , the wakefield amplitude is relatively insensitive to uncertainties in the pulse duration and/or the plasma uniformity. This is shown in Fig. 11, where the peak wakefield amplitude  $E_{\max}$  is shown as a function of the pulse length  $L$  at a fixed density and intensity. The parameters are identical to the sine profile laser pulse examples shown in Fig. 2(a) and (b), only now the pulse length  $L$  is varied. The solid curve is for  $a_0 = 0.5$ , the dashed curve is for  $a_0 = 2$ , and the field amplitude is normalized to  $E_N = E_0(a_0^2/2)(1 + a_0^2/2)^{-1/2}$ , which is the maximum wakefield amplitude for a square pulse profile. Notice that the electric field amplitude is maximum for  $L \simeq 0.75\lambda_p$  and is fairly insensitive to changes in the pulse length. Also, the curve for the  $a_0 = 2$  case is broader due to an increase in the nonlinear plasma wavelength. Similarly, for the case of a circularly polarized Gaussian pulse profile,  $a^2 = a_0^2 \exp(-\zeta^2/L^2)$ , the wakefield amplitude behind the pulse ( $\zeta^2 \gg L^2$ ) is given by [82]

$$E_{\max}/E_0 = (\sqrt{\pi}a_0^2/2)k_p L \exp(-k_p^2 L^2/4) \quad (32)$$

assuming  $a_0^2 \ll 1$ . Equation (32) explicitly shows the dependence of the wake amplitude on the pulse length  $L$ . In particular, the wake amplitude achieves a maximum value of  $E_{\max}/E_0 = a_0^2(\pi/2e)^{1/2} \simeq 0.76a_0^2$  when  $L = \lambda_p/\pi\sqrt{2}$ .

To summarize the optimal pulse length conditions for the square, sine, and Gaussian pulse profiles discussed above, it is convenient to express the pulse length in terms of the full-width-half-maximum length,  $L_{\text{FWHM}}$ , and the root-mean-square length,  $L_{\text{rms}}$ , of the pulse intensity profile [153]. For the square pulse, the wakefield is maximum  $E_{\max} = a_0^2 E_0$  when  $L_{\text{FWHM}} = 0.5\lambda_p$  ( $k_p L_{\text{rms}} = 0.91$ ). For the sine pulse, the

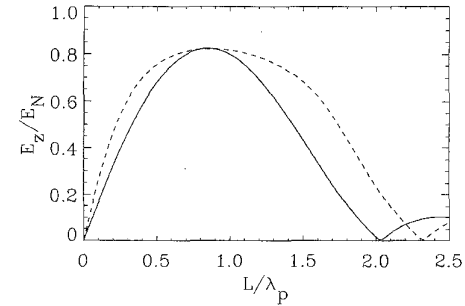


Fig. 11. Amplitude of the axial electric field  $E_z$  plotted as a function of laser pulse length,  $L$ , for the LWFA examples shown in Fig. 2. The solid curve is for  $a_0 = 0.5$ , the dashed curve is for  $a_0 = 2.0$ , the laser pulse envelope is given by  $a = a_0 \sin(\pi|\zeta|/L)$  for  $-L \leq \zeta \leq 0$ , and plasma density is held constant at  $n_0 = 1.2 \times 10^{16} (\lambda_p = 0.03 \text{ cm})$ .

wakefield is maximum  $E_{\max} = 0.82a_0^2 E_0$  when  $L_{\text{FWHM}} = 0.37\lambda_p$  ( $k_p L_{\text{rms}} = 0.85$ ). For the Gaussian pulse, the wakefield is maximum  $E_{\max} = 0.76a_0^2 E_0$  when  $L_{\text{FWHM}} = 0.37\lambda_p$  ( $k_p L_{\text{rms}} = 1$ ). These results assume  $a_0^2 \ll 1$  and circular polarization.

Furthermore, since the laser pulse in the LWFA is of short duration,  $L \simeq \lambda_p$ , various instabilities which can be detrimental to the propagation of long pulses can be reduced. Schemes which utilize long laser pulses,  $L \gg \lambda_p$ , such as the PBWA and the self-modulated LWFA, are subject to various instabilities, some of which are discussed in Section VII. Electron acceleration in LWFA experiments has been reported by Nakajima *et al.* [30], as discussed in the Introduction. In addition, optical interferometry techniques have been used to measure the plasma waves generated in LWFA experiments [106], [107].

### B. Plasma Beat-Wave Accelerator

In the PBWA, a large amplitude plasma wave is resonantly driven by the beating of two long pulse lasers [1], [25]–[29], [52]–[79]. The resonance condition on the frequencies of the two lasers is  $\Delta\omega \equiv \omega_1 - \omega_2 \simeq \omega_p$ . When this is satisfied, large amplitude plasma waves can be generated. Consider two lasers with a combined normalized vector potential given by  $a = a_1 \cos(k_1 z - \omega_1 t) + a_2 \cos(k_2 z - \omega_2 t)$ , where  $k_{1,2}$  are the wavenumbers. The ponderomotive force,  $\nabla a^2/2$ , will have a resonant beat term  $(a^2)_{\text{res}} = a_1 a_2 \cos(\Delta k z - \Delta\omega t)$ , where  $\Delta k \equiv k_1 - k_2$ . In the linear regime, plasma wave generation is described by  $(\partial^2/\partial t^2 + \omega_p^2)\phi = \omega_p^2(a^2/2)_{\text{res}}$ , and the ponderomotive beat term can resonantly drive a plasma wave when  $\Delta\omega \simeq \omega_p$ . When the resonance condition is exactly satisfied,  $\Delta\omega = \omega_p$ , secular growth of the plasma wave results,  $\phi = -\phi_p \sin(\Delta k z - \Delta\omega t)$ , where  $\phi_p = a_1 a_2 k_p |\zeta|/4$  and  $|\zeta| = |z - ct|$  is the distance behind the front of the laser beams. Hence, the amplitude of the plasma wave within the laser pulse is [58]

$$E_{\max}/E_0 = a_1 a_2 k_p |\zeta|/4. \quad (33)$$

Furthermore, notice that the phase velocity of the plasma wave,  $v_p = \Delta\omega/\Delta k$ , is given by  $v_p/c \simeq 1 - \omega_p^2/2\omega_1^2$  in the limit  $\omega_p^2/\omega_1^2 \ll 1$ , i.e., the plasma wave phase velocity is approximately equal to the group velocity of the driving lasers.

In effect, the laser beat-wave acts as a series of laser pulses, each of normalized amplitude  $a_1 a_2$  and of duration  $\Delta\tau = 2\pi/\Delta\omega$ . Each of these pulses generates a wake of amplitude  $E_{\max}/E_0 = \pi a_1 a_2/2$ . The total plasma wave amplitude generated by a laser beat-wave of length  $L = N\lambda_p$  is  $E_{\max}/E_0 = N\pi a_1 a_2/2$ , where  $N$  is the number of laser beat periods within the pulse.

The result given by (33) was based on linear plasma theory,  $|\phi| \ll 1$ . Various nonlinear effects were neglected. In particular, as discussed in Section III-B, as the plasma wave amplitude increases the plasma wave period increases. Since the period of the beat wave is fixed, whereas the period of the plasma wave is increasing, the plasma wave will eventually become out of phase with the laser beat wave. This resonant detuning of the plasma wave from the beat wave will limit the amplitude of the plasma wave [53].

The nonlinear dynamics of the beat-wave generation in 1-D with  $\omega_p^2/\omega^2 \ll 1$  can be examined using the nonlinear Poisson equation, (13), with  $n_b = 0$ . Analysis of (13) indicates that the nonlinear plasma wavelength is given by  $\lambda_{Np} = (4/k_p)(1+\phi_p)^{1/2} E_2(\hat{\rho})$ , where  $\phi_p$  is the maximum amplitude of the plasma wave,  $\hat{\rho} = 1 - (1 + \phi_p)^{-2}$ , and  $E_2$  is the complete elliptic integral of the second kind. In the limit  $\phi_p^2 \ll 1$ ,  $\lambda_{Np} \simeq \lambda_p(1 + 3\phi_p^2/16)$ , which indicates that the nonlinear plasma wavelength increases as the plasma wave amplitude increases. Hence, in the limit  $\phi_p^2 \ll 1$ , the nonlinear plasma wavenumber  $k_{Np} = 2\pi/\lambda_{Np}$  is given by

$$k_{Np} \simeq k_p(1 - 3\phi_p^2/16). \quad (34)$$

The detuning and saturation of the plasma wave can be estimated as follows [58]. The growth of the plasma wave will stop when the phase difference between the laser beat-wave and the plasma wave is  $\pi/2$ , i.e.,  $\int d\zeta (k_p - k_{Np}) \simeq \pi/2$ . Using the linear result for the plasma wave amplitude,  $\phi_p = a_1 a_2 k_p |\zeta|/4$ , gives a detuning distance  $L_t = (2\pi/a_1^2 a_2^2)^{1/3} 4/k_p$ . Hence, the plasma wave growth will saturate after a distance  $L_t$  behind the front of the laser beam, at which point the plasma wave amplitude is  $\phi_t = (2\pi a_1 a_2)^{1/3} = E_{\max}/E_0$ . A more careful derivation [53] of resonant detuning gives a maximum value of the electric field at saturation of

$$E_{\max}/E_0 = (16 a_1 a_2/3)^{1/3} \quad (35)$$

which assumes that the laser beat frequency is exactly equal to the ambient plasma frequency  $\Delta\omega = \omega_p$ .

Saturation occurs because the plasma wave period increases as the wave grows. Hence, to partially compensate for the increasing nonlinear plasma period, the plasma wave can be driven to higher amplitudes by using a laser beat period which is slightly longer [55]. In other words, the beat frequency is slightly detuned such that  $\Delta\omega < \omega_p$ . Tang *et al.* [55] showed that the optimum detuning, which maximizes the plasma wave amplitude at saturation, is given by

$$\Delta\omega_{\text{opt}} = \omega_p[1 - (9 a_1 a_2)^{2/3}/8]. \quad (36)$$

This gives a maximum saturation amplitude of

$$E_{\max}/E_0 = 4(a_1 a_2/3)^{1/3}. \quad (37)$$

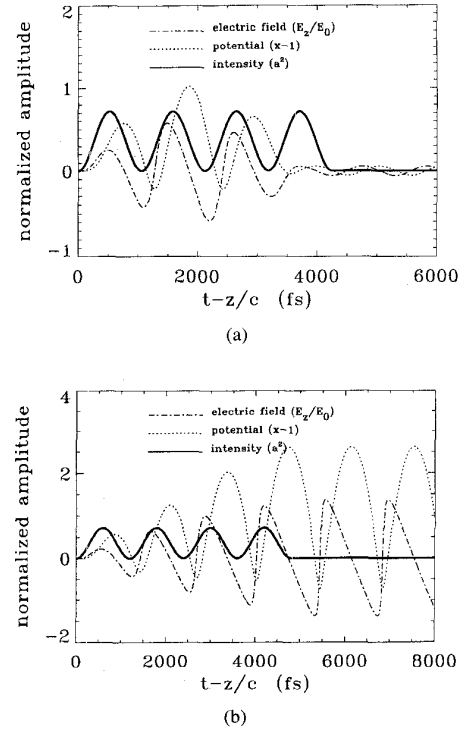


Fig. 12. Examples of a PBWA consisting of four beat pulses with  $a_0 = 1.2$  in a plasma of density  $n_0 = 10^{16} \text{ cm}^{-3}$ : (a) without optimization,  $\Delta\omega = \omega_p$ , showing the effects of detuning, and (b) with optimization,  $\Delta\omega < \omega_p$ . The solid curve shows the normalized intensity profile  $a^2$ , the dotted curve the potential  $\phi$ , and the dashed line the axial field  $E_z/E_0$ . The pulses are linearly polarized and move to the left (from [120]).

The above results are valid in the limit of weak pump amplitudes  $a_1 a_2 \ll 1$  for which the plasma wave is driven to saturation over a large number of beat periods. In the highly nonlinear regime,  $a_1 a_2 \gtrsim 1$ , however, the same general concepts apply to beat-wave generation, i.e., the plasma wave amplitude is limited by the increasing nonlinear plasma wavelength and the plasma wave amplitude can be optimized by increasing the beat-wave period such that  $\Delta\omega < \omega_p$ . To illustrate this, (13) is solved numerically [120] for a laser beat wave consisting of four beat periods, as shown in Fig. 12. The amplitude of the lasers is  $a_1 = a_2 = a_0$ , with  $a_0 = 1.2$ , and linear polarization is assumed, such that  $(a_1 a_2)_s = a_0^2/2$ , where the subscript  $s$  refers to an averaging over the fast laser period. The ambient plasma density is  $n_0 = 10^{16} \text{ cm}^{-3}$  ( $\lambda_p = 330 \mu\text{m}$ ). The case  $\Delta\omega = \omega_p$  is shown in Fig. 12(a), and it is clear that the plasma wave amplitude saturates (reaches maximum amplitude) after just the second beat pulse. In fact, the effect of the third and fourth beat pulses is to drive the plasma wave down to a very low amplitude. In Fig. 12(b) the beat period has been optimized numerically such that the plasma wave amplitude after the fourth beat pulse is maximized, i.e., the beat period is decreased  $\Delta\omega < \omega_p$  such that the length of the beat pulse is closer to the final nonlinear plasma wavelength  $\lambda_{Np}$ . This results in a dramatic increase in the final amplitude of the plasma wave electric field,  $E_{\max} \simeq 1.4 E_0 = 13 \text{ GV/m}$ , in comparison to the  $\Delta\omega = \omega_p$  case.

In addition to resonant detuning, the plasma wave amplitude in the PBWA can be limited by laser-plasma instabilities. Experiments at Ecole Polytechnique observed saturation of the beat-generated plasma wave by a parametric coupling to ion waves [73], [74]. In general, since the laser pulse lengths in the PBWA are long,  $L > \lambda_p$ , the beams are subject to various instabilities, some of which are discussed in Section VII. Several experiments have observed acceleration in the PBWA [25]–[29], as discussed in the Introduction.

### C. Multiple Laser Pulses

In the previous section discussing the PBWA, it was pointed out that 1) the laser beat wave acted in effect as a series of short laser pulses; 2) as the plasma wave grew the plasma period increased which led to a loss of resonance with respect to the laser beat pulses; and 3) the beat period, i.e., the width of the beat pulses, could be adjusted and optimized to maximize the plasma wave amplitude. These general principles can be extended to describe plasma wave generation by a series of short laser pulses [91], [118]–[122]. For example, the resonant laser-plasma accelerator (RLPA) [119], [120] uses an optimized train of short laser pulses to drive a plasma wave, in which the width of each pulse and the spacing between pulses is independently controlled. By optimizing the pulse widths and interpulse spacings, resonance with the plasma wave can be maintained and saturation of the plasma wave by resonant detuning can be eliminated. A sequence of  $n$  pulses is optimized when the pulse widths and spacings are chosen to maximize the plasma wave amplitude.

For square pulses in the linear regime ( $a^2, E_{\max}/E_0 \ll 1$ ), the optimum pulse train consists of  $n$  identical pulses, each of width  $L = \lambda_p/2$  and separated by a distance  $(2\ell + 1)\lambda_p/2$ , where  $\ell$  is an integer. The plasma wave amplitude will be  $n$  times the single pulse value,  $E_{\max}/E_0 = na_0^2$ . This result neglects nonlinear effects. In particular, as the nonlinear plasma wavelength increases, resonant detuning will eventually saturate the plasma wave amplitude.

In the nonlinear regime, however, resonance can only be maintained by optimizing both the pulse widths and spacings of each individual pulse. In the 1-D limit with  $\omega_p^2/\omega^2 \ll 1$ , this can be examined by solving (13). For square pulse profiles, analytic solutions can be obtained. It can be shown [119], [120] that the optimal width of the  $n$ th pulse  $L_n$ , the nonlinear wavelength  $\lambda_{Nn}$ , and the electric field amplitude  $E_{zn}$  of the wake behind the  $n$ th pulse are given by

$$L_n = (2/k_p)x_n^{1/2}E_2(\rho_n) \quad (38)$$

$$\lambda_{Nn} = (4/k_p)x_n^{1/2}E_2(\hat{\rho}_n) \quad (39)$$

$$E_{zn}/E_0 = x_n^{1/2} - x_n^{-1/2} \quad (40)$$

where  $x_n = \gamma_{\perp 1}^2 \gamma_{\perp 2}^2 \cdots \gamma_{\perp n}^2$ ,  $\gamma_{\perp n}^2 = 1 + a_n^2$ ,  $a_n$  is the amplitude of the  $n$ th pulse,  $E_2$  is the complete elliptic integral of the second kind,  $\rho_n^2 = 1 - \gamma_{\perp n}^2 x_n^{-1/2}$  and  $\hat{\rho}_n^2 = 1 - x_n^{-1/2}$ . The optimal spacing between the end of the  $n$ th pulse and the beginning of the  $n+1$ th pulse is given by  $(2\ell + 1)\lambda_{Nn}/2$  ( $\ell = \text{integer}$ ). The maximum normalized electric field of the wake,  $E_{\max}/E_0$ , for an optimized train of  $n$  square pulses of equal amplitudes  $a_n = a_0$ , is plotted in Fig. 13 versus

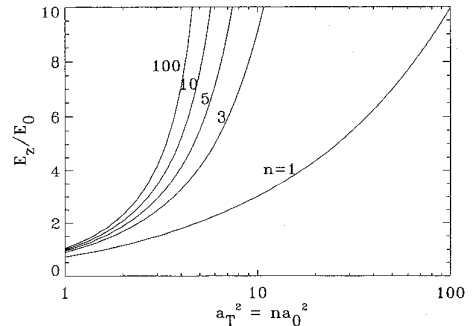


Fig. 13. The maximum electric field amplitude,  $E_z/E_0$ , versus the quantity  $a_T^2 = n a_0^2$ , for  $n = 1, 3, 5, 10$ , and  $100$  optimized square laser pulses with  $a_0 = 1$  (from [119]).

the quantity  $a_T^2 = n a_0^2$  [119], [120]. The curves show the results for 1, 3, 5, 10, and 100 pulses. In the linear regime,  $E_{zn} = nE_{z1} = n a_0^2 E_0$ , i.e., these curves are just straight lines. Fig. 13, however, shows that in the nonlinear regime,  $n$  pulses are more efficient than the linear result, i.e.,  $E_{zn} > nE_{z1}$ . In the highly nonlinear regime, this enhancement can be quite dramatic. Furthermore, Fig. 13 indicates that just a few optimized square pulses are far more efficient than a single pulse.

For square pulse profiles, both the width of the pulse and the spacing between pulses increase for subsequent pulses in the train, since the nonlinear wavelength of the plasma wave is increasing. For more realistic pulse profiles, the pulse length does not necessarily increase as  $\lambda_{Np}$  increases. Consider the case in which the electric field envelope of each pulse is modeled by a half period of a sine function, e.g.,  $a = a_1 \sin \pi \zeta / L_1$  ( $0 < \zeta < L_1$ ) for the first pulse. The result from a numerical optimization [119], [120] of (13) for a train of four sine pulses is shown in Fig. 14. Here, the plasma density is  $n_0 = 10^{16} \text{ cm}^{-3}$  and the pulses are linearly polarized with equal amplitudes  $a_n = a_0 = 1.2$ . Notice that the width of the pulses is decreasing, i.e., the width of the first pulse is 940 fs, whereas the width of the fourth laser pulse is 200 fs. From Fig. 14, it can be seen that the pulses are optimized when they reside in the region of the plasma wave for which  $\phi < 0$  and  $d\phi/d\zeta < 0$ , where  $\zeta = z - ct$ . This is the phase region of the plasma wave within which the laser pulse drives the plasma wave most efficiently. As in the square wave case,  $\lambda_{Nn}$ , and thus the spacing between pulses, increases with each succeeding pulse. For this example, the total laser fluence for the pulse train is  $I\tau_{\text{tot}} = 2.2 \text{ MJ/cm}^2$  and the final accelerating field is  $E_{\max} \simeq 1.9E_0 = 18 \text{ GV/m}$ .

Several techniques may be used to generate a train of short intense pulses using CPA laser systems [120]. One possible method is to divide the amplified stretched pulse by use of beam splitters, then send the separate pulses to separate compressors with adjustable lengths and delays. Alternatively, Fourier filtering can be used by placing a mask in the pulse stretcher to modify the phase and/or amplitude of the frequency components of the pulse in such a way that, when it is recompressed, a series of pulses with arbitrary spacings and widths will be produced. Preliminary experiments using similar methods have been reported [123], [154], [155].

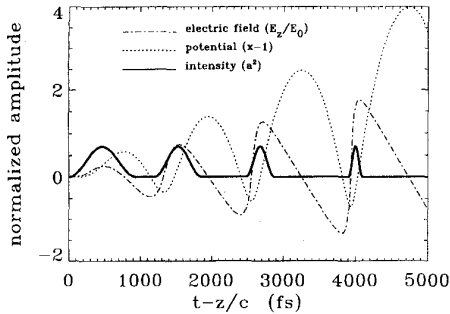


Fig. 14. An RLPA consisting of four optimized sine-shaped laser pulses with  $a_0 = 1.2$  and  $n_0 = 10^{16} \text{ cm}^{-3}$ . The solid curve shows the normalized intensity profile  $a^2$ , the dotted curve the potential  $\phi$ , and the dashed line the axial field  $E_z/E_0$ . The pulses are linearly polarized and move to the left (from [120]).

#### D. Self-Modulated LWFA

In the previous section it was described how a train of laser pulses can be used to generate a large amplitude wakefield. Under appropriate conditions, however, it is possible for a single long laser pulse to break up into a train of short pulses, each of these short pulses having a width on the order of  $\lambda_p$ . Associated with the break-up of the long pulse is a large amplitude plasma wave. This process is referred to as self-modulation [31]–[35], [96], [97], [108]–[117] and was first observed in fluid simulations [96], [108], [109] of relativistically guided laser pulses. The break-up of a long pulse can occur via forward Raman scattering in the 1-D limit [114], [115] or via an envelope self-modulation instability in the 2-D limit [111]–[113]. Physically, envelope self-modulation occurs from the plasma wave producing periodic regions of enhanced focusing and diffraction [69]. This process is discussed in more detail in Sections VI-F and VII-B.

To operate in the self-modulated regime [96], [97], [108]–[113], it is desirable that 1) the pulse length be long compared to the plasma wavelength,  $L > \lambda_p$ , and 2) the pulse power be larger than the power required to guide a long laser beam,  $P > P_c(1 - \Delta n/\Delta n_c)$ . Here,  $P_c = 17\omega^2/\omega_p^2$  GW is the critical power required for relativistic optical guiding,  $\Delta n$  is the depth of a preformed parabolic density channel (if present),  $\Delta n_c = 1/\pi r_e r_0^2$  is the critical channel depth, and  $r_e$  is the classical electron radius. The optical guiding of laser pulses by relativistic effects and density channels will be discussed more completely in Section VI. In the remainder of this section, it will be assumed that the laser pulse is propagating in an initially uniform plasma ( $\Delta n = 0$ ). Since  $\lambda_p \sim n_0^{-1/2}$  and  $P_c \sim n_0^{-1}$ , then for fixed laser parameters the conditions  $L > \lambda_p$  and  $P > P_c$  can usually be satisfied by operating at a sufficiently high plasma density.

Consider the possibility of generating wakefields with a 300 fs ( $L = 90 \mu\text{m}$ ) laser pulse of wavelength  $\lambda = 1 \mu\text{m}$  and power  $P = 10 \text{ TW}$ . To operate in the standard LWFA configuration,  $L \simeq \lambda_p$  implies a density of  $n_0 \simeq 1.4 \times 10^{17} \text{ cm}^{-3}$ . At this density  $P \ll P_c \simeq 140 \text{ TW}$  and the effects of relativistic guiding are unimportant. To operate in the self-modulated regime, it is desirable that  $L > \lambda_p$  and  $P > P_c$ . Choosing a plasma density such that  $P = 1.5P_c$  implies

$n_0 \simeq 2.8 \times 10^{17} \text{ cm}^{-3}$  and  $L \simeq 4.5\lambda_p$ . Hence, for this laser pulse, the self-modulated regime can be reached by increasing the plasma density by a factor of 20 compared to standard LWFA configuration. Furthermore, the corresponding energy gain can be enhanced by nearly a factor of 10 compared to the standard LWFA configuration, as is indicated by simulations discussed below [110].

The advantages of the self-modulated LWFA over the standard LWFA are simplicity and enhanced acceleration. Simplicity in that a matching condition of  $L \simeq \lambda_p$ , a preformed density channel and/or special pulse tailoring are not required. Enhanced acceleration is achieved for several reasons: 1) the self-modulated LWFA operates at higher density, hence a larger wakefield will be generated, since  $E_z \sim \sqrt{n_0}$ , as indicated by (31); 2) since  $P > P_c$ , the laser pulse will tend to focus to a higher intensity, thus increasing  $a_0$  and  $E_z$ ; 3) the wakefield is resonantly excited, i.e., excited by a series of beamlets as opposed to a single pulse as in the standard LWFA; and 4) relativistic optical guiding allows the modulated pulse structure to propagate for several Rayleigh lengths, thus extending the acceleration distance. The disadvantages of the self-modulated LWFA are: 1) at higher densities the laser pulse group velocity ( $\simeq$  the plasma wakefield phase velocity) decreases and, hence, electron dephasing from the plasma wakefield can limit the acceleration distance, and 2) the modulated pulse structure eventually diffracts.

The properties of the self-modulated LWFA are illustrated by the following simulations [110]. Two cases will be considered: 1) a standard LWFA in which  $L \simeq \lambda_p$  and  $P < P_c$ , and 2) a self-modulated LWFA, in which  $L > \lambda_p$  and  $P > P_c$ . The laser parameters for both cases are identical: a Gaussian axial intensity profile with a pulse length  $L = 90 \mu\text{m}$  (300 fs),  $\lambda = 1 \mu\text{m}$ ,  $a_0 = 0.7$ ,  $r_0 = 31 \mu\text{m}$  (in vacuum), which corresponds to  $Z_R = 3 \text{ mm}$ ,  $P = 10 \text{ TW}$ , and a pulse energy of  $W = 1.5 \text{ J}$ . The simulation begins at  $c\tau = 0$  as the laser pulse enters the plasma, initially converging such that in vacuum it would focus to a minimum spot size of  $r_0 = 31 \mu\text{m}$  at  $c\tau = 3Z_R$ . The plasma density is initially increasing, reaching full density at  $c\tau = 2Z_R$ . The simulation continues until  $c\tau = 10Z_R = 3 \text{ cm}$ . In both cases, the acceleration and trapping of a continuous electron beam with initial energy of 3 MeV and normalized emittance  $\epsilon_n = 130 \text{ mm-mrad}$  is considered. The electron beam is initially converging such that in vacuum it would focus to a minimum rms radius  $r_b = 200 \mu\text{m}$  at  $c\tau = 3Z_R$ . With such a large initial emittance, only a small fraction ( $\sim 1\%$ ) of the particles will be trapped and accelerated.

For the standard LWFA, Case I, the requirement  $L = \lambda_p = 90 \mu\text{m}$  implies a density of  $n_0 = 1.4 \times 10^{17} \text{ cm}^{-3}$ . At this density,  $P \ll P_c = 140 \text{ TW}$ , such that relativistic guiding effects are unimportant. In fact, the presence of the plasma has little effect on the evolution of the laser pulse, which reaches a peak intensity of  $|\hat{a}_f|^2 = 0.56$  at  $c\tau = 3Z_R$ . The evolution of the spot size, Fig. 15, is very close to vacuum diffraction. This is also evident in Fig. 16(a) (dashed line), where the peak accelerating field, plotted versus time, is symmetric about the focus,  $c\tau = 3Z_R$ . After  $c\tau = 10Z_R = 3 \text{ cm}$ , a small fraction ( $\sim 0.1\%$ ) of the test electron beam particles has been trapped

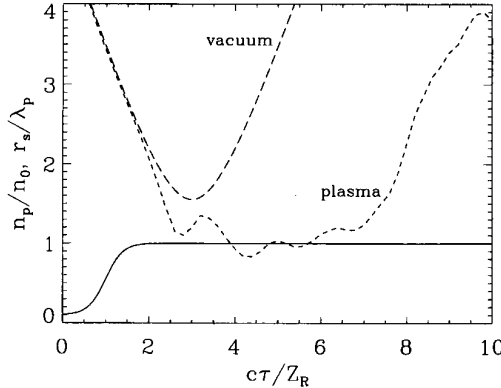


Fig. 15. Ambient plasma density  $n_p/n_0$  (solid line) and spot size  $r_s/\lambda_p$  (dashed line) versus propagation distance  $c\tau$  for a self-modulated LWFA with  $n_0 = 2.8 \times 10^{18} \text{ cm}^{-3}$ . The laser is initially converging such that the minimum spot size in vacuum is reached at  $c\tau = 3Z_R$ . Here,  $r_s$  is the spot size of the leading beamlet and is defined to be the radius enclosing 86.5% of the laser power (from [110]).

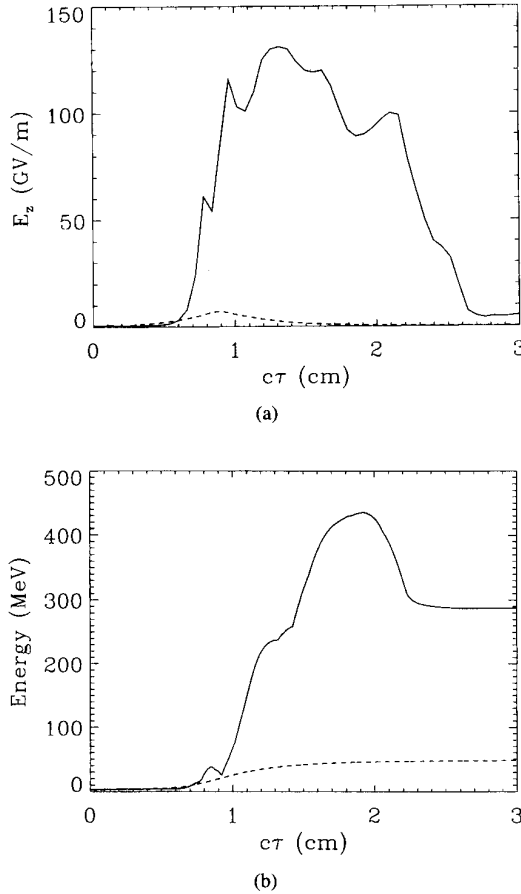


Fig. 16. (a) Peak accelerating field and (b) peak energy of the injected particles versus propagation distance  $c\tau$  for the standard LWFA case (dashed line) with  $n_0 = 1.4 \times 10^{17} \text{ cm}^{-3}$  and the self-modulated LWFA case (solid line) with  $n_0 = 2.8 \times 10^{18} \text{ cm}^{-3}$  (from [110]).

and accelerated. At  $c\tau = 2 \text{ cm}$ , the peak particle energy is 48 MeV, which implies an average acceleration of 2.4 GeV/m, as shown in Fig. 16(b) (dashed line).

For the self-modulated LWFA, Case II, the density is increased such that  $P = 1.5P_c = 10 \text{ TW}$ , which implies

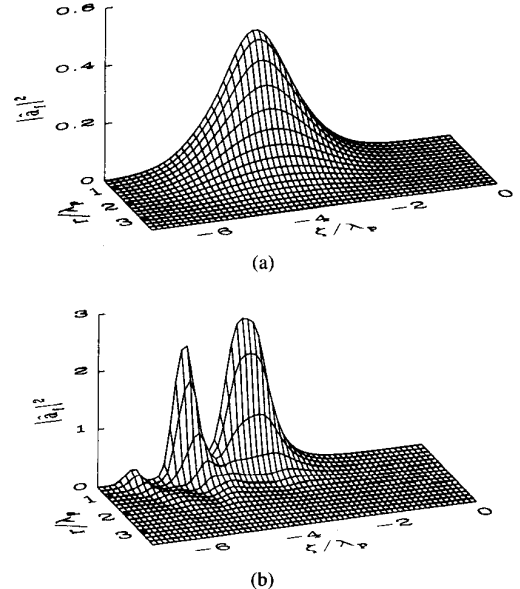


Fig. 17. Normalized laser intensity  $|\hat{a}_f|^2$  for the self-modulated LWFA case, sampled over a coarse grid (the numerical grid is much finer), at (a)  $c\tau = 2Z_R$  and (b)  $c\tau = 3.2Z_R$ . The laser pulse is moving to the right (from [110]).

$n_0 = 2.8 \times 10^{18} \text{ cm}^{-3}$ , which is 20 times higher than in Case I. At this density  $L > \lambda_p = 20 \mu\text{m}$ , i.e., the laser pulse now extends over  $\simeq 4.5\lambda_p$ . Fig. 17 shows the laser intensity at (a)  $c\tau = 2Z_R$  and (b)  $c\tau = 3.2Z_R$ . The axial electric field and the plasma density response on axis at  $c\tau = 3.2Z_R$  are shown in Fig. 18(a) and (b), respectively. The laser pulse has become modulated (three peaks are observable, separated by  $\lambda_p$ ) and the plasma wave is highly nonlinear. In addition, relativistic optical guiding effects have focused the laser to a much higher intensity than was observed in Case I. The evolution of the laser spot size is shown in Fig. 15, indicating that the pulse has focused to a smaller spot size and remains guided over  $\simeq 5.5Z_R$ . A plot of the peak accelerating field versus time, Fig. 16(a) (solid line), shows that the highly nonlinear fields persist as the laser pulse is optically guided. A maximum accelerating field of  $\simeq 130 \text{ GV/m}$  was obtained. Because of the larger fields, a greater fraction (2%) of the test electron beam particles was trapped and accelerated. The peak particle energy of 430 MeV is observed at  $c\tau = 6Z_R = 1.8 \text{ cm}$ . At  $c\tau = 10Z_R = 3 \text{ cm}$ , however, the peak particle energy has dropped to 290 MeV due to the reduced group velocity of the laser pulse, which causes the electrons to slip out of phase with the wakefield and become decelerated. Fig. 16(b) (solid line) shows acceleration to 430 MeV over 1.8 cm which gives an average gradient of 24 GeV/m. This is an order of magnitude increase compared to the standard LWFA of Case I.

As discussed in the Introduction, electron acceleration in the self-modulated regime has been observed in several experiments [31]–[35]. In addition, observation of the plasma wave in the self-modulated regime by coherent Thomson scattering of a frequency double probe pulse has been reported [117].

#### E. Limits on Laser-Driven Acceleration

Several mechanisms can limit the energy gain in a laser-driven accelerator: laser diffraction, electron detuning, pump

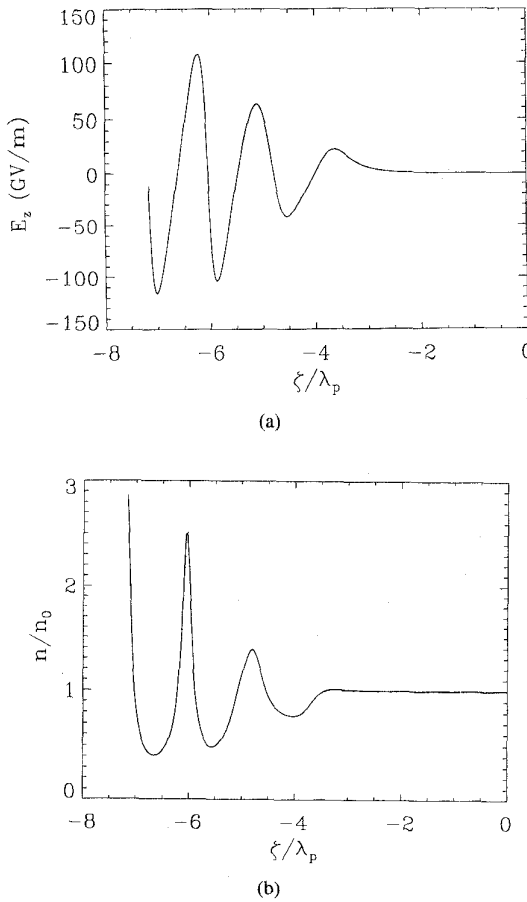


Fig. 18. Axial electric field  $E_z$  (a) and plasma electron density on axis  $n/n_0$  (b) versus  $\zeta/\lambda_p$  plotted at  $c\tau = 3.2Z_R$  for the self-modulated LWFA case (from [110]).

depletion, and laser-plasma instabilities. In vacuum a laser pulse undergoes Rayleigh diffraction, i.e., the laser spot size evolves according to  $r_s = r_0(1 + z^2/Z_R^2)^{1/2}$ , where  $r_0$  is the minimum spot size at the focal point  $z = 0$  and  $Z_R = kr_0^2/2$  is the Rayleigh length. Without some form of optical guiding, the laser-plasma interaction distance will be limited to a few  $Z_R$ . Electron detuning, wherein a highly relativistic electron outruns the plasma wave, can limit the energy gain to a detuning length  $L_d$  as discussed in Section III-C. As the laser driver excites a plasma wave, it loses energy, i.e., it pump depletes [58], [61], [89], [92], [102]. The pump depletion length  $L_{pd}$  can be estimated by equating the laser pulse energy to the energy left behind in the wakefield,  $E_z^2 L_{pd} \simeq E_L^2 L$ , where  $E_L$  is the laser field.

As an illustration, consider an LWFA in the standard configuration driven by a circularly polarized square profile laser pulse with  $L \simeq \lambda_{Np}/2$ . The detuning and pump depletion lengths are given by [89], [92], [102]

$$L_d \simeq (\omega^2/\omega_p^2) \lambda_p \begin{cases} 1, & \text{for } a_0^2 \ll 1 \\ 2a_0^2/\pi, & \text{for } a_0^2 \gg 1 \end{cases} \quad (41)$$

$$L_{pd} \simeq (\omega^2/\omega_p^2) \lambda_p \begin{cases} a_0^{-2}, & \text{for } a_0^2 \ll 1 \\ a_0/3\pi, & \text{for } a_0^2 \gg 1. \end{cases} \quad (42)$$

For the parameters  $a_0 = 0.5$ ,  $\lambda = 1 \mu\text{m}$ , and  $r_0 = \lambda_p = 33 \mu\text{m}$  ( $P = 12 \text{ TW}$ ,  $n_0 = 10^{18} \text{ cm}^{-3}$ ), the relevant propagation lengths are  $Z_R = 0.34 \text{ cm}$ ,  $L_d \simeq 3.6 \text{ cm}$ , and  $L_{pd} \simeq 14 \text{ cm}$ , i.e.,  $Z_R \ll L_d < L_{pd}$ . Furthermore, since  $L_d, L_{pd} \sim n_0^{-3/2}$ , the detuning length and pump depletion lengths can be increased by operating at lower densities. Since  $L \sim \lambda_p$  in the standard LWFA, lower densities correspond to longer laser pulse durations  $L \sim n_0^{-1/2}$ . In principle, a static magnetic field can be introduced to reduce detuning, as in the surfatron configuration [54]. Use of an active medium has also been proposed as a method to reduce pump depletion [104].

The energy gain in the standard LWFA for a laser pulse undergoing vacuum diffraction is given by  $\Delta W_v \simeq e\pi Z_R E_z$  which, in the limit  $a_0^2 \ll 1$ , can be written as [95]

$$\Delta W_v [\text{MeV}] \simeq 580(\lambda/\lambda_p)P [\text{TW}]. \quad (43)$$

To increase the energy gain beyond this value in a single stage, some form of optical guiding is necessary to prevent diffraction. Various methods for optical guiding are discussed in Section VI. If diffraction is overcome, detuning will limit the energy gain. In the standard LWFA, the single-stage energy gain after a detuning length  $\Delta W_d = eL_d E_z$  can be written in the limit  $a_0^2 \ll 1$  as

$$\Delta W_d [\text{GeV}] \simeq I [\text{W/cm}^2]/n_0 [\text{cm}^{-3}]. \quad (44)$$

For example,  $P = 100 \text{ TW}$ ,  $r_0 = 100 \mu\text{m}$ ,  $I = 6.4 \times 10^{17} \text{ W/cm}^2$ ,  $\tau_L = 1 \text{ ps}$ ,  $n_0 = 10^{16} \text{ cm}^{-3}$ ,  $\lambda_p = 330 \mu\text{m}$ , and  $\lambda = 1 \mu\text{m}$  imply  $\Delta W_v = 180 \text{ MeV}$  and  $\Delta W_d = 64 \text{ GeV}$ . These estimates assume that laser-plasma instabilities do not significantly degrade the laser pulse. The effects of various instabilities are discussed in Section VII.

## VI. OPTICAL GUIDING IN PLASMAS

The optical guiding mechanisms discussed below are based on the principle of refractive guiding. Refractive guiding becomes possible when the radial profile of the index of refraction,  $\eta_R(r)$ , exhibits a maximum on axis, i.e.,  $\partial\eta_R/\partial r < 0$ . Since  $\eta_R \simeq ck/\omega$ ,  $\partial\eta_R/\partial r < 0$  implies that the phase velocity along the propagation axis is less than it is off-axis. This causes the laser phase fronts to curve such that the beam focuses toward the axis.

The index of refraction for a small amplitude electromagnetic wave propagating in a plasma of uniform density  $n = n_0$ , in the 1-D limit, is given by  $\eta_R = ck/\omega = (1 - \omega_p^2/\omega^2)^{1/2}$ . For large amplitude waves, however, variations in the electron density and mass will occur, i.e.,  $\omega_p^2 \rightarrow (\omega_p^2/\gamma)n/n_0$ . Hence, a general expression for the index of refraction for a large amplitude electromagnetic wave in a plasma is

$$\eta_R(r) \simeq 1 - \frac{\omega_p^2}{2\omega^2} \frac{n(r)}{n_0\gamma(r)} \quad (45)$$

assuming  $\omega_p^2/\omega^2 \ll 1$ . The  $\eta_R(r)$  profile can be modified through the relativistic factor  $\gamma(r)$  or the density  $n(r)$ . The leading order motion of the electrons in the laser field is the quiver motion  $\mathbf{p}_\perp = mca$  and, hence,  $\gamma \simeq \gamma_\perp = (1 + a^2)^{1/2}$ . A laser intensity profile peaked on axis  $\partial a^2/\partial r < 0$  leads

to  $\partial\eta_R/\partial r < 0$  and the possibility of guiding (i.e., relativistic self-focusing). The density profile can have contributions from a preformed density channel  $\Delta n_p \sim \Delta nr^2/r_0^2$  or a plasma wave  $\delta n \sim \delta n_0(r) \cos k_p \zeta$ , i.e.,  $n = n_0 + \Delta n_p + \delta n$ . A radial density profile which has a minimum on axis (i.e., a channel) implies  $\partial\eta_R/\partial r < 0$ . In the limits  $a^2 \ll 1$ ,  $|\Delta n_p/n_0| \ll 1$  and  $|\delta n/n_0| \ll 1$ , the refractive index can be written as

$$\eta_R(r) \simeq 1 - \frac{\omega_p^2}{2\omega^2} \left( 1 - \frac{a^2}{2} + \frac{\Delta n_p}{n_0} + \frac{\delta n}{n_0} \right). \quad (46)$$

In the above expression, the  $a^2/2$  term is responsible for relativistic optical guiding [65]–[69], [88], [89], [95]–[97], [130], [156]–[174], the  $\Delta n_p/n_0$  term is responsible for preformed density channel guiding [64], [69], [95]–[100], [175]–[178], and the  $\delta n/n_0$  term is responsible for self-channeling [96], [160], [161], [164]–[174], plasma wave guiding [69], [88], [89], and self-modulation of long laser pulses [96], [97], [108]–[117].

### A. Relativistic Optical Guiding

The self-focusing of laser beams by relativistic effects was first considered by Litvak [156] and Max *et al.* [157]. In the standard theory of relativistic optical guiding [156]–[159], only the effects of the transverse quiver motion of the electrons are included in the expression for  $\eta_R$ , i.e.,  $n = n_0$ ,  $\gamma = \gamma_\perp(r)$ , and

$$\eta_R \simeq 1 - (\omega_p^2/2\omega^2)(1 + a^2)^{-1/2}. \quad (47)$$

Analysis of the paraxial wave equation with an index of refraction of this form indicates that when the laser pulse power exceeds a critical power,  $P \geq P_c$ , relativistic effects can prevent the diffraction of the laser pulse. For a circularly polarized Gaussian laser pulse of the form  $a = a_0 \exp(-r^2/r_s^2)(\cos k\zeta e_x + \sin k\zeta e_y)$ ,  $P/P_c = k_p^2 a_0^2 r_s^2 / 16$ . In practical units the critical power can be written as [156]–[171]

$$P_c[\text{GW}] \simeq 17(\omega/\omega_p)^2. \quad (48)$$

An equation for the laser spot size can be derived by analyzing the paraxial wave equation with an index of refraction of the form given by (47). In the limit  $a^2 \ll 1$ ,  $(1 + a^2)^{-1/2} \simeq 1 - a^2/2$ , and the laser spot size evolves according to [65], [83], [84], [159]

$$\frac{d^2R}{dz^2} = \frac{1}{Z_R^2 R^3} \left( 1 - \frac{P}{P_c} \right) \quad (49)$$

where  $R = r_s/r_0$  is the normalized spot size,  $r_0$  is the minimum spot size in vacuum, and  $Z_R = kr_0^2/2$  is the vacuum Rayleigh length. The first term on the right of (49) represents vacuum diffraction, whereas the second term represents relativistic self-focusing. The solution to (49) is  $r_s^2/r_0^2 = 1 + (1 - P/P_c)z^2/Z_R^2$ , which indicates that the spot size will focus when  $P > P_c$ . In fact, (49) predicts “catastrophic” focusing. This is due to the approximation  $(1 + a^2)^{-1/2} \simeq 1 - a^2/2$  in the  $a^2 \ll 1$  limit. If the full relativistic factor  $(1 + a^2)^{-1/2}$  is kept in the wave equation [159], however, it can be shown that a laser beam can be guided when  $P > P_c$ , i.e., the laser spot size will remain constant or oscillate about its matched beam radius.

The self-consistent nonlinear theory developed by Sprangle *et al.* [88], [89], [96] showed, however, that relativistic optical guiding is ineffective in preventing the diffraction of sufficiently short pulses,  $L \lesssim \lambda_p/\gamma_\perp$ . This is due to the fact that the index of refraction becomes modified by the laser pulse on the plasma frequency time scale, not the laser frequency time scale. Typically, relativistic guiding only effects the body of long pulses,  $L > \lambda_p$ .

In the 1-D limit,  $r_s^2 k_p^2 \gg 1$ , nonlinear quasi-static theory [88], [89] indicates that the self-consistent electron fluid response satisfies  $n/\gamma n_0 = (1 + \phi)^{-1}$ , hence

$$\eta_R \simeq 1 - (\omega_p^2/2\omega^2)(1 + \phi)^{-1} \quad (50)$$

where  $\phi$  is the normalized electrostatic potential which satisfies the nonlinear Poisson equation, (13), assuming  $\omega_p^2/\omega^2 \ll 1$ . For long laser pulses with sufficiently smooth envelopes,  $|\partial a^2/\partial \zeta| \ll k_p a^2$ ,  $\partial^2 \phi / \partial \zeta^2$  can be neglected in (13) which implies  $1 + \phi = (1 + a^2)^{1/2}$ . The index of refraction has the form given by (47) and, hence, the standard theory of relativistic focusing [156]–[159] can be applied to the body of long pulses. Although long pulses can be guided by relativistic effects, they can also be subject to various instabilities (e.g., Raman, self-modulation, and laser-hose instabilities), which are discussed in more detail in the subsequent sections.

Short laser pulses with pulse lengths  $L \simeq \lambda_p$  can generate plasma waves (as in the standard LWFA). A linear plasma wave has the form  $\phi = \phi_0 \sin k_p \zeta$ . At the front of the pulse ( $\zeta = 0$ )  $\phi = 0$  and, hence, (50) indicates that the front of the pulse will not be guided. Since the plasma wave takes a finite time to be excited, on the order of  $\omega_p^{-1}$ , the relativistic guiding effect described by (50) also takes a finite time ( $\sim \omega_p^{-1}$ ) to take effect. Hence, relativistic guiding will not be efficient in guiding short pulses and the leading portion ( $|\zeta| < k_p^{-1}$ ) of a long pulse will erode by diffraction.

Simulations [96] confirm the inability of relativistic guiding to prevent the diffraction of short laser pulses. The results are shown in Fig. 19 for the parameters  $\lambda_p = 0.03$  cm ( $n_0 = 1.2 \times 10^{16}$  cm $^{-3}$ ),  $r_s = \lambda_p$  (Gaussian radial profile),  $\lambda = 1$   $\mu\text{m}$  ( $Z_R = 28$  cm), and  $P = P_c$ . The initial axial laser profile is given by  $|\hat{a}_f(\zeta)| = a_0 \sin(-\pi\zeta/L)$  for  $0 < -\zeta < L = c\tau_L$ , where  $a_0 = 0.9$  for the above parameters. Simulations are performed for two laser pulse lengths,  $L = \lambda_p$  ( $\tau_L = 1$  ps) and  $L = \lambda_p/4$  ( $\tau_L = 0.25$  ps). The spot size at the pulse center versus propagation distance  $c\tau$  is shown in Fig. 19 for (a) the vacuum diffraction case, (b) the  $L = \lambda_p/4$  pulse, and (c) the  $L = \lambda_p$  pulse. The  $L = \lambda_p/4$  pulse diffracts almost as if in vacuum. The  $L = \lambda_p$  pulse experiences a small amount of initial guiding before diffracting. A preformed parabolic plasma density channel can guide the  $L = \lambda_p$  pulse, as shown in Fig. 19(d), where the channel depth is given by  $\Delta n = 1/\pi r_e r_s^2 = 1.3 \times 10^{15}$  cm $^{-3}$  ( $r_e = e^2/m_e c^2$ ) and the density on axis is  $n_0 = 1.2 \times 10^{16}$  cm $^{-3}$ .

### B. Tailored Pulse Propagation

A laser pulse with an appropriately tailored envelope can propagate many Rayleigh lengths without significantly altering its original profile [96], [97], [130]. Consider a long laser

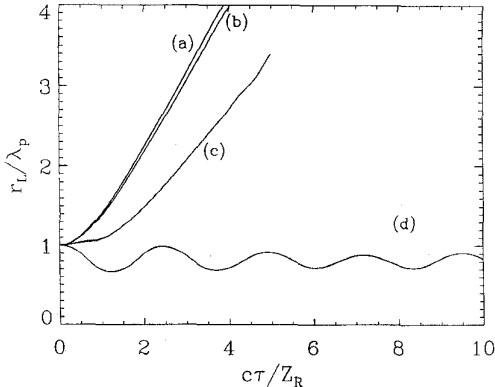


Fig. 19. Laser spot size  $r_s$  versus propagation distance  $c\tau$  for (a) vacuum diffraction, (b) an ultrashort pulse with  $L = \lambda_p/4$ , and (c) a short pulse with  $L = \lambda_p$ . Here,  $P = P_c$ ,  $a_0 = 0.9$ , and  $\lambda_p = 0.03$  cm. Guiding of the  $L = \lambda_p$  pulse in a preformed parabolic plasma density channel with  $\Delta n = 1/r_e r_s^2$  is shown by (d) (from [96]).

pulse,  $L > \lambda_p$ , in which the spot size is tapered from a large value at the front to a small value at the back, so that the laser power,  $P \sim r_s^2 |\hat{a}_f|^2$ , is constant throughout the pulse and equal to  $P_c$ . The leading portion ( $\ll \lambda_p$ ) of the pulse will diffract as if in vacuum, as discussed in the previous section. Since  $r_s$  is large at the front of the pulse, however, the Rayleigh length is also large. Hence, the locally large spot size allows the pulse front to propagate a long distance, whereas the body of the pulse will be relativistically guided. Also, since  $|\hat{a}_f|^2$  increases slowly throughout the pulse, detrimental wakefield effects (e.g., self-modulation) are reduced.

The effectiveness of pulse tailoring has been observed in simulations [96], [97], [130]. The results of such a simulation [97] are shown in Figs. 20–22. The initial normalized intensity profile,  $|\hat{a}_f|^2$ , is shown in Fig. 20(a). The local spot size at the front ( $\zeta = 0$ ) of the pulse is large,  $r_L \simeq 8\lambda_p$ , and tapers down over  $\zeta = -2\lambda_p$  to  $r_L = \lambda_p$  (a Gaussian radial profile assumed throughout). The initial axial laser envelope is given by  $|\hat{a}_f(\zeta)| = a_L \sin(-\pi\zeta/4\lambda_p)$  for  $0 < -\zeta < 2\lambda_p$  such that  $P = P_c$  at each  $\zeta$  slice, i.e.,  $r_L(\zeta)a_0(\zeta) = 0.9\lambda_p$ . Also,  $\lambda = 1 \mu\text{m}$  and  $\lambda_p = 30 \mu\text{m}$  ( $n_0 = 1.2 \times 10^{18} \text{ cm}^{-3}$ , initially a uniform plasma), such that  $P = P_c = 16 \text{ TW}$ . This gives a peak value of  $a_0 = 0.9$  at the back of the pulse where  $r_L = \lambda_p$ , which corresponds to a Rayleigh length of  $Z_R = 0.28 \text{ cm}$ . The pulse intensity then terminates over a distance of  $L_{\text{fall}} = \lambda_p/2$ . The pulse energy is approximately 3 J and the pulse length is approximately  $L = 2\lambda_p = 60 \mu\text{m}$  (200 fs). Because  $L_{\text{fall}} < \lambda_p$ , a large amplitude wakefield will be excited behind the pulse.

Fig. 20(b) shows the normalized intensity profile after propagating  $c\tau = 10Z_R = 2.8 \text{ cm}$ . The pulse is somewhat distorted, but largely intact. The evolution of the pulse spot size at the position of peak intensity versus propagation distance is shown in Fig. 21(b), indicating that guiding has been achieved over the  $10Z_R$  simulation region. The axial electric field of the wake on axis after  $c\tau = 10Z_R$  is shown in Fig. 22. The evolution of a continuous electron beam with an initial normalized emittance  $\epsilon_n = 1.0 \text{ mm-mrad}$ , rms radius  $r_b = 5 \mu\text{m}$ , and energy  $E_b = 2 \text{ MeV}$  was

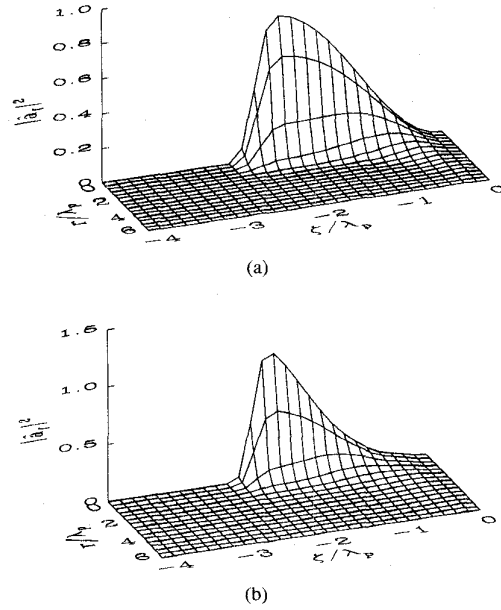


Fig. 20. Surface plot of the normalized laser intensity,  $|\hat{a}_f|^2$ , at (a)  $\tau = 0$  and at (b)  $c\tau = 10Z_R$  for a tailored-pulse LWFA (from [97]).

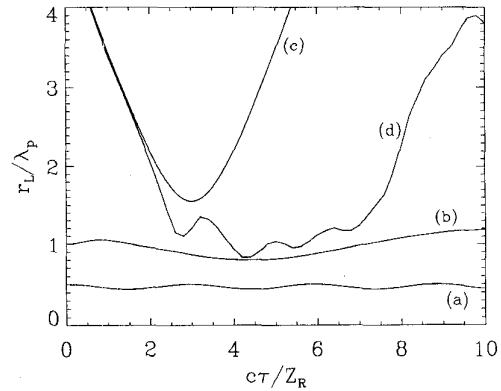


Fig. 21. Laser spot size  $r_s$  at the position of peak intensity versus propagation distance  $c\tau/Z_R$  for (a) a channel-guided LWFA, (b) a tailored-pulse LWFA, (c) vacuum diffraction, and (d) the self-modulated LWFA of Figs. 16–18 (from [97]).

simulated using the self-consistent wakefields. After  $c\tau = 2.8 \text{ cm}$ , approximately 60% of the beam electrons were trapped and accelerated. The peak energy of the beam electrons experienced an average gradient of 27 GeV/m (750 MeV in 2.8 cm). Additional simulations [130] indicate that a tailored pulse can be constructed, in effect, by overlapping as few as five Gaussian pulses, each with a different spot size.

### C. Plasma Density Channel Guiding

A preformed plasma density channel can guide short intense laser pulses [64], [69], [95]–[100], [175]–[178]. Consider a parabolic density channel of the form  $n = n_0 + \Delta n(r^2/r_0^2)$ , where  $\Delta n \geq 0$ . For a low power,  $P \ll P_c$ , low intensity  $a^2 \ll 1$  laser pulse, the index of refraction is given approximately by

$$\eta_R = 1 - \frac{\omega_p^2}{2\omega^2} \left( 1 + \frac{\Delta n}{n_0} \frac{r^2}{r_0^2} \right). \quad (51)$$

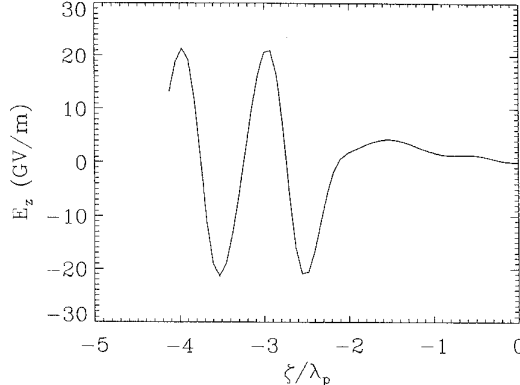


Fig. 22. Axial electric field  $E_z$  on axis at  $c\tau = 10Z_R$  for the tailored-pulse LWFA of Fig. 20 (from [97]).

Analysis of the paraxial wave equation with an index of refraction of this form indicates that the spot size  $r_s$  of a Gaussian laser beam of the form  $a^2 = a_0^2 \exp(-2r^2/r_s^2)$  will evolve according to [69] and [111]

$$\frac{d^2 R}{dz^2} = \frac{1}{Z_R^2 R^3} \left( 1 - \frac{\Delta n}{\Delta n_c} R^4 \right) \quad (52)$$

where  $R = r_s/r_0$ . This indicates that a parabolic channel can guide a Gaussian beam with  $r_s = r_0$  provided that the density channel depth is equal to the critical depth,  $\Delta n = \Delta n_c$ , where the critical channel depth is given by [69], [95], [96]

$$\Delta n_c = 1/\pi r_e r_0^2 \quad (53)$$

where  $r_e = e^2/m_e c^2$  is the classical electron radius. In practical units

$$\Delta n_c [\text{cm}^{-3}] = 1.1 \times 10^{20}/r_0^2 [\mu\text{m}]. \quad (54)$$

For  $\Delta n \neq \Delta n_c$ , the beam spot size will oscillate about its matched value (given by  $R^4 = \Delta n_c/\Delta n$ ), provided that the channel is sufficiently broad.

Simulations indicate that preformed density channels are effective in guiding ultrashort ( $L \sim \lambda_p$ ) high-intensity ( $a^2 \sim 1$ ) laser pulses. The results of a simulation [97] of a channel-guided LWFA are shown in Figs. 21, 23, and 24. In this example, the initial axial laser profile is given by  $|\hat{a}_f(\zeta)| = a_0 \sin(-\pi\zeta/L)$  for  $0 < -\zeta < L$ , with  $a_0 = 0.72$  and  $L = 120 \mu\text{m}$  (400 fs). Also,  $\lambda = 1 \mu\text{m}$  and  $r_0 = 60 \mu\text{m}$  (Gaussian radial profile), which implies  $Z_R = 1.1 \text{ cm}$  and  $P = 40 \text{ TW}$ . The density on axis is chosen such that  $L = \lambda_p$  ( $n_0 = 7.8 \times 10^{16} \text{ cm}^{-3}$ ) and a preformed density channel with a parabolic profile is assumed with  $\Delta n = 1/\pi r_e r_0^2 = 3.2 \times 10^{16} \text{ cm}^{-3}$ .

Fig. 21(a) shows the evolution of the laser spot size versus propagation distance,  $c\tau$ . The laser pulse remains well guided by the density channel, with the laser spot size exhibiting small oscillations about its initial value over the full  $20Z_R = 23 \text{ cm}$  simulation length. After  $c\tau = 20Z_R$ , the pulse profile shows very little distortion from its initial profile. A surface plot of the electron density profile at  $c\tau = 20Z_R$  is shown in Fig. 23. The initial unperturbed parabolic profile can be seen at the right ( $\zeta = 0$ ), and the distortion of the channel by the laser

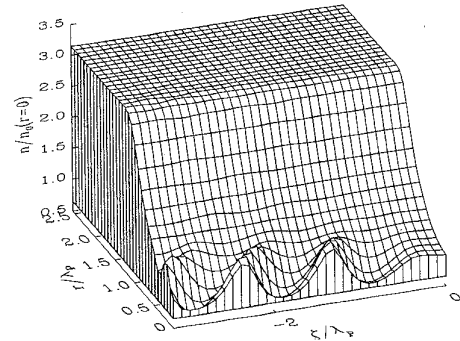


Fig. 23. Surface plot of the plasma electron density  $n/n_0$  at  $c\tau = 20Z_R$  for a channel-guided LWFA. The initial density profile is parabolic with a depth given by  $\Delta n = 1/\pi r_e r_s^2$  (from [97]).

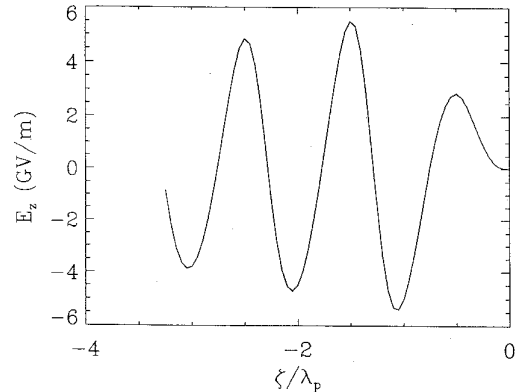


Fig. 24. Axial electric field  $E_z$  on axis at  $c\tau = 20Z_R$  for the channel-guided LWFA of Fig. 23 (from [97]).

pulse, including the excitation of a large amplitude wakefield along the axis, is evident in the region  $\zeta < 0$ . A plot of the axial electric field along the axis at  $c\tau = 20Z_R$  is shown in Fig. 24. The effect of the wakefield on a continuous electron beam with an initial normalized emittance  $\epsilon_n = 1.0 \text{ mm-mrad}$ , rms radius  $r_b = 10 \mu\text{m}$ , and energy  $E_b = 2 \text{ MeV}$  was also simulated. After  $c\tau = 20 \text{ cm}$ , approximately 70% of the beam electrons were trapped and accelerated. The peak electron energy increases nearly linearly with propagation distance with an average acceleration gradient of  $5.25 \text{ GeV/m}$  ( $1 \text{ GeV}$  in  $20 \text{ cm}$ ).

The above discussion applies to essentially parabolic channel profiles. Other channel profiles, however, may offer different advantages. Durfee *et al.* [176] discuss the formation of “leaky” channels, in which the channel is approximately parabolic out to some radius, after which the density falls off to zero, as shown in Fig. 25. Higher order transverse modes may not be guided by such a channel, and Antonson and Mora [179] have described how leaky channels can stabilize certain instabilities, such as small angle forward Raman scattering [109], [114], self-modulation [111]–[113], and laser-hosing [180], [181]. Hollow channels (e.g., a square channel with density zero on axis out to the channel radius) may also have some beneficial properties with regard to acceleration [64], [98]–[100]. Within the channel, where the plasma density is

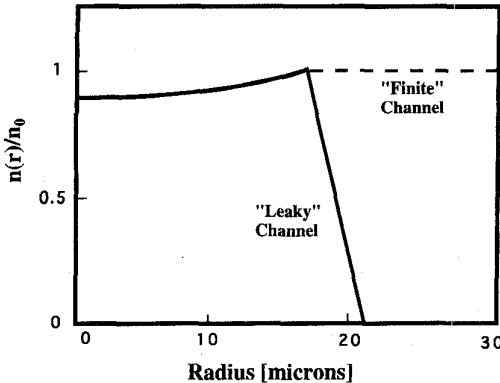


Fig. 25. Schematic of the radial profile of the plasma density for a leaky and nonleaky channel (from [179]).

zero, the transverse profile of the axial wakefield is uniform, thus providing uniform acceleration of an injected beam [100]. The wakefield in such a channel, however, may be damped due to resonant absorption in the channel walls [182].

#### D. Ponderomotive Self-Channeling

The radial ponderomotive force of a long laser pulse propagating in an initially uniform plasma can expel electrons from the axis thus creating a density channel (i.e., self-channeling) [96], [160], [161], [164]–[174]. This can enhance the effects of relativistic self-focusing. Consider a long axially uniform laser pulse propagating in an initially uniform plasma. The steady-state radial force balances indicates that the space-charge force is equal to the ponderomotive force, i.e.,  $\nabla_{\perp}\phi = \nabla_{\perp}\gamma_{\perp}$ , where  $\gamma_{\perp} = (1 + a^2)^{1/2}$  (circular polarization). This implies a density perturbation via Poisson's equation,  $\nabla_{\perp}^2\phi = k_p^2\delta n/n_0$ , given by [96], [160], [161], [164], [165]

$$\delta n/n_0 = k_p^{-2}\nabla_{\perp}^2(1 + a^2)^{1/2} \quad (55)$$

assuming  $|\delta n/n_0| \leq 1$ . In the limit  $a^2 \ll 1$ , a Gaussian laser pulse  $a^2 = a_0^2 \exp(-2r^2/r_0^2)$  creates a Gaussian density channel  $\delta n = -\delta n(0)(1 - 2r^2/r_0^2)\exp(-2r^2/r_0^2)$ . Along the axis, the depth of the ponderomotive channel is given by

$$\delta n(0) = a_0^2\Delta n_c \quad (56)$$

where  $\Delta n_c$  is given by (53). Analysis of the paraxial wave equation with a density perturbation given by  $\delta n/n_0 = k_p^{-2}\nabla_{\perp}^2a^2/2$  indicates that the normalized spot size of a Gaussian laser pulse evolves according to [164]

$$\frac{d^2R}{dz^2} = \frac{1}{Z_R^2 R^3} \left( 1 - \frac{P}{P_c} - \frac{\delta n(0)}{2\Delta n_c} R^{-2} \right) \quad (57)$$

where  $\delta n(0)$  is given by (56) and  $a^2 \ll 1$  was assumed. Hence, in the limit  $P/P_c \ll 1$ , the ponderomotive channel depth required to guide a laser pulse is  $\delta n(0) \geq 2\Delta n_c$ . Clearly, when  $a_0 < 1$ , ponderomotive self-channeling alone will not guide the laser pulse. Furthermore,  $|\delta n/n_0| < 1$  implies  $a_0^2 < 2(P/P_c)^{1/2}$  and  $\delta n(0) < 2(P/P_c)^{1/2}\Delta n_c$ . Hence,  $P/P_c \leq 1$  implies  $\delta n(0) < 2\Delta n_c$ , which again indicates that the ponderomotive channel alone will not guide the laser pulse. For laser powers approaching the critical power

$P \rightarrow P_c$ , guiding is achieved predominantly by relativistic self-focusing. Ponderomotive self-channeling can enhance this effect, but does not dramatically alter the power threshold for guiding. More detailed studies [160], [165] that include the effects of relativistic self-focusing and ponderomotive self-channeling conclude that the threshold power for guiding is  $P \geq 16.2(\omega^2/\omega_p^2)$  GW.

#### E. Plasma Wave Guiding

In Section III-E, it was discussed how an ultrashort ( $L < \lambda_p$ ) laser pulse could be frequency upshifted if properly phased within a plasma wave wakefield. Similarly, it is possible for an ultrashort laser pulse to be guided by a plasma wave, if the laser pulse is properly phased within the wakefield [69], [88], [89]. The effective index of refraction for a low power  $P/P_c \ll 1$ , low intensity  $a^2 \ll 1$  laser pulse propagating in a plasma wave is given by

$$\eta_R \simeq 1 - (\omega_p^2/2\omega^2)(1 + \delta n/n_0) \quad (58)$$

where  $\delta n$  is the density oscillation of the plasma wave and it is assumed that the plasma wave remains unaffected by the laser pulse. Consider a 3-D plasma wave of the form  $\delta n = \delta \hat{n}(r) \sin k_p(z - ct)$ , i.e., where  $d\delta \hat{n}/dr < 0$  and  $\delta \hat{n} > 0$ . In regions where  $\sin k_p \zeta < 0$ , the plasma wave acts as a local density channel and enhances focusing, in regions where  $\sin k_p \zeta > 0$ , the plasma wave enhances diffraction.

The evolution of a “test” laser pulse in an externally generated plasma wave can be analyzed using the paraxial wave equation. Consider a 3-D nonevolving plasma wave of the form  $\delta n = \delta n_0 \sin k_p(z - ct) \exp(-2r^2/r_p^2)$ , i.e., the plasma wave has a Gaussian radial profile with a radius  $r_p$  and a phase velocity  $v_p \simeq c$ . It can be shown that the spot size  $r_s$  of a Gaussian laser pulse evolves according to [69]

$$\frac{d^2R}{dz^2} = \frac{1}{Z_R^2 R^3} \left[ 1 + \frac{2\delta n_0 R_p^2 \sin k_p \zeta}{\Delta n_c (1 + R_p^2/R^2)^2} \right] \quad (59)$$

where  $\Delta n_c = 1/\pi r_e r_0^2$  is the critical channel depth,  $R_p = r_p/r_0$ , and  $P/P_c \ll 1$  and  $a^2 \ll 1$  have been assumed. Consider an ultrashort pulse  $L \ll \lambda_p$  centered about  $k_p \zeta = -\pi/2$  such that  $\sin k_p \zeta \simeq -1$ . Equation (59) indicates that this pulse will be guided by the plasma wave,  $r_s = r_0$ , provided [69]

$$\delta n_0 \geq \Delta n_c (1 + R_p^2)^2 / 2R_p^2. \quad (60)$$

For  $r_p = r_0$ , this gives  $\delta n_0 \geq 2\Delta n_c$ . Notice that a test laser pulse experiences maximum focusing at the minimum of  $\delta n$  (e.g.,  $k_p \zeta = -\pi/2$ ); whereas maximum frequency upshifting occurs at the maximum of  $-d\delta n/d\zeta$  (e.g.,  $k_p \zeta = -\pi$ ). In general, for a sinusoidal plasma wave, a test laser pulse will experience both enhanced focusing and frequency upshifting over a  $|k_p \Delta \zeta| = \pi/4$  phase region of the plasma wave. Furthermore, (59) describes how a plasma wave can lead to the modulation of a long ( $L > \lambda_p$ ) laser pulse [69], as illustrated schematically in Fig. 26.

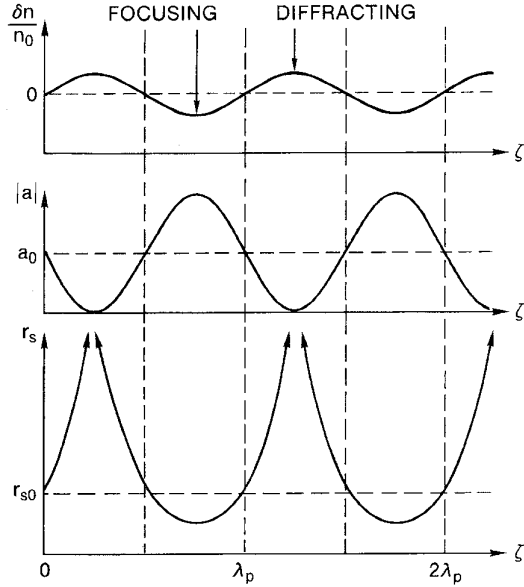


Fig. 26. Schematic of the focusing effects of an externally generated plasma wave on an initially uniform, low intensity radiation beam. This illustrates the tendency for the radiation to form beamlets which are optically guided in the regions of minimum density (from [69]).

#### F. Self-Modulation of Guided Laser Pulses

In the absence of instabilities, a long laser pulse,  $L > \lambda_p$ , with a power above the guiding threshold,  $P > P_c(1 - \Delta n/\Delta n_c)$ , can be, in principle, optically guided. Since the pulse is long, however, it is subject to various instabilities, e.g., stimulated Raman scattering and hose-modulation instabilities, as are discussed in Section VII. One optical guiding phenomena which can affect a long pulse is envelope self-modulation [96], [97], [108]–[117], wherein the laser pulse intensity becomes severely modulated at the plasma wavelength  $\lambda_p$ . Specifically, a plasma wave, excited initially by the ponderomotive force associated the finite rise of the laser pulse, can strongly affect the focusing properties of the pulse body by introducing periodic regions of enhanced focusing and diffraction [69].

The process of envelope self-modulation can be understood by considering a long laser pulse,  $L \gg \lambda_p$ , with  $P = P_c(1 - \Delta n/\Delta n_c)$  on which a finite wakefield exists. The plasma density modulation of the wake is of the form  $\delta n = \delta n_0(r) \cos(k_p \zeta)$ , which modifies the plasma refractive index, as indicated by (46) and (58). This density oscillation acts on the laser pulse as an axially periodic density channel. In regions of a local density channel, i.e., where  $\partial \delta n / \partial r > 0$ , the radiation focuses. In regions where  $\partial \delta n / \partial r < 0$ , diffraction is enhanced. This causes the laser pulse envelope to become modulated at  $\lambda_p$ , which subsequently enhances the growth of the plasma wave, and the process proceeds in a highly nonlinear manner. The end result can be a fully self-modulated laser pulse, composed of a series of laser “beamlets” of length  $\simeq \lambda_p/2$ , which can remain optically guided over several Rayleigh lengths. Associated with the periodic beamlet structure are large amplitude wakefields which can trap and accelerate a trailing electron beam [110].

This process forms the basis of the self-modulated LWFA discussed in Section V-D.

It should be noted that self-modulation, as described above, is an inherently 2-D effect, i.e., the plasma wave leads to enhanced focusing/diffraction and modulation results from a radial transport of laser pulse energy. In the 1-D limit, however, modulation can result via forward Raman scattering and an axial transport of laser pulse energy. The remainder of this section is concerned primarily with self-modulation in the 2-D limit. Forward Raman scattering is discussed further in Section VII-A.

An equation for the evolution of the laser spot size can be derived by analyzing the paraxial wave equation with an index of refraction of the form given by (46), assuming an initial density profile which is parabolic,  $n^{(0)} = n_0 + \Delta n r^2/r_0^2$ , and the self-consistent plasma response,  $(\partial^2/\partial \zeta^2 + k_p^2)\phi = k_p^2 a^2/2$ . In the limits  $a^2 \ll 1$  and  $r_0^2 k_p^2 \gg 1$ , the spot size evolves according to [111]

$$\frac{\partial^2 R}{\partial \hat{\tau}^2} = \frac{1}{R^3} \left( 1 - \frac{P}{P_c} - \frac{\Delta n}{\Delta n_c} R^4 \right) \\ = 4R \int_0^\zeta d\zeta' \cos k_p(\zeta' - \zeta) \frac{\partial}{\partial \zeta'} \frac{P(\zeta')/P_c}{[R^2(\zeta) + R^2(\zeta')]^2} \quad (61)$$

where  $R = r_s/r_0$ ,  $\zeta = z - ct$ , and  $\hat{\tau} = c\tau/Z_R$ . The second, third, and fourth terms on the left in (61) represent the effects of vacuum diffraction, relativistic focusing, and channel focusing, respectively, whereas the term on the right side represents the nonlinear coupling of the envelope to the plasma wave. Equation (61) correctly describes well-known laser pulse evolution, such as the inability of relativistic guiding to prevent the diffraction of short pulses  $L < \lambda_p$  [88], [89], [96].

The evolution of a long axially uniform laser beam can be examined in the limit where the effects of the plasma wave are neglected, i.e., the nonlinear coupling term on the right side of (61) is set equal to zero. Matched beam propagation ( $r_s = r_0 = \text{constant}$ ) requires that the power satisfy [111], [169]  $1 - P/P_c - \Delta n/\Delta n_c = 0$ . In general, it can be shown that the spot size will remain guided (oscillate about its matched beam value) when  $1 - P/P_c - \Delta n/\Delta n_c \leq 0$ .

The effects of the plasma wave on the spot size evolution can be examined by including the right side of (61). The initial effects of the plasma wave on the spot size can be estimated by approximating  $R(\zeta') = R(\zeta)$  within the integral in (61), i.e., initially the spot size is uniform throughout the pulse. Equation (61) takes on the form

$$\frac{\partial^2 R}{\partial \hat{\tau}^2} = \frac{1}{R^3} \left( 1 - \frac{P}{P_c} - \frac{\delta n}{2\Delta n_c} - \frac{\Delta n}{\Delta n_c} R^4 \right) \quad (62)$$

where  $\delta n$  is the initial density perturbation given by

$$\frac{\delta n}{n_0} = \int_0^\zeta d\zeta' \cos k_p(\zeta - \zeta') \frac{\partial}{\partial \zeta'} \frac{a^2(\zeta')}{2}. \quad (63)$$

The rise associated with the front of the pulse gives a nonzero value of  $\partial a^2 / \partial \zeta$  which generates a finite amplitude density wake. Throughout the body of a long flat-top pulse, this density wake has the form  $\delta n = \delta n_0 \cos k_p \zeta$ . Clearly, the effect of

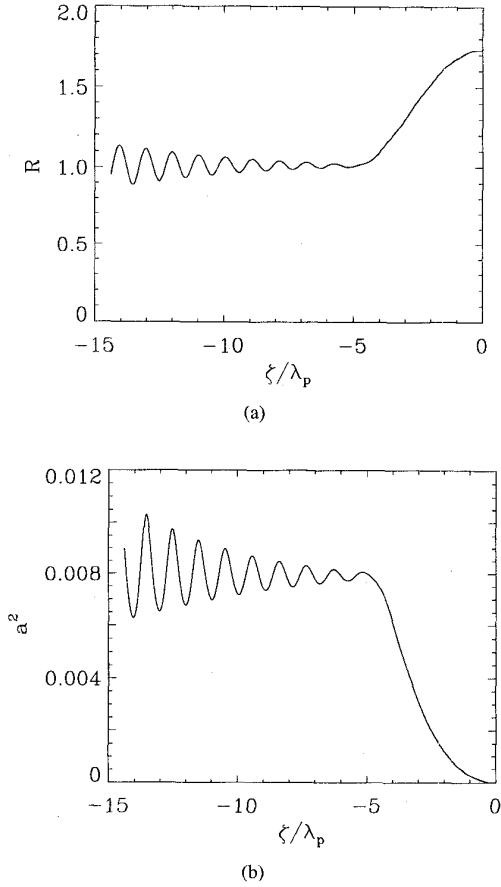


Fig. 27. Numerical solution of (61) showing self-modulation: (a) the normalized spot size  $R = r_s/r_0$  and (b) the normalized envelope profile  $a^2$  versus  $\zeta$  at  $c\tau = 1.4Z_R$ . Initially, the spot size is uniform and the intensity has a slow rise followed by a long flat-top region ( $\zeta \leq -5\lambda_p$ ) with  $P = P_c$ .

the  $\delta n(\zeta)$  term in (62) is to produce  $\zeta$ -periodic regions of enhanced focusing and diffraction [69]. This leads to self-modulation.

Pulse modulation is illustrated by a simulation of a long pulse (a long rise,  $L_{\text{rise}} = 5\lambda_p$ , followed by a long flat-top region,  $L_{\text{flat}} = 15\lambda_p$ ) with  $\Delta n = 0$  and  $P = P_c$  ( $a_0 = 0.09$ ,  $r_s = 10\lambda_p$ ), as obtained by numerically solving (61). Fig. 27 shows the evolution of 1) the normalized spot size  $R$  (initially,  $R = 1$ ), and 2) the normalized intensity on axis  $|\hat{a}_f|^2 = a_0^2(\tau = 0)/R^2$ , plotted versus  $\zeta$  at  $c\tau = 1.4Z_R$ . Note that the front portion of the pulse with  $P < P_c$  is diffracting. Clearly, the modulation is growing as a function of both the propagation distance and the distance behind the pulse front. Simulations [111] indicate that strong self-modulation occurs when  $P \geq P_M$ , where  $P_M = P_c(1 - \Delta n/\Delta n_c)$  is the threshold power for guiding. For  $P < P_M/2$  modulation is reduced, since the pulse envelope is everywhere (at all  $\zeta$ ) diffracting. This is illustrated in Fig. 28, where the normalized modulation amplitude  $\delta R/\langle R \rangle$  is plotted versus  $c\tau/Z_R$ , where  $\langle R \rangle$  is the  $\zeta$ -averaged value of  $R$ , as obtained from (61) for a flat-top pulse profile with  $L_{\text{rise}} = 0.1\lambda_p$ ,  $\Delta n = 0$ , and  $P/P_c = 0.25$ , 0.5, and 0.75. The specific growth rates for the self-modulation instability are discussed in Section VII-B. A fluid simulation

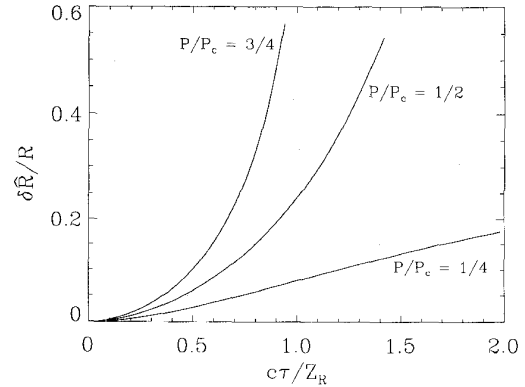


Fig. 28. Numerical solution of (61) showing the normalized modulation amplitude  $\delta \hat{R}/\langle R \rangle$  versus  $c\tau$  for a flat-top pulse with  $L_{\text{rise}} = 0.1\lambda_p$  and  $P/P_c = 0.25$ , 0.5, and 0.75 (from [111]).

of the self-modulated LWFA, including the effects of forward Raman scattering, is presented in Section V-D.

#### G. Optical Guiding Experiments

Several recent experiments have observed some form of optical guiding [172]–[178], [183], [184]. Multifoci have been observed for short pulses propagating in a gas at powers well below the critical power for relativistic self-focusing in a plasma [183]. In the neutral gas, the pulse self-focuses due to nonlinear effects associated with the refractive index. As the pulse focuses, the intensity exceeds the ionization threshold, thus forming a plasma. Within the plasma, the pulse diffracts. In such a way multiple ionization “sparks” were observed [183]. More recently, short (100 fs) pulses were observed to propagate over 20 m in air with a significant portion of the initial pulse energy trapped in a filament of radius  $r_0 = 40 \mu\text{m}$  with an intensity near  $10^{14} \text{ W/cm}^2$  [184]. This mode of propagation may result from a balance between self-focusing in the neutral gas and diffraction due to plasma formation [184], [185]. It is not clear that this is the case in the experiment, however, since some fraction of the initial laser pulse energy exists out to a large radius ( $\sim 1 \text{ cm}$ ). At higher intensities, short pulses propagating in gas were observed to diffract more quickly than they would in vacuum, since the ionization taking place at the front of the pulse can create a plasma density profile which is peaked on axis thus causing ionization induced refraction [79].

The guiding of modest intensity (up to  $10^{14} \text{ W/cm}^2$ ) laser pulses by preformed plasma density channels has been experimentally demonstrated by Durfee *et al.* [175], [176]. In these experiments, a pump laser pulse was passed through an axicon lens to create a long ( $\lesssim 2 \text{ cm}$ ) focus in a gas. The pump pulse ionized and heated the gas, creating a long plasma channel by hydrodynamic expansion. A second probe pulse was propagated along the axis of the channel. Up to 75% of the probe pulse energy was guided in the channel over a distance up to  $70Z_R$  (2.2 cm). These experiments were well diagnosed and simulated, and single mode, multimode, and “leaky” mode propagation of the channeled beam were observed.

Density channels have also been formed by other methods [177], [178]. In a laser preionized high-density (25% critical)

plasma, channels were formed [177] by a relatively long pulse (500 ps) laser with intensities near  $10^{16} \text{ W/cm}^2$ . A channel was formed, 800  $\mu\text{m}$  long by 100  $\mu\text{m}$  wide, extending the entire length of the initial plasma, with a depth near 50% of the initial density. Capillary discharges [178] have been used to create long (1 cm), axially uniform channels in high density ( $10^{20} \text{ cm}^{-3}$ ) plasma with radii on the order of 25–50  $\mu\text{m}$ . Initial experiments [178] have demonstrated that such a channel is capable of guiding of short (100 fs), intense ( $10^{17} \text{ W/cm}^2$ ) laser pulses in one and two dimensions.

Experiments on relativistic guiding and ponderomotive self-channeling have also been performed [172]–[174]. Borisov *et al.* report the propagation of a 270-fs KrF laser (248 nm) pulse over a distance of 3–4 mm ( $>100Z_R$ ) through a noble gas at a pressure of 1–5 atm [173]. The channel radius was approximately 1.5  $\mu\text{m}$ , the laser intensity was near  $5 \times 10^{18} \text{ W/cm}^2$ , and the plasma density was on the order of  $10^{21} \text{ cm}^{-3}$ . Since the laser power was somewhat above the relativistic guiding threshold, the long propagation distance was attributed to a combination of relativistic guiding and ponderomotive self-channeling. Monot *et al.* [174] report the propagation of a 1- $\mu\text{m}$  15-TW 400-fs laser pulse through a pulsed hydrogen gas jet ( $n_e \simeq 10^{19} \text{ cm}^{-3}$ ). For powers above the critical power for relativistic guiding, the laser pulse, with an intensity near  $10^{19} \text{ W/cm}^2$ , was observed to propagate through the entire 3 mm length ( $\simeq 10Z_R$ ) of the gas jet.

## VII. LASER-PLASMA INSTABILITIES

Laser-plasma instabilities can limit the laser propagation distance and degrade the performance of a laser-driven accelerator. This section will provide a brief overview of a few instabilities which are relevant to laser-driven accelerators: stimulated forward and backward Raman scattering [124], [186]–[203], self-modulation [108]–[114], and laser-hose instabilities [180], [181]. Other instabilities, such as parametric coupling to ion modes, which have been observed in PBWA experiments [73], [74], will not be discussed.

### A. Stimulated Raman Scattering

Stimulated Raman scattering involves the interaction of a light wave with an electron plasma wave [124], [186]–[188]. In its most basic form, it consists of the decay of the pump laser field, of frequency and wave vector ( $\omega_0, k_0$ ), into an electron plasma wave ( $\omega, k$ ) and two daughter light waves, namely a Stokes wave ( $\omega_0 - \omega, k_0 - k$ ) and an anti-Stokes wave ( $\omega_0 + \omega, k_0 + k$ ). Typically,  $\omega \simeq \omega_p + i\Gamma$  where the growth rate  $\Gamma$  is usually obtained through a standard linear instability analysis. In such an analysis, the pump laser field is assumed to be a 1-D plane wave of the form  $a_p \sim a_0 \exp(i(k_0 z - \omega_0 t))$ . Perturbations are introduced,  $\delta a \sim \exp(i(\mathbf{k} \cdot \mathbf{r} - \omega t))$  and the linearized equations are then solved to determine the behavior of the instability. Since the pump laser is assumed to be a 1-D plane wave, the 3-D evolution of the pump laser is not taken into consideration. In particular, the effects of diffraction and self-focusing are neglected. Strictly speaking, the resulting analysis is only valid for times short compared to the characteristic evolution time  $T_E$  of the pump laser, e.g.,

$t < T_E \sim Z_R/c$ . In practice, however, the growth rates obtained from such an analysis can be adequate estimates provided that the mode frequency and growth rate are large compared to  $T_E^{-1}$ .

For an infinite 1-D plane wave pump field, the purely temporal growth rates, i.e.,  $\delta a \sim \exp(\Gamma t)$  with  $\Gamma$  independent of  $t$ , can be obtained in a straightforward manner. The basic treatment of forward and backward Raman scattering is presented by Kruer [124]. Temporal growth rates for the various Raman modes in various regimes have been recently summarized by Antonson and Mora [109]. For short laser pulses, however, the growth and propagation of the instability with respect to the laser pulse front must be correctly taken into consideration. Antonson and Mora [109] first applied convective instability analysis, or a spatial-temporal analysis, to Raman instabilities to account for the short-pulse nature of the instability. Such an analysis, in effect, yields growth rates which are a function of both space and time.

1) *Backward Raman Scattering*: In backward Raman scattering (BRS), the pump wave ( $\omega_0, k_0$ ) decays into a plasma wave ( $\omega, k$ ) and a backward going scattered wave ( $\omega_0 - \omega, k_0 - k$ ), where  $\omega \simeq \omega_p$  and  $k \simeq 2k_0$ . The standard temporal growth rate [124], in the limits  $a_0^2 \ll 1$  and  $\omega_p \ll \omega_0$ , i.e., the weakly coupled regime, is  $\Gamma = (a_0/2)(\omega_p \omega_0)^{1/2}$ . In general, the scattered mode can propagate at some angle  $\theta$  with respect to the pump wave (sidescatter), and the growth rate is given by  $\sin \theta/2$  times the BRS result. The spatial-temporal analysis indicates that the number of *e*-folds of the BRS instability,  $N_e = \Gamma t$ , is given by [109]

$$N_e \simeq (a_0^2 k_p k_0 / 8)^{1/2} |\zeta|. \quad (64)$$

In effect, since the scattered wave is moving opposite to the pump, the temporal growth is modified by  $ct \rightarrow |\zeta|/2$ , where  $\zeta = z - ct$  is a measure of the distance back from the front of the laser pulse.

Typically, BRS is the fastest growing of the SRS instabilities. In laser-plasma accelerators, BRS is significant for a number of reasons. At low pump laser intensities, the spectrum of the backscattered radiation can be used to determine  $\omega - \omega_p$  and, hence, the plasma density can be determined experimentally. For high pump intensities, however, it has been observed that the backscattered spectrum broadens [196] and, in some cases, becomes extremely broad [203], so that the  $\omega - \omega_p$  peak can no longer be distinguished. Raman sidescatter and backscatter can erode the back of a long pulse,  $L > \lambda_p$ , since energy is being transported out of the pulse. This has been observed in fluid [109], [113] and particle simulations [115], [116]. At very high intensities, simulations [115] indicate that BRS erodes the front portion of a long pulse in the high-density self-modulated regime. In the body of the pulse, BRS is suppressed, possibly due to plasma heating.

As the BRS mode grows to large amplitude, it can trap the background plasma electrons, thus heating the plasma and creating a fast tail on the electron distribution. The phase velocity of the BRS plasma wave is  $v_p = \omega/k = \omega_p/2k_0 \ll c$ . Since  $v_p/c \ll 1$ , the plasma wave can trap the background thermal electrons. The resulting fast electrons can be sub-

sequently trapped by Raman scattered modes propagating at smaller angles  $\theta$ , which will accelerate the electrons to higher energies [18], [189], [199]. Eventually, these background electrons can be trapped and accelerated to very high energies by the plasma wave associated with the forward Raman instability or the self-modulation instability, which has  $v_p \simeq c$ . This mechanism may explain how background plasma electrons can be trapped and accelerated to high energies, as is observed in recent experiments [31]–[35] on and simulations [115], [116] of the self-modulated LWFA (i.e., a laser pulse in the high-density self-modulated/forward Raman scattering regime). Direct wavebreaking of a relativistic plasma wave can also result in the acceleration of background plasma electrons [33].

For high pump intensities, theory predicts that stimulated backscattering occurs in the strongly coupled or Compton regime [109], [186]–[188] for which  $|\omega - \omega_0| \sim \Gamma \gg \omega_p$ . In addition, 1-D nonlinear theory predicts that for a linearly polarized pump laser field, stimulated backscattered harmonic (SBH) radiation can be generated [192], [193] at frequencies given approximately by  $\omega = N\omega_0$ , where  $N = 2\ell + 1$  and  $\ell$  is an integer, i.e., odd harmonics. The temporal growth rate of the SBH radiation is given by

$$\Gamma = \sqrt{3}\omega_0 \left( \frac{\omega_p^2 F_\ell}{4\omega_0^2 \gamma_{\perp 0}} \right)^{1/3} \quad (65)$$

where  $\gamma_{\perp 0} = (1 + a_0/2)^{1/2}$ ,  $F_\ell = b[J_\ell(b) - J_{\ell+1}(b)]^2$  is the harmonic coupling function, and  $b = (2\ell + 1)a_0^2/4\gamma_{\perp 0}^2$ . Equation (65) is valid for arbitrary laser intensities  $a_0$ . For  $a_0 \ll 1$ , the growth rate of the fundamental ( $\omega = \omega_0$ ) backscattered mode is given by  $\Gamma/\omega_0 = \sqrt{3}(\omega_p a_0/4\omega_0)^{2/3}$ . The function  $F_\ell^{1/3}$ , proportional to the growth rate, is plotted in Fig. 29 [192], [193] versus  $a_0^2/4\gamma_{\perp 0}^2$  for various harmonics  $N = (2\ell + 1)$ . It is clear that the generation of higher harmonics requires  $a_0 \gtrsim 1$ . Thermal effects, i.e., trapping of the background plasma electrons, can severely limit the generation of higher harmonics [192], [193]. For example, to observe the third (fifth) harmonic using a  $\lambda_0 = 1 \mu\text{m}$ ,  $a_0 = 2.6$  laser in a plasma of density  $n_0 = 10^{19} \text{ cm}^{-3}$ , the longitudinal energy spread on the plasma electrons must satisfy  $E_{\text{th}} < 77 \text{ eV}$  (22 eV).

2) *Forward Raman Scattering*: In forward Raman scattering (FRS) [124], [186]–[188], the scattered waves propagate parallel (or nearly parallel) to the pump wave, and the associated plasma wave has a phase velocity  $v_p \simeq c$ . Hence, the plasma wave can be used to accelerate electrons to ultrahigh energies. The FRS instability can serve as the basis for an LWFA [1], [18], [114], in which a single long ( $L > \lambda_p$ ) laser pulse becomes modulated via FRS and drives a large amplitude plasma wave. As with the envelope self-modulation instability described below, FRS can be used to drive a the self-modulated LWFA [108]–[116].

The physical mechanism of FRS can be understood by the following 1-D description [114]. Consider a long uniform laser pulse propagating in the presence of an initially small amplitude plasma wave of the form  $\delta n = \delta n_0 \sin k_p \zeta$  with

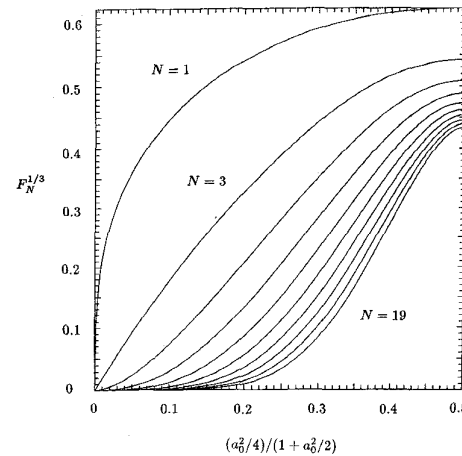


Fig. 29. The function  $F_N^{1/3}$ , proportional to the growth rate of the SBH radiation, versus the parameter  $(a_0^2/4)/(1 + a_0^2/2)$  (from [192]).

$\delta n_0 > 0$ . Since the local group velocity  $v_g$  is given by  $v_g/c \simeq 1 - \omega_p^2(\zeta)/2\omega_0^2$ , the local group velocity decreases in regions where  $\delta n > 0$  and increases in regions where  $\delta n < 0$ . This tends to modulate the laser pulse such that the intensity modulations are 90 degrees out of phase with the density wave, i.e.,  $a \simeq a_0 + \delta a$ , where  $\delta a = \delta a_0 \cos k_p \zeta$  and  $\delta a_0 > 0$ . This intensity modulation feeds back via  $(\partial^2/\partial \zeta^2 + k_p^2)\delta n/n_0 = (\partial^2/\partial \zeta^2)a^2/2$  and drives the plasma wave to larger amplitudes, thus resulting in the FRS instability.

Several regimes of the FRS can be identified [109], [114], [194], such as a four-wave regime, in which both  $\omega_0 \pm \omega_p$  modes are resonant, and a three-wave regime, in which only  $\omega_0 - \omega_p$  is resonant with the pump laser and the plasma wave. The temporal growth rate in the four-wave resonant regime is  $\Gamma_R = \omega_p^2 a_0 / 2\sqrt{2}\omega_0$ , the temporal growth rate in the four-wave nonresonant regime is  $\Gamma_N = \sqrt{3}\omega_p(a_0\omega_p^2/4\omega_0^2)^{2/3}/2$ , and the temporal growth rate in the three-wave regime is  $\Gamma_3 = \omega_p a_0 (\omega_p/\omega_0)^{1/2}/4$ . The spatial-temporal analysis [109], [110], [114], [198] indicates, however, that as the FRS instability grows, it passes through these various regimes, depending on the relative value of  $|\zeta|/\tau$ , where  $\zeta = z - ct$  and  $\tau = t$  are the independent coordinates. The number of  $e$ -foldings for these three FRS modes and the corresponding spatial-temporal regimes are roughly given by [109], [110], [114]

$$N_e \simeq 2\Gamma_R(|\zeta|\tau/c)^{1/2}, \text{ for } a_0^2|\zeta|/\tau \gg 2\omega_p^2/\omega_0^2 \quad (66)$$

$$N_e \simeq 1.5\Gamma_N(4|\zeta|\tau^2/c)^{1/3}, \\ \text{for } 16\omega_p^5/\omega_0^5 \ll a_0^2|\zeta|/\tau \ll 2\omega_p^2/\omega_0^2 \quad (67)$$

$$N_e \simeq 2\Gamma_3(|\zeta|\tau/c)^{1/2}, \text{ for } a_0^2|\zeta|/\tau \ll 16\omega_p^5/\omega_0^5 \quad (68)$$

where  $a_0^2 \ll 1$ ,  $\omega_p^2/\omega_0^2 \ll 1$  are assumed. Decker *et al.* [114] describe that, for a fixed  $\zeta$  within the pulse, the FRS instability transitions through the various regimes as a function of time.

The above results, (66)–(68), describe direct FRS for which  $\theta = 0$ , where  $\mathbf{k}_s \cdot \mathbf{k}_0 = k_s k_0 \cos \theta$ , i.e.,  $\theta$  is the angle between the pump  $\mathbf{k}_0$  and scattered  $\mathbf{k}_s$  wave vectors. Similar analyses [109], [114] can be applied to describe near FRS and Raman

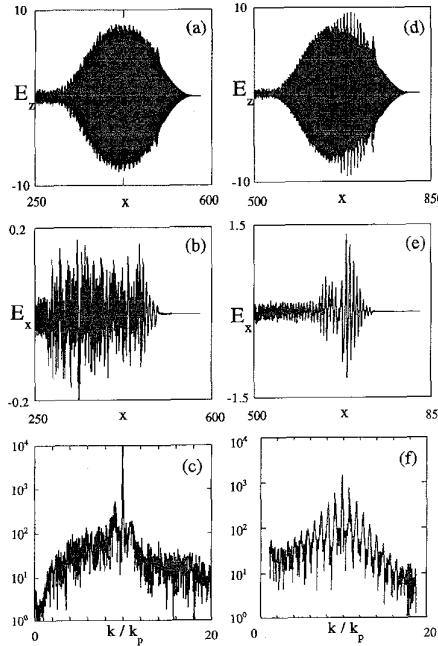


Fig. 30. Results of a 1-D particle simulation of forward Raman scattering with  $a_0 = 0.8$ ,  $\omega/\omega_p = 10.0$ , and  $L = 150c/\omega_p$ : (a) laser field  $E_L/E_0$ , (b) plasma wave field  $E_z/E_0$ , and (c) Fourier spectrum  $E_L(k)$  at  $\omega_p t = 250$ , (d) laser field, (e) plasma wave field, and (f) Fourier spectrum at  $\omega_p t = 500$ . The  $z$  axis is in units of  $c/\omega_p$  (from [115]).

sidescatter, in which the scattered wave propagates at a finite angle  $\theta$  (i.e.,  $k_{s\perp} \neq 0$ ), assuming a plane wave pump field. For example, Antonson and Mora [109] describe small angle FRS and find a growth rate similar to (68) (proportional to  $\Gamma_3$ ). Decker *et al.* [114] describe a four-wave nonresonant regime of near FRS, the growth rate of which depends on  $k_{s\perp}$ . Furthermore, when  $k_{s\perp} = 1/r_0$ , the growth rate of the four-wave nonresonant regime of near FRS has an identical scaling to that of the envelope self-modulation instability [111] in the long-pulse regime, as discussed in the following section.

As a side note, the paraxial approximation to the wave operator,  $(\nabla_\perp^2 + 2ik_0\partial/\partial c\tau)$  is not sufficient to describe direct ( $\theta = 0$ ) FRS. Direct FRS requires an axial transport of laser energy (within the  $\zeta = z - ct$  frame) and an axial modulation of the laser power. In the paraxial approximation, however, the laser group velocity is effectively  $c$  and an axial transport of energy from one  $\zeta$  location to another is not possible. Retention of the term  $(\nabla_\perp^2 + 2\partial^2/\partial\zeta\partial c\tau)$  is necessary to describe on-axis FRS. This was done in the fluid simulation of the self-modulated LWFA presented in Section V-D, i.e., the effects of both the FRS and self-modulation instabilities are included.

The growth rates presented for both the BRS mode, (64), and the FRS modes, (66)–(68), assumed a plane wave pump field with  $a_0^2 \ll 1$  (low intensity limit). For a circularly polarized plane wave pump field, these results can be generalized [114], [198] to describe the regime  $a_0 \gtrsim 1$  by substituting  $a_0 \rightarrow a_0/\gamma_\perp$  and  $\omega_p^2 \rightarrow \omega_p^2/\gamma_\perp$  into the expressions for the growth rates, where  $\gamma_\perp = (1 + a_0^2)^{1/2}$ .

In addition, it is also possible for an FRS mode to undergo multiple scattering, sometimes referred to as cascading [18], [67], [115], [186]–[188], resulting in multiple waves with frequencies  $\omega_0 \pm \ell\omega_p$  ( $\ell = \text{integer}$ ). It is possible to interpret this as photon acceleration, or phase-modulation by the plasma wave, of the scattered wave [114]. Numerous high-order Stokes and anti-Stokes lines have been observed in simulations of FRS [115]. The larger the plasma wave amplitude, the larger the number of high-order Stokes/anti-Stokes lines present. Multiple [32]–[35], [117] (up to the fifth [33]) anti-Stokes lines have been observed in FRS/self-modulated LWFA experiments.

A 1-D particle simulation [115] of FRS is presented in Fig. 30 for a  $1 \mu\text{m}$  laser pulse with a 600 fs rise time and an intensity  $I = 8.9 \times 10^{17} \text{ W/cm}^2$  propagation through a plasma of density  $n_0 = 10^{19} \text{ cm}^{-3}$  (approximately corresponding to the experiments of [196]), i.e.,  $a_0 = 0.8$ ,  $\omega_0/\omega_p = 10$ , and  $L = 150c/\omega_p$ . Fig. 30 shows the electric field of the laser pulse, the electric field of the plasma wave, and Fourier spectrum of the laser field at  $\omega_p t = 250$  (1.4 ps) and  $\omega_p t = 500$  (2.8 ps). At  $\omega_p t = 250$ , BRS is dominant and FRS is beginning to occur at the pulse head. BRS depletes the laser energy at the pulse head, creating a steepened front. The ponderomotive force of the steepened front generates a plasma wake which apparently acts as a seed for FRS. This is evident in Fig. 30(a) and (b), where the location of the onset of FRS corresponds to the location of local laser pulse depletion. At  $\omega_p t = 500$ , the laser pulse has become strongly modulated due to FRS and a large amplitude plasma wave is present. The nonlinear state of the modulation leads to spectral cascading, i.e.,  $\omega_0 \pm \ell\omega_p$ , as is clearly evident in Fig. 30(f).

### B. Self-Modulation and Laser-Hose Instabilities

Recently, a formalism has been developed [111], [181] to describe the 3-D evolution laser pulses in plasmas, including the effects of diffraction, relativistic and channel guiding, finite pulse duration, and coupling to the self-consistent plasma wave generated by the pulse structure. This formalism has been used to describe a class of “whole-beam” instabilities, which includes self-modulation [96], [108]–[113] and laser-hose [180], [181] instabilities. In this formalism, equations are derived to describe the evolution of the local laser pulse spot size  $x_s(\zeta, t)$  and the local laser pulse centroid  $x_c(\zeta, t)$ , where the transverse profile of the laser field is assumed to be a Gaussian of the form  $a \sim \exp[-(x - x_c)^2/x_s^2]$  (the  $y$  profile can be similarly defined). The self-modulation instability consists of a periodic “sausaging” of the laser spot size  $x_s$  and the laser-hose consists of a periodic “kinking” of the laser centroid  $x_c$ , as shown schematically in Fig. 31. In their most basic forms, the hose/modulation instabilities are described by spot size and centroid perturbations of the forms  $\delta x_{s,c} \sim \exp(\Gamma_{s,c}t + ik_p\zeta)$ , i.e., they have a period equal to the plasma wavelength  $\lambda_p = 2\pi/k_p$  and a growth rate which is a function of both space and time,  $\Gamma_{s,c} = \Gamma_{s,c}(\zeta, t)$ . Intrinsically, these instabilities involve a coupling to a plasma wave, and the dynamics of the instabilities is determined by the enhanced diffraction and focusing properties of the plasma wave on the laser pulse.

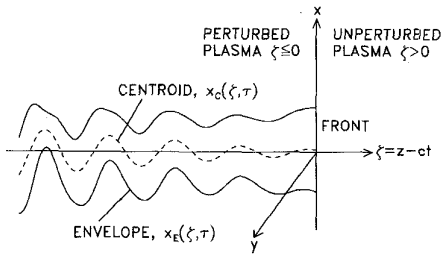


Fig. 31. Schematic of the hose-modulation instability showing the laser pulse centroid  $x_c = x_C$  and envelope  $x_s = x_E$  in the  $\zeta = z - ct$  frame (from [181]).

The physical mechanism underlying self-modulation has been described previously in Section VI-F. The physical mechanism for laser hosing [180], [181] is somewhat similar. Consider a long,  $L > \lambda_p$ , guided laser pulse,  $P/P_c = 1 - \Delta n/\Delta n_c$ , with a centroid which is initially perturbed at the plasma wavelength,  $x_c \simeq x_{c0} \sin k_p \zeta$ , where  $x_{c0} > 0$ . This periodic centroid displacement will drive an asymmetric plasma wave. Notice that for  $x_c^2/x_s^2 \ll 1$ , the intensity profile is approximately  $a^2 \simeq a_0^2(1 + 4xx_c/x_s^2)\exp(-2x^2/x_s^2)$ . At a fixed  $x$  position above the axis,  $x = x_0$ , the laser intensity modulation has the form  $a^2(x_0)/a_0^2 \sim 1 + 4(x_0 x_{c0}/x_s^2) \sin k_p \zeta$ , which drives a plasma wave. At a fixed  $x$  position below the axis,  $x = -x_0$ , the laser intensity is similarly modulated, but 180 degrees out of phase with respect to the  $x = x_0$  modulation. Hence, the plasma wave driven below the axis is 180 degrees out of phase with respect to the plasma wave driven above the axis, which results in an asymmetric (with respect to  $x$ ) plasma wave. Roughly speaking, the plasma wave has the form  $\delta n \sim -\delta n_0(x/x_s) \cos k_p \zeta$ , where  $\delta n_0 > 0$ . The laser pulse will tend to focus into the regions of reduced plasma density. For the asymmetric plasma wave, the laser pulse evolves in such a way as to enhance the initial centroid perturbation and the process proceeds in an unstable manner.

Equations describing the behavior of the spot size  $x_s(\zeta, \tau)$  and centroid  $x_c(\zeta, \tau)$  can be derived by analyzing the paraxial wave equation including the effects of a performed parabolic density channel and the self-consistent plasma response given by (63). In the limits  $a^2 \ll 1$  and  $k_p^2 r_0^2 \gg 1$ ,  $x_s$  and  $x_c$  obey equations of the form [181]

$$\frac{\partial^2 \hat{x}_c}{\partial \hat{\tau}^2} + \frac{\Delta n}{\Delta n_c} \hat{x}_c = -4k_p \int_0^\zeta d\zeta' \sin k_p (\zeta' - \zeta) \times [x_c(\zeta') - x_c(\zeta)] F_c(\zeta', \zeta) \frac{P(\zeta')}{P_c} \quad (69)$$

$$\begin{aligned} \frac{\partial^2 \hat{x}_s}{\partial \hat{\tau}^2} + \left( \frac{\hat{x}_s P}{\hat{y}_s P_c} + \frac{\Delta n}{\Delta n_c} \hat{x}_s^4 - 1 \right) \hat{x}_s^{-3} \\ = 4\hat{x}_s \int_0^\zeta d\zeta' \cos k_p (\zeta' - \zeta) \frac{\partial}{\partial \zeta'} \left[ F_s(\zeta', \zeta) \frac{P(\zeta')}{P_c} \right]. \end{aligned} \quad (70)$$

Also,  $\hat{y}_s$  obeys an equation similar to (70). In the above,  $\hat{x}_c = x_c/r_0$ ,  $\hat{x}_s = x_s/r_0$ ,  $\hat{y}_s = y_s/r_0$ ,  $\hat{\tau} = c\tau/Z_R$ ,  $Z_R = kr_0^2/2$ ,  $\Delta n_c = (\pi r_e r_0^2)^{-1}$  is the critical channel depth, and

$P(\zeta)/P_c = a^2 x_s y_s k_p^2 / 16$  is the laser power over the critical power. The functions  $F_{s,c}(\zeta', \zeta)$ , which depend on  $x_s$ ,  $y_s$ , and  $x_c$ , couple the spot size dynamics to the centroid dynamics. In the absence of a centroid perturbation ( $x_c = 0$ ),  $F_{s,c} = 1$ , the laser pulse remains axisymmetric ( $x_s = y_s = r_s$ ), and (70) reduces to the spot size equation [111], (61), discussed in Section VI-F.

The right side of (69) indicates that if  $x_c(\zeta) = x_c(\zeta')$  initially,  $x_c(\zeta)$  will not increase. Hence, the laser-hose instability requires a nonuniform head-to-tail centroid displacement [181]  $\partial x_c / \partial \zeta \neq 0$ . The right side of (70) indicates that axial gradients in the laser power  $\partial P / \partial \zeta \neq 0$  will lead to modulations in the laser envelopes  $x_s, y_s$ , as discussed in Section VI-F. Both the self-modulation and laser-hose instabilities can occur in either a uniform plasma ( $\Delta n = 0$ ) or in a preformed density channel.

For sufficiently small perturbations,  $x_s/r_0 \ll 1$  and  $x_c/r_0 \ll 1$ , (69) and (70) decouple and self-modulation and the laser-hose instability can be analyzed independently. Asymptotic growth rates can be obtained in various regimes using standard methods [111], [180], [181] by perturbing about the matched beam equilibrium. The number of *e*-folds  $N_e = \Gamma_{c,s}\tau$  in the various regimes is given by [111], [181]

Long pulse regime:  $k_p |\zeta| Z_R / c\tau \gg \alpha_1 P_c / P$

$$N_e = \frac{3\sqrt{3}}{4} \left( \alpha_2 \frac{P}{P_c} k_p |\zeta| \frac{c^2 \tau^2}{Z_R^2} \right)^{1/3}. \quad (71)$$

Intermediate regime:  $\alpha_3 P / P_c \ll k_p |\zeta| Z_R / c\tau \ll \alpha_1 P_c / P$

$$N_e = \left( \alpha_3 \frac{P}{P_c} k_p |\zeta| \frac{c\tau}{Z_R} \right)^{1/2}. \quad (72)$$

Short pulse regime:  $k_p |\zeta| Z_R / c\tau \ll \alpha_3 P / P_c$

$$N_e = \frac{3\sqrt{3}}{4} \left( \alpha_3 \frac{P}{P_c} k_p^2 |\zeta|^2 \frac{c\tau}{Z_R} \right)^{1/3}. \quad (73)$$

For the laser-hose,  $\alpha_1 = \alpha_2 = \alpha_3 = 1$ . For self-modulation,  $\alpha_1 = \sqrt{2}(2 - P/P_c)^{3/2}$  ( $\sqrt{2} \leq \alpha_1 \leq 4$ ),  $\alpha_2 = 2$ , and  $\alpha_3 = \sqrt{2}(2 - P/P_c)^{-1/2}$  ( $1 \leq \alpha_3 \leq \sqrt{2}$ ). Hence, the number of *e*-folds is a function of the dimensionless parameters  $P/P_c$ ,  $k_p |\zeta|$ , and  $c\tau/Z_R$ .

Some insight can be gained by comparing  $N_e$  for self-modulation in the long-pulse regime to that of FRS in the four-wave nonresonant regime. Equations (67) and (71) indicate that self-modulation is dominant provided  $k_p^2 r_0^2 \ll k_0^2/k_p^2$ . This supports the assertion that self-modulation dominates in the 2-D limit, whereas FRS dominates in the 1-D limit. These two growth rates, however, occur in different spatial-temporal regimes, hence, comparison of the growth of self-modulation and FRS is more complicated. As mentioned in the previous section, it is interesting to note that the growth rate of four-wave nonresonant near FRS [114], as obtained from an instability analysis for a plane wave pump field, gives a growth rate similar to that for self-modulation in the long pulse regime, (71), when the transverse wavenumber for the scattered wave is given by  $k_{s\perp} = 1/r_0$ .

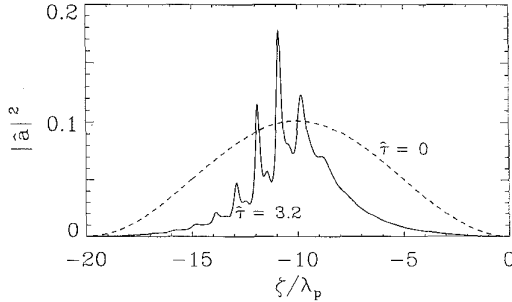


Fig. 32. Normalized laser intensity  $|\hat{a}|^2$  versus  $\zeta$  at  $c\tau = 0$  (dashed line) and at  $c\tau = 3.2Z_R$  (solid line). The laser, which is moving to the right, is modulated at wavelength  $\lambda_p = 30 \mu\text{m} = r_0/2$  (from [181]).

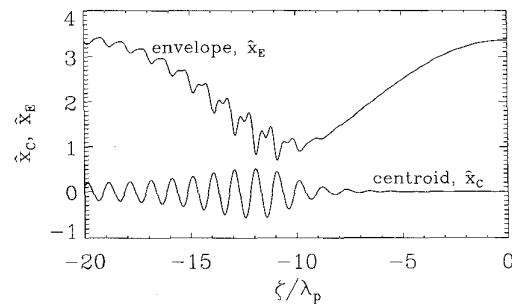


Fig. 33. Laser envelope  $x_E$  (upper curve) and centroid  $x_C$  (lower curve) versus  $\zeta$  at  $c\tau = 3.2Z_R$  for an initial perturbation of 1% in  $x_C$ . Perturbations grow at wavelength  $\lambda_p = 30 \mu\text{m} = r_0/2$  (from [181]).

To illustrate the behavior of the coupled self-modulation and laser-hose instabilities, (69) and (70) are solved numerically [181]. Consider an initially uniform plasma of density  $n_0 = 1.2 \times 10^{18} \text{ cm}^{-3}$  ( $\lambda_p = 30 \mu\text{m}$ ) and a 16-TW 1-ps laser pulse with wavelength  $\lambda = 1 \mu\text{m}$  and initial spot size  $r_0 = 60 \mu\text{m}$  ( $Z_R = 1.1 \text{ cm}$ ). For these parameters,  $P(\zeta) = P_c$  at the center of the pulse. Initially,  $\hat{x}_s = \hat{y}_s = 1$  and the centroid has a 1% random perturbation such that  $|\partial \ln x_c / \partial \zeta| \ll 1/\lambda$ .

As the laser propagates, the high-intensity center of the pulse remains guided ( $\hat{x}_s \simeq 1$ ). The front and back portions of the pulse with  $P < P_c$ , however, diffract, and the coupled hose-modulation instabilities grow within the guided portion of the pulse as illustrated in Figs. 32 and 33. Fig. 32 shows the normalized laser intensity on axis  $|\hat{a}|^2 = 16P(\zeta)/(P_c \hat{x}_s \hat{y}_s k_p^2 r_0^2)$  at  $\hat{\tau} = 0$  (dashed curve) and at  $\hat{\tau} = 3.2$ . Fig. 33 shows  $\hat{x}_s(\zeta)$  and  $\hat{x}_c(\zeta)$  at  $\hat{\tau} = 3.2$  and indicates a significant level of hosing, with  $|\hat{x}_c|$  as large as 0.5. Coupling between the hose and the modulation instabilities is clearly evident, i.e., in addition to the modulation of the envelope at  $\lambda_p$ , the second harmonic at  $\lambda_p/2$  is present. The spatial modulation of the laser envelope at  $\lambda_p/2$  is due to the dependence of the driving terms on the centroid motion. The second harmonic is not observed when the initial centroid perturbation is sufficiently small, 0.1% for the present parameters.

The presence of the laser-hose instability can strongly modify the structure of the wakefield generated by the laser pulse. To illustrate this point, consider the case when the initial centroid perturbation is 10% [181]. Here, the centroid

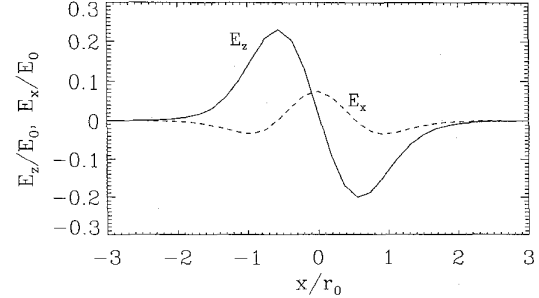


Fig. 34. Transverse profiles of the axial wakefield  $E_z$  (solid line) and the transverse wakefield  $E_x$  (dashed line) at  $c\tau = 1.8Z_R$  and  $\zeta = -18\lambda_p$  for a hose-dominated case with an initial perturbation of 10% in  $x_C$  (from [181]).

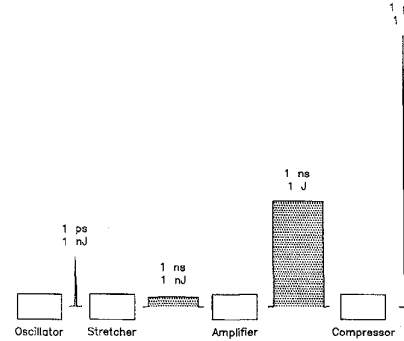


Fig. 35. Schematic of the chirped-pulse amplification laser technique (courtesy of G. Mourou).

motion dominates both the development of the wakefield and the evolution of the envelope. The spot size modulations are dominated by the second harmonic component. Fig. 34 shows the transverse profiles of both the longitudinal and transverse wakefields, at  $\hat{\tau} = 1.8$ , near the back of the pulse. The transverse field,  $E_x$ , is nearly symmetric and peaked on axis while the longitudinal field,  $E_z$ , is nearly antisymmetric and vanishes on axis. This wakefield symmetry is opposite that which occurs without hosing, i.e., in the absence of the hose instability,  $E_x$  is antisymmetric and vanishes on axis, while  $E_z$  is symmetric and peaked on axis.

While the modulation instability can enhance the wakefield amplitude and acceleration in the LWFA, the laser-hose instability should generally be avoided. To avoid significant levels of hosing, the initial laser centroid must be sufficiently smooth. Equations (71)–(73) indicate that the growth of the hose instability can be reduced by decreasing the pulse length ( $k_p |\zeta|$ ), the laser power ( $P/P_c$ ), and/or the interaction distance ( $c\tau/Z_R$ ). Further simulations [181] indicate that by appropriately varying (i.e., detuning) either the plasma density and/or the depth of the preformed plasma channel as a function of  $z$  in the laboratory frame, the hose and modulation instability can be substantially reduced.

### VIII. CONCLUSION

Theoretical studies of plasma-based accelerators, for the most part, can be divided into three main categories: 1) the

calculation of the wakefields (i.e., the plasma response) for a nonevolving drive beam; 2) the evolution of the drive beam; and 3) the evolution of the accelerated electron beam. Plasma wave generation by a nonevolving beam is well understood (i.e., analytical solutions or simple numerical models exist) in the 3-D linear regime and in the 1-D nonlinear regime. Issues pertaining to the evolution of the drive beam are guiding and stability. Theoretical studies indicate that a laser pulse can be guided over an extended distance (many Rayleigh lengths) in a preformed density channel. At high powers and intensities, relativistic self-focusing, ponderomotive self-channeling, and plasma wave effects are also important. Numerous instabilities can affect drive beam propagation. Of these, Raman scattering, self-modulation, and electron and laser hosing are the most significant and have been discussed in some detail. Analytic studies of drive beam evolution, for the most part, are limited to the linear regime in which, for example, analytic expressions for instability growth rates are readily obtained. The self-consistent problem of plasma wave generation by an evolving drive beam is typically of sufficient complexity as to require numerical simulation. Self-consistent simulations of plasma-based accelerators have been performed in the 2-D nonlinear regime using both fluid and particle-in-cell codes.

A practical concern of plasma-based accelerators, which has not been addressed in this paper, is the evolution of the accelerated electron beam. This includes beam loading and efficiency considerations [43], as well as the quality (i.e., emittance and energy spread) of the accelerated beam. Since the longitudinal and transverse dimensions of the plasma wave are typically small, e.g., wavelengths on the order of 300  $\mu\text{m}$ , the dimensions of the injected electron beam must also be small. To maintain low emittance and energy spread, the injected beam must be of subpicosecond duration, tightly focused, and synchronized to the plasma wave. This problem is currently being investigated and is the subject of other papers in this special issue.

Perhaps the two most fundamental questions concerning plasma-based accelerators are 1) can an ultrahigh accelerating field be generated and 2) can this accelerating field be sustained over a sufficiently long propagation distance so as to provide a substantial single-stage electron energy gain. Theory and simulation indicate that these requirements can be met. Experimentally, several groups [18]–[35] have measured ultrahigh accelerating fields and accelerated electrons, as is summarized in Tables I and II. Acceleration gradients and energy gains as high as 100 GV/m and 44 MeV, respectively, have been obtained by the experiments at Rutherford [33]. Much of the recent experimental success can be attributed to the development of chirped-pulse amplification [11], which has revolutionized laser technology by providing compact sources of multiterawatt subpicosecond laser pulses. Except for relativistic self-focusing and ponderomotive self-channeling effects, none of these accelerator experiments has utilized an external method for beam guiding. Recent experiments at the University of Maryland [176] have demonstrated a viable method for the production of a plasma density channel and the subsequent propagation of a guided laser pulse over many Rayleigh lengths, however, at a relatively low laser

intensity. Preliminary experimental results on plasma channels formed by capillary discharges [178] indicate the guiding of higher intensity ( $\simeq 10^{17} \text{ W/cm}^2$ ) laser pulses. If a plasma channel is used in conjunction with an ultrahigh intensity laser pulse in the standard LWFA configuration, then linear theory predicts a maximum single-stage energy gain of  $\Delta W [\text{GeV}] \simeq I [\text{W/cm}^2]/n_0 [\text{cm}^{-3}]$ . Hence, a picosecond laser pulse with an intensity of  $10^{18} \text{ W/cm}^2$  in a plasma of density  $10^{16} \text{ cm}^{-3}$  may provide a single-stage energy gain as high as 100 GeV over a distance on the order of 10 m.

#### APPENDIX: COMPACT TERAWATT LASERS

A compact terawatt laser system, based on the technique of CPA, was first demonstrated in 1988 by Mourou and co-workers [11]. The CPA technique allows for ultrashort ( $\tau_L \leq 1 \text{ ps}$ ) pulses to be efficiently amplified in solid-state media (e.g., Nd:glass, Ti:sapphire, and Cr:LiSAF), and has enabled the power of a compact system (per  $\text{cm}^2$  of amplifying medium) to rise from the GW to the TW level [10]–[17]. In CPA, a low energy pulse from an ultrashort pulse mode-locked oscillator is temporally stretched by a pair of gratings. The chirped long duration pulse avoids undesirable high field effects, such as self-focusing in the amplifying medium, and can reach much higher energies in the solid-state regenerative and single pass amplifiers. The amplified pulse is then compressed by a second matched pair of gratings. The CPA method is schematically shown in Fig. 35. This method has been applied to compact systems to produce subpicosecond pulses in the 1–20 TW range [10]–[13]. The average power of table-top CPA systems is currently limited to  $\lesssim 10 \text{ W}$  [15], [16]. Efforts are also underway to apply the CPA method to large scale systems with the goal of producing laser pulses with extremely high power (100 TW–1 PW) [14]–[17]. In fact, 125 TW has recently been achieved at Lawrence Livermore National Laboratory [17].

#### ACKNOWLEDGMENT

The authors acknowledge many insightful conversations with N. E. Andreev, G. Bonnaud, C. E. Clayton, W. P. Leemans, W. B. Mori, G. Mourou, T. Katsouleas, J. B. Rosenzweig, G. Shvets, C. W. Siders, and D. Umstadter.

#### REFERENCES

- [1] T. Tajima and J. M. Dawson, "Laser electron accelerator," *Phys. Rev. Lett.*, vol. 43, pp. 267–270, 1979.
- [2] "Laser acceleration of particles," in *Proc. AIP Conf.*, vol. 91, P. J. Channell, Ed. New York: Amer. Inst. Phys., 1982.
- [3] "Laser acceleration of particles," in *Proc. AIP Conf.*, vol. 130, C. Joshi and T. Katsouleas, Eds. New York: Amer. Inst. Phys., 1985.
- [4] "Advanced accelerator concepts," in *Proc. AIP Conf.*, vol. 156, F. E. Mills, Ed. New York: Amer. Inst. Phys., 1987.
- [5] "Special issue on plasma-based high-energy accelerators," *IEEE Trans. Plasma Sci.*, T. Katsouleas, Ed., vol. PS-15, 1987.
- [6] "Advanced accelerator concepts," in *Proc. AIP Conf.*, vol. 193, C. Joshi, Ed. New York: Amer. Inst. Phys., 1989.
- [7] "Advanced accelerator concepts," in *Proc. AIP Conf.*, vol. 279, J. Wurtele, Ed. New York: Amer. Inst. Phys., 1993.
- [8] "Advanced accelerator concepts," in *Proc. AIP Conf.*, vol. 335, P. Schoessow, Ed. New York: Amer. Inst. Phys., 1995.
- [9] "Special Issue on plasma based accelerators," *IEEE Trans. Plasma Sci.*, T. Katsouleas and R. Bingham, Eds., 1996.
- [10] D. Strickland and G. Mourou, "Compression of amplified chirped optical pulses," *Opt. Commun.*, vol. 56, pp. 219–221, 1985.

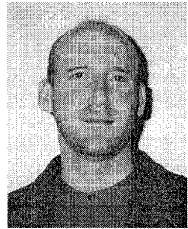
- [11] P. Maine, D. Strickland, P. Bado, M. Pessot, and G. Mourou, "Generation of ultrahigh peak power pulses by chirped-pulse amplification," *IEEE J. Quantum Electron.*, vol. QE-24, pp. 398–403, 1988.
- [12] M. Ferray, L. A. Lompire, O. Gobert, A. L'Huillier, G. Mainfray, C. Manus, and A. Sanchez, "Multiterawatt picosecond Nd:glass laser system at 1053 nm," *Opt. Commun.*, vol. 75, pp. 278–281, 1990.
- [13] F.G. Patterson, R. Gonzales, and M. D. Perry, "Compact 10-TW, 800-fs, Nd:glass laser," *Opt. Lett.*, vol. 16, pp. 1107–1109, 1991.
- [14] C. Sauteret, D. Husson, G. Thiell, S. Seznec, S. Gary, A. Migus, and G. Mourou, "Generation of 20-TW pulses of picosecond duration using chirped-pulse amplification in a Nd:glass power chain," *Opt. Lett.*, vol. 16, pp. 238–240, 1991; J. P. Watteau, G. Bonnau, J. Coutant, R. Dautray, A. Decoster, M. Louis-Jacquet, J. Ouvry, J. Sauteret, S. Seznec, and D. Teychenne, "Experimental program on the 20-TW laser system," *Phys. Fluids B*, vol. 4, pp. 2217–2223, 1992.
- [15] G. Mourou and D. Umstadter, "Development and applications of compact high-intensity lasers," *Phys. Fluids B*, vol. 4, pp. 2315–2325, 1992.
- [16] M. D. Perry and G. Mourou, "Terawatt to petawatt subpicosecond lasers," *Sci.*, vol. 64, pp. 917–924, 1994.
- [17] M. D. Perry, *Laser Focus World*, p. 9, Sept. 1995.
- [18] C. Joshi, T. Tajima, J. M. Dawson, H. A. Baldis, and N. A. Ebrahim, "Forward Raman instability and electron acceleration," *Phys. Rev. Lett.*, vol. 47, pp. 1285–1288, 1981.
- [19] J. B. Rosenzweig, D. B. Cline, B. Cole, H. Figueroa, W. Gai, R. Konecny, J. Norem, P. Schoessow, and J. Simpson, "Experimental observation of plasma wakefield acceleration," *Phys. Rev. Lett.*, vol. 61, pp. 98–101, 1988.
- [20] J. B. Rosenzweig, P. Schoessow, B. Cole, W. Gai, R. Konecny, J. Norem, and J. Simpson, "Experimental measurement of nonlinear plasma wakefields," *Phys. Rev. A*, vol. 39, pp. 1586–1589, 1989.
- [21] J. B. Rosenzweig, P. Schoessow, B. Cole, C. Ho, W. Gai, R. Konecny, S. Mtingwa, J. Norem, M. Rosing, and J. Simpson, "Demonstration of electron beam self-focusing in plasma wake fields," *Phys. Fluids B*, vol. 2, pp. 1376–1383, 1990.
- [22] K. Nakajima, A. Enomoto, H. Kobayashi, H. Nakanishi, Y. Nishida, A. Ogata, S. Ohasawa, T. Oogoe, T. Shoji, and T. Urano, *Nucl. Instrum. Methods A*, vol. 292, p. 12, 1990.
- [23] A. Ogata, "Plasma lens and wake experiments in Japan," in *Advanced Accelerator Concepts*, in *Proc. AIP Conf. Advanced Accelerator Concepts*, vol. 279, J. S. Wurtele, Ed. New York: Amer. Inst. Phys., 1993, pp. 420–449; H. Nakanishi, A. Enomoto, A. Ogata, K. Nakajima, D. Whittum, Y. Yoshida, T. Ueda, T. Kobayashi, H. Shibata, S. Tagawa, N. Yugami, and Y. Nishida, *Nucl. Instrum. Meth.*, vol. A328, p. 596, 1993.
- [24] A. K. Berezin, Ya. B. Fainberg, V. A. Kiselev, A. F. Linnik, V. V. Uskov, V. A. Balakirev, I. N. Onishchendo, G. L. Sidelnikov, and G. V. Sotnikov, "Wake field excitation in plasma by a relativistic electron pulse with a controlled number of short bunches," *Fizika Plazmy*, vol. 20, pp. 663–670, 1994; *Plasma Phys. Rep.*, vol. 20, pp. 596–602, 1994.
- [25] Y. Kitagawa, T. Matsumoto, T. Minamihata, K. Sawai, K. Matsuo, K. Mima, K. Nishihara, H. Azechi, K. A. Tanaka, H. Takabe, and S. Nakai, "Beat-wave excitation of plasma wave and observation of accelerated electrons," *Phys. Rev. Lett.*, vol. 68, pp. 48–51, 1992.
- [26] C. E. Clayton, K. A. Marsh, A. Dyson, M. Everett, A. Lal, W. P. Leemans, R. Williams, and C. Joshi, "Ultrahigh-gradient acceleration of injected electrons by laser-excited relativistic electron plasma waves," *Phys. Rev. Lett.*, vol. 70, pp. 37–40, 1993.
- [27] C. E. Clayton, M. J. Everett, A. Lal, D. Gordon, K. A. Marsh, and C. Joshi, "Acceleration and scattering of injected electrons in plasma beat-wave accelerator experiments," *Phys. Plasmas*, vol. 1, pp. 1753–1760, 1994; M. Everett, A. Lal, D. Gordon, C. E. Clayton, K. A. Marsh, and C. Joshi, "Trapped electron acceleration by a laser-driven relativistic plasma wave," *Nature*, vol. 368, pp. 527–529, 1994.
- [28] N. A. Ebrahim, "Optical mixing of laser light in a plasma and electron acceleration by relativistic electron plasma waves," *J. Appl. Phys.*, vol. 76, pp. 7645–7647, 1994.
- [29] F. Amiranoff, J. Ardonceau, M. Bercher, D. Bernard, B. Cros, A. Debraine, J. M. Dieulot, J. Fusellier, F. Jacquet, J. M. Joly, M. Juillard, G. Matthieu, P. Matricon, P. Mine, B. Montes, P. Mora, R. Morano, J. Morillo, F. Moulin, P. Poilleux, A. Specka, and C. Stenz, "Electron acceleration in the plasma beat-wave experiment at Ecole Polytechnique," in *Advanced Accelerator Concepts*, *AIP Conf. Proc.*, vol. 335, P. Schoessow, Ed. New York: Amer. Inst. Phys., 1995, pp. 612–634.
- [30] K. Nakajima, T. Kawakubo, H. Nakanishi, A. Ogata, Y. Kitagawa, R. Kodama, K. Mima, H. Shiraga, K. Suzuki, K. Yamakawa, T. Zhang, Y. Kato, D. Fisher, M. Downer, T. Tajima, Y. Sakawa, T. Shoji, N. Yugami, and Y. Nishida, "Proof-of-principle experiments of laser wakefield acceleration using a 1 ps 10 TW Nd:glass laser," in *Proc. AIP Conf. Advanced Accelerator Concepts*, vol. 335, P. Schoessow, Ed. New York: Amer. Inst. Phys., 1995, pp. 145–155.
- [31] K. Nakajima, D. Fisher, T. Kawakubo, H. Nakanishi, A. Ogata, Y. Kato, Y. Kitagawa, R. Kodama, K. Mima, H. Shiraga, K. Suzuki, K. Yamakawa, T. Zhang, Y. Sakawa, T. Shoji, Y. Nishida, N. Yugami, M. Downer, and T. Tajima, "Observation of ultrahigh gradient electron acceleration by a self-modulated intense short laser pulse," *Phys. Rev. Lett.*, vol. 74, pp. 4428–4431, 1995.
- [32] C. Coverdale, C. B. Darrow, C. D. Decker, W. B. Mori, K. C. Tzeng, K. A. Marsh, C. E. Clayton, and C. Joshi, "Propagation of intense subpicosecond laser pulses through underdense plasmas," *Phys. Rev. Lett.*, vol. 74, pp. 4659–4662, 1995.
- [33] A. Modena, Z. Najmudin, A. E. Dangor, C. E. Clayton, K. A. Marsh, C. Joshi, V. Malka, C. B. Darrow, C. Danson, D. Neely, and F. N. Walsh, "Electron acceleration from the breaking of relativistic plasma waves," *Nature*, vol. 337, pp. 606–608, 1995.
- [34] R. Wagner, S. Y. Chen, A. Maksimchuk, E. Dodd, J. K. Kim, and D. Umstadter, "MeV-electron acceleration by the combined action of low- and high-phase-velocity plasma waves parametrically driven by a high-intensity laser," *Bullet. Amer. Phys. Soc.*, vol. 40, p. 1799, 1995.
- [35] A. Ting, C. Moore, and M. Baine, private communication, 1996.
- [36] J. M. Dawson, "Nonlinear electron oscillations in a cold plasma," *Phys. Rev.*, vol. 133, pp. 383–387, 1959.
- [37] A. I. Akhiezer and R. V. Polovin, "Theory of wave motion of an electron plasma," *Zh. Eksp. Teor. Fiz.*, vol. 30, pp. 915–928, 1956; *Sov. Phys. JETP*, vol. 3, pp. 696–705, 1956.
- [38] Y. B. Fainberg, V. A. Balakirev, I. N. Onishchendo, G. L. Sidelnikov, and G. V. Sotnikov, "Wakefield excitation in plasma by a train of relativistic electron bunches," *Fizika Plazmy*, vol. 20, pp. 674–681, 1994; *Plasma Phys. Rep.*, vol. 20, pp. 606–612, 1994, and references therein.
- [39] P. Chen, J. M. Dawson, R. W. Huff, and T. Katsouleas, "Acceleration of electrons by the interaction of a bunched electron beam with a plasma," *Phys. Rev. Lett.*, vol. 54, pp. 693–696, 1985.
- [40] R. D. Ruth, A. W. Chao, P. L. Morton, and P. B. Wilson, "A plasma wakefield accelerator," *Particle Accelerators*, vol. 17, pp. 171–189, 1985.
- [41] P. Chen, J. J. Su, J. M. Dawson, K. L. F. Bane, and P. B. Wilson, "Energy transfer in the plasma wakefield accelerator," *Phys. Rev. Lett.*, vol. 56, pp. 1252–1255, 1986.
- [42] T. Katsouleas, "Physical mechanisms in the plasma wakefield accelerator," *Phys. Rev. A*, vol. 33, pp. 2056–2064, 1986.
- [43] T. Katsouleas, S. Wilks, P. Chen, J. M. Dawson, and J. J. Su, "Beam loading in plasma accelerators," *Particle Accelerators*, vol. 22, pp. 81–99, 1987.
- [44] R. Keinigs and M. E. Jones, "Two-dimensional dynamics of the plasma wakefield accelerator," *Phys. Fluids*, vol. 30, pp. 252–263, 1987.
- [45] J. J. Su, T. Katsouleas, J. M. Dawson, P. Chen, M. Jones, and R. Keinigs, "Stability of the driving bunch in the plasma wakefield accelerator," *IEEE Trans. Plasma Sci.*, vol. PS-15, pp. 192–198, 1987.
- [46] J. B. Rosenzweig, "Nonlinear plasma dynamics in the plasma wakefield accelerator," *Phys. Rev. Lett.*, vol. 58, pp. 555–558, 1987.
- [47] ———, "Trapping, thermal effects, and wave breaking in the nonlinear plasma wakefield accelerator," *Phys. Rev. A*, vol. 38, pp. 3634–3642, 1988.
- [48] J. B. Rosenzweig, B. Breizman, T. Katsouleas, and J. J. Su, "Acceleration and focusing of electrons in two-dimensional nonlinear plasma wakefields," *Phys. Rev. A*, vol. 44, pp. R6189–R6192, 1991.
- [49] J. Krall, G. Joyce, and E. Esarey, "Vlasov simulations of very large amplitude wave generation in the plasma wakefield accelerator," *Phys. Rev. A*, vol. 44, pp. 6854–6861, 1991.
- [50] N. Barov and J. B. Rosenzweig, "Propagation of short electron pulses in underdense plasmas," *Phys. Rev. E*, vol. 49, pp. 4407–4416, 1994.
- [51] J. Krall and G. Joyce, "Transverse equilibrium and stability of the primary beam in the plasma wakefield accelerator," *Phys. Plasmas*, vol. 2, pp. 1326–1331, 1995.
- [52] C. Joshi, W. B. Mori, T. Katsouleas, J. M. Dawson, J. M. Kindel, and D. W. Forslund, "Ultrahigh gradient particle acceleration by intense laser-driven plasma density waves," *Nature*, vol. 311, pp. 525–529, 1984.
- [53] M. N. Rosenbluth and C. S. Liu, "Excitation of plasma waves by two laser beams," *Phys. Rev. Lett.*, vol. 29, pp. 701–705, 1972.
- [54] T. Katsouleas and J. M. Dawson, "Unlimited electron acceleration in laser-driven plasma waves," *Phys. Rev. Lett.*, vol. 51, pp. 392–395, 1983.
- [55] C. M Tang, P. Sprangle, and R. Sudan, "Excitation of plasma waves in the plasma beat-wave accelerator," *Appl. Phys. Lett.*, vol. 45, pp.

- 375–377, 1984; “Dynamics of space-charge waves in the laser beat-wave accelerator,” *Phys. Fluids*, vol. 28, pp. 1974–1983, 1985.
- [56] T. Tajima, “High-energy laser plasma accelerators,” *Laser Particle Beams*, vol. 3, pp. 351–413, 1985.
- [57] R. J. Noble, “Plasma wave generation in the beat-wave accelerator,” *Phys. Rev. A*, vol. 32, pp. 460–471, 1985.
- [58] T. Katsouleas, C. Joshi, J. M. Dawson, F. F. Chen, C. E. Clayton, W. B. Mori, C. Darrow, and D. Umstadter, “Plasma accelerators,” in *Proc. AIP Conf. Laser Acceleration Particles*, vol. 130, C. Joshi and T. Katsouleas, Eds., New York: Amer. Inst. Phys., 1985, pp. 63–98.
- [59] K. Mima, T. Ohsuga, H. Takabe, K. Nishihara, T. Tajima, E. Zaidman, and W. Horton, “Wakeless triple-soliton accelerator,” *Phys. Rev. Lett.*, vol. 57, pp. 1421–1424, 1986.
- [60] C. McKinstry and D. Dubois, “Relativistic solitary-wave solutions of the beat-wave equations,” *Phys. Rev. Lett.*, vol. 57, pp. 2022–2025, 1986.
- [61] W. Horton and T. Tajima, “Pump depletion in the plasma-beat-wave accelerator,” *Phys. Rev. A*, vol. 34, pp. 4110–4119, 1986.
- [62] C. J. McKinstry and D. W. Forslund, “The detuning of relativistic Langmuir waves in the beat-wave accelerator,” *Phys. Fluids*, vol. 30, pp. 904–908, 1987.
- [63] W. B. Mori, “On beat-wave excitation of relativistic plasma waves,” *IEEE Trans. Plasma Sci.*, vol. PS-15, pp. 88–106, 1987.
- [64] D. C. Barnes, T. Kurki-Suonio, and T. Tajima, “Laser self-trapping for the plasma fiber accelerator,” *IEEE Trans. Plasma Sci.*, vol. PS-15, pp. 154–160, 1987.
- [65] E. Esarey, A. Ting, and P. Sprangle, “Relativistic focusing and beat-wave phase velocity control in the plasma beat-wave accelerator,” *Appl. Phys. Lett.*, vol. 53, pp. 1266–1268, 1988.
- [66] W. B. Mori, C. Joshi, J. M. Dawson, D. W. Forslund, and J. M. Kindel, “Evolution of self-focusing of intense electromagnetic waves in plasma,” *Phys. Rev. Lett.*, vol. 60, pp. 1298–1301, 1988.
- [67] P. Gibbon and A. R. Bell, “Cascade focusing in the beat-wave accelerator,” *Phys. Rev. Lett.*, vol. 61, pp. 1599–1562, 1988.
- [68] C. J. McKinstry and D. A. Russell, “Nonlinear focusing of coupled waves,” *Phys. Rev. Lett.*, vol. 61, pp. 2929–2932, 1988.
- [69] E. Esarey, A. Ting, and P. Sprangle, “Optical guiding and beat-wave phase velocity control in the plasma beat-wave accelerator,” in *Proc. AIP Conf. Advanced Accelerator Concepts*, vol. 193, C. Joshi, Ed., New York: Amer. Inst. Phys., 1989, pp. 71–86; E. Esarey and A. Ting, “Comment on cascade focusing in the beat-wave accelerator,” *Phys. Rev. Lett.*, vol. 65, p. 1961, 1990.
- [70] C. E. Clayton, C. Joshi, C. Darrow, and D. Umstadter, “Relativistic plasma wave excitation by collinear optical mixing,” *Phys. Rev. Lett.*, vol. 54, pp. 2343–2346, 1985.
- [71] N. A. Ebrahim, “Lasers, plasmas, and particle accelerators—Novel particle accelerating techniques for the 21st century,” *Phys. Canada*, vol. 45, pp. 178–188, 1989.
- [72] A. E. Dangor, A. K. L. Dymoke-Bradshaw, and A. E. Dyson, “Observation of relativistic plasma waves generated by the beat-wave with 1 micron lasers,” *Physica Scripta*, vol. T30, pp. 107–109, 1990.
- [73] F. Amiranoff, M. Laberge, J. R. Marques, F. Moulin, E. Fabre, B. Cros, G. Matthieussent, P. Benkheiri, F. Jacquet, J. Meyer, P. Mine, C. Stenz, and P. Mora, “Observation of modulation instability in Nd-laser beat-wave experiments,” *Phys. Rev. Lett.*, vol. 66, pp. 3710–3713, 1992.
- [74] F. Moulin, F. Amiranoff, M. Laberge, J. R. Marques, B. Cros, G. Matthieussent, D. Bernard, F. Jacquet, P. Mine, A. Specka, C. Stenz, and P. Mora, “Coupling between electron and ion waves in Nd-laser beat-wave experiments,” *Phys. Plasmas*, vol. 1, pp. 1318–1327, 1994.
- [75] M. J. Everett, A. Lal, D. Gordon, C. E. Clayton, W. B. Mori, T. W. Johnston, and C. Joshi, “Coupling between high-frequency plasma waves in laser-plasma interactions,” *Phys. Rev. Lett.*, vol. 74, pp. 2236–2239, 1995.
- [76] M. J. Everett, A. Lal, D. Gordon, K. Wharton, C. E. Clayton, W. B. Mori, and C. Joshi, “Evolution of stimulated Raman into stimulated compton scattering of laser light via wave breaking of plasma waves,” *Phys. Rev. Lett.*, vol. 74, pp. 1355–1358, 1995.
- [77] W. P. Leemans, C. E. Clayton, K. A. Marsh, and C. Joshi, “Stimulated Compton scattering from preformed underdense plasmas,” *Phys. Rev. Lett.*, vol. 67, pp. 1434–1437, 1991.
- [78] W. P. Leemans, C. E. Clayton, W. B. Mori, K. A. Marsh, A. Dyson, and C. Joshi, “Plasma physics aspects of tunnel-ionized gases,” *Phys. Rev. Lett.*, vol. 68, pp. 321–324, 1992.
- [79] W. P. Leemans, C. E. Clayton, W. B. Mori, K. A. Marsh, P. K. Kaw, A. Dyson, C. Joshi, and J. M. Wallace, “Experiments and simulations of tunnel-ionized plasmas,” *Phys. Rev. A*, vol. 46, pp. 1091–1105, 1992.
- [80] D. J. Sullivan and B. B. Godfrey, “The plasma beatwave accelerator—II simulations,” in *Proc. AIP Conf. Laser Acceleration Particles*, vol. 91, P. J. Channell, Ed., New York: Amer. Inst. Phys., 1982, pp. 43–68.
- [81] W. B. Mori, “Computer simulations on the acceleration of electrons by fast large-amplitude plasma waves driven by laser beams,” Masters thesis, Univ. California Los Angeles, 1984.
- [82] L. M. Gorbulov and V. I. Kirsanov, “Excitation of plasma waves by an electromagnetic wave packet,” *Zh. Eksp. Teor. Fiz.*, vol. 93, pp. 509–518, 1987; *Sov. Phys. JETP*, vol. 66, pp. 290–294, 1987.
- [83] P. Sprangle, E. Esarey, A. Ting, and G. Joyce, “Laser wakefield acceleration and relativistic optical guiding,” *Appl. Phys. Lett.*, vol. 53, pp. 2146–2148, 1988.
- [84] E. Esarey, A. Ting, P. Sprangle, and G. Joyce, “The laser wakefield accelerator,” *Comments Plasma Phys. Controlled Fusion*, vol. 12, pp. 191–204, 1989.
- [85] V. N. Tsytovich, U. DeAngelis, and R. Bingham, “Beat-wave-wake acceleration by short high intensity laser pulses,” *Comments Plasma Phys. Controlled Fusion*, vol. 12, pp. 249–256, 1989.
- [86] T. Katsouleas, W. B. Mori, and C. B. Darrow, “Laser wakefield acceleration with highly relativistic pumps,” in *Proc. AIP Conf. Advanced Accelerator Concepts*, vol. 193, C. Joshi, Ed., New York: Amer. Inst. Phys., 1989, pp. 165–171.
- [87] S. V. Bulanov, V. I. Kirsanov, and A. S. Sakharov, “Excitation of ultrarelativistic plasma waves by pulse of electromagnetic radiation,” *Pis'ma Zh. Eksp. Teor. Fiz.*, vol. 50, pp. 176–178, 1989; *JETP Lett.*, vol. 50, pp. 198–201, 1989.
- [88] P. Sprangle, E. Esarey, and A. Ting, “Nonlinear theory of intense laser-plasma interactions,” *Phys. Rev. Lett.*, vol. 64, pp. 2011–2014, 1990; “Nonlinear interaction of intense laser pulses in plasmas,” *Phys. Rev. A*, vol. 41, pp. 4463–4469, 1990.
- [89] A. Ting, E. Esarey, and P. Sprangle, “Nonlinear wakefield generation and relativistic focusing of intense laser pulses in plasmas,” *Phys. Fluids B*, vol. 2, pp. 1390–1394, 1990.
- [90] V. I. Berezhiani and I. G. Murusidze, “Relativistic wakefield generation by an intense laser pulse in a plasma,” *Phys. Lett. A*, vol. 148, pp. 338–340, 1990.
- [91] ———, “Interaction of highly relativistic short laser pulses with plasmas and nonlinear wakefield generation,” *Physica Scripta*, vol. 45, pp. 87–90, 1992.
- [92] S. V. Bulanov, I. N. Inovenkov, V. I. Kirsanov, N. M. Naumova, and A. S. Sakharov, “Nonlinear depletion of ultrashort and relativistically strong laser pulses in an underdense plasma,” *Phys. Fluids B*, vol. 4, pp. 1935–1942, 1992.
- [93] P. K. Kaw, A. Sen, and T. Katsouleas, “Nonlinear 1-D laser pulse solitons in a plasma,” *Phys. Rev. Lett.*, vol. 68, pp. 3172–3175, 1992.
- [94] J. M. Rax and N. J. Fisch, “Nonlinear relativistic interaction of an ultrashort laser pulse with a cold plasma,” *Phys. Fluids B*, vol. 4, pp. 1323–1331, 1992; “Ultrahigh intensity laser-plasma interaction: A Lagrangian approach,” *Phys. Fluids B*, vol. 5, pp. 2578–2583, 1993.
- [95] P. Sprangle and E. Esarey, “Interaction of ultrahigh laser fields with beams and plasmas,” *Phys. Fluids B*, vol. 4, pp. 2241–2248, 1992.
- [96] P. Sprangle, E. Esarey, J. Krall, and G. Joyce, “Propagation and guiding of intense laser pulses in plasmas,” *Phys. Rev. Lett.*, vol. 69, pp. 2200–2203, 1992.
- [97] E. Esarey, P. Sprangle, J. Krall, A. Ting, and G. Joyce, “Optically guided laser wakefield acceleration,” *Phys. Fluids B*, vol. 5, pp. 2690–2697, 1993.
- [98] J. S. Wurtele, “The role of plasma in advanced accelerators,” *Phys. Fluids B*, vol. 5, pp. 2363–2370, 1993.
- [99] S. V. Bulanov and F. Pegoraro, “Acceleration of charged particles and photons in the wake of a short laser pulse in a thin channel,” *Laser Phys.*, vol. 4, pp. 1120–1131, 1994.
- [100] T. C. Chiou, T. Katsouleas, C. Decker, W. B. Mori, J. S. Wurtele, G. Shvets, and J. J. Su, “Laser wakefield acceleration and optical guiding in a hollow plasma channel,” *Phys. Plasmas*, vol. 2, pp. 310–318, 1995.
- [101] D. Teychenne, G. Bonnaud, and J. L. Bobin, “Wave-breaking limit to the wakefield effect in an underdense plasma,” *Phys. Rev. E*, vol. 48, pp. R3248–R3251, 1993.
- [102] ———, “Electrostatic and kinetic energies in the wake wave of a short laser pulse,” *Phys. Plasmas*, vol. 1, pp. 1771–1773, 1994.
- [103] R. Bingham, U. DeAngelis, M. R. Amin, R. A. Cairns, and B. McNamara, “Relativistic Langmuir waves generated by ultrashort pulse lasers,” *Plasma Phys. Controlled Fusion*, vol. 34, pp. 557–567, 1992.
- [104] D. L. Fisher and T. Tajima, “Superluminous laser pulse in an active medium,” *Phys. Rev. Lett.*, vol. 71, pp. 4338–4321, 1993; D. L. Fisher, T. Tajima, M. C. Downer, and C. W. Siders, “Envelope evolution of a

- laser pulse in an active medium," *Phys. Rev. E*, vol. 51, pp. 4860–4868, 1995.
- [105] H. Hamster, A. Sullivan, S. Gordon, W. White, and R. W. Falcone, "Subpicosecond, electromagnetic pulses from intense laser-plasma interaction," *Phys. Rev. Lett.*, vol. 71, pp. 2725–2728, 1993.
- [106] J. R. Marques, J. P. Geindre, F. Amiranoff, P. Audebert, J. C. Gauthier, A. Antonetti, and G. Grillon, "Temporal and spatial measurements of the electron density perturbation produced in the wake of an ultra-short laser pulse," submitted to *Phys. Rev. Lett.*, 1995.
- [107] M. C. Downer, C. W. Siders, D. F. Fisher, S. P. LeBlanc, B. Rau, E. Gaul, T. Tajima, A. Babine, A. Stepanov, and A. Sergeev, "Laser wakefield photon accelerator: Optical diagnostics for the laser wakefield accelerator based on longitudinal interferometry," *Bullet. Amer. Phys. Soc.*, vol. 40, p. 1862, 1995.
- [108] N. E. Andreev, L. M. Gorbunov, V. I. Kirsanov, A. A. Pogosova, and R. R. Ramazashvili, "Resonant excitation of wakefields by a laser pulse in a plasma," *Pis'ma Zh. Eksp. Teor. Fiz.*, vol. 55, pp. 551–555, 1992; *JETP Lett.*, vol. 55, pp. 571–576, 1992.
- [109] T. M. Antonsen, Jr. and P. Mora, "Self-focusing and Raman scattering of laser pulses in tenuous plasmas," *Phys. Rev. Lett.*, vol. 69, pp. 2204–2207, 1992; *Phys. Fluids B*, vol. 5, pp. 1440–1452, 1993.
- [110] J. Krall, A. Ting, E. Esarey, P. Sprangle, and G. Joyce, "Enhanced acceleration in a self-modulated laser wakefield accelerator," *Phys. Rev. E*, vol. 48, pp. 2157–2161, 1993.
- [111] E. Esarey, J. Krall, and P. Sprangle, "Envelope analysis of intense laser pulse self-modulation in plasmas," *Phys. Rev. Lett.*, vol. 72, pp. 2887–2890, 1994.
- [112] N. E. Andreev, L. M. Gorbunov, V. I. Kirsanov, A. A. Pogosova, and R. R. Ramazashvili, "The theory of laser self-resonant wake field accelerator," *Physica Scripta*, vol. 49, pp. 101–109, 1994.
- [113] N. E. Andreev, V. I. Kirsanov, and L. M. Gorbunov, "Stimulated processes and self-modulation of a short intense laser pulse in the laser wakefield accelerator," *Phys. Plasmas*, vol. 2, pp. 2573–2582, 1995.
- [114] W. B. Mori, C. D. Decker, D. E. Hinkel, and T. Katsouleas, "Raman forward scattering of short-pulse high-intensity lasers," *Phys. Rev. Lett.*, vol. 72, pp. 1482–1485, 1994; W. B. Mori, C. D. Decker, T. Katsouleas, and D. E. Hinkel, "Spatial temporal theory of Raman forward scattering," *Phys. Plasmas*, submitted 1995.
- [115] C. D. Decker, W. B. Mori, and T. Katsouleas, "Particle-in-cell simulations of Raman forward scattering from short-pulse high-intensity lasers," *Phys. Rev. E*, vol. 50, pp. R3338–R3341, 1994; C. D. Decker, W. B. Mori, K. C. Tzeng, and T. Katsouleas, "The evolution of ultra-intense, short-pulse lasers in underdense plasmas," *Phys. Plasmas*, submitted 1995; K. C. Tzeng, W. B. Mori, and C. D. Decker, "The anomalous absorption and scattering of short pulse high intensity lasers in underdense plasmas," *Phys. Rev. Lett.*, submitted 1995.
- [116] S. V. Bulanov, F. Pegoraro, and A. M. Pukhov, "Two-dimensional regimes of self-focusing, wakefield generation, and induced focusing of a short intense laser pulse in an underdense plasma," *Phys. Rev. Lett.*, vol. 74, pp. 710–713, 1995.
- [117] C. I. Moore, K. Krushelnick, A. Ting, R. Burris, A. Fisher, P. Sprangle, E. Esarey, and D. Umstadter, "Thomson scattering characterization of wakefield plasma waves in the laser wakefield accelerator," *Bullet. Amer. Phys. Soc.*, vol. 40, p. 1797, 1995.
- [118] K. Nakajima, "Plasma-wave resonator for particle-beam acceleration," *Phys. Rev. A*, vol. 45, pp. 1149–1156, 1992.
- [119] D. Umstadter, E. Esarey, and J. Kim, "Nonlinear plasma waves resonantly driven by optimized laser pulse trains," *Phys. Rev. Lett.*, vol. 72, pp. 1224–1227, 1994.
- [120] D. Umstadter, J. Kim, E. Esarey, E. Todd, and T. Neubert, "Resonant laser-driven plasma waves for electron acceleration," *Phys. Rev. E*, vol. 51, pp. 3484–3497, 1995.
- [121] S. Dalla and M. Lontano, "Large amplitude plasma wave excitation by means of sequences of short laser pulses," *Phys. Rev. E*, vol. 49, pp. R1819–R1822, 1994.
- [122] G. Bonnaud, D. Teychenne, and J. L. Bobin, "Wake-field effect induced by multiple laser pulses," *Phys. Rev. E*, vol. 50, pp. R36–R39, 1994.
- [123] X. Liu, R. Wagner, A. Maksimchuk, E. Goodman, J. Workman, D. Umstadter, and A. Mingus, "Nonlinear temporal diffraction and frequency shifts resulting from pulse shaping in chirped-pulse amplification systems," *Opt. Lett.*, vol. 20, pp. 1163–1165, 1995.
- [124] W. L. Kruer, *The Physics of Laser Plasma Interactions*. Reading, MA: Addison-Wesley, 1988.
- [125] P. Chen, "A possible final focusing mechanism for linear colliders," *Particle Accelerators*, vol. 20, pp. 171–182, 1987.
- [126] P. Chen, J. J. Su, T. Katsouleas, S. Wilks, and J. M. Dawson, "Plasma focusing for high-energy beams," *IEEE Trans. Plasma Sci.*, vol. PS-15, pp. 218–225, 1987.
- [127] W. K. H. Panofsky and W. A. Wenzel, *Rev. Sci. Instrum.*, vol. 27, p. 967, 1956.
- [128] E. Esarey, A. Ting, P. Sprangle, D. Umstadter, and X. Liu, "Nonlinear analysis of relativistic harmonic generation by intense lasers in plasmas," *IEEE Trans. Plasma Sci.*, vol. 21, pp. 95–104, 1993.
- [129] E. Esarey and M. Piloff, "Trapping and acceleration in nonlinear plasma waves," *Phys. Plasmas*, vol. 2, pp. 1432–1436, 1995.
- [130] J. Krall, E. Esarey, P. Sprangle, and G. Joyce, "Propagation of radius-tailored laser pulses over extended distances in a uniform plasma," *Phys. Plasmas*, vol. 1, pp. 1738–1743, 1994.
- [131] T. Katsouleas and W. B. Mori, "Wave-breaking amplitude of relativistic oscillations in a thermal plasma," *Phys. Rev. Lett.*, vol. 61, pp. 90–93, 1988.
- [132] D. Teychenne, G. Bonnaud, and J. L. Bobin, "Oscillatory relativistic motion of a particle in a power-law or sinusoidal-shaped potential well," *Phys. Rev. E*, vol. 49, pp. 3253–3263, 1994.
- [133] R. L. Williams, C. E. Clayton, C. Joshi, T. Katsouleas, and W. B. Mori, *Laser Particle Beams*, vol. 8, p. 427, 1990.
- [134] P. Mora, "Particle acceleration in a relativistic wave in the adiabatic regime," *Phys. Fluids B*, vol. 4, pp. 1630–1634, 1992; *J. Appl. Phys.*, vol. 71, p. 2087, 1992; P. Mora and F. Amiranoff, *J. Appl. Phys.*, vol. 66, p. 3476, 1989.
- [135] C. D. Decker and W. B. Mori, "Group velocity of large amplitude electromagnetic waves in a plasma," *Phys. Rev. Lett.*, vol. 72, pp. 490–493, 1994; *Phys. Rev. E*, vol. 51, pp. 1364–1375, 1995.
- [136] E. Esarey, P. Sprangle, M. Piloff, and J. Krall, "Theory and group velocity of ultrashort, tightly focused laser pulses," *J. Opt. Soc. Amer. B*, vol. 12, pp. 1695–1703, 1995.
- [137] H. H. Kuehl, C. Y. Zhang, and T. Katsouleas, "Interaction of a weakly nonlinear laser pulse in a plasma," *Phys. Rev. E*, vol. 47, pp. 1249–1261, 1993.
- [138] E. Esarey, J. Krall, and P. Sprangle, "Plasma wave phase velocities in laser-driven accelerators," to be published.
- [139] W. P. Leemans, C. W. Siders, E. Esarey, N. E. Andreev, G. Shvets, and W. B. Mori, "Plasma guiding and wakefield generation for second-generation experiments," this issue, pp. 331–342.
- [140] S. C. Wilks, J. M. Dawson, W. B. Mori, T. Katsouleas, and M. E. Jones, "Photon accelerator," *Phys. Rev. Lett.*, vol. 62, pp. 2600–2603, 1989.
- [141] E. Esarey, A. Ting, and P. Sprangle, "Frequency shifts induced in laser pulses by plasma waves," *Phys. Rev. A*, vol. 42, pp. 3526–3531, 1990.
- [142] V. A. Mironov, A. M. Sergeev, E. V. Vanin, and G. Brodin, "Localized nonlinear wave structures in the nonlinear photon accelerator," *Phys. Rev. A*, vol. 42, pp. 4862–4866, 1990.
- [143] C. W. Siders, S. P. Le Blanc, A. Babine, A. Stepanov, A. Sergeev, T. Tajima, and M. C. Downer, "Plasma-based accelerator diagnostics based upon longitudinal interferometry with ultrashort optical pulses," this issue, pp. 301–315.
- [144] M. Rosing, E. Chojnacki, W. Gai, C. Ho, R. Konecny, S. Mtingwa, J. Norem, P. Schoessow, and J. Simpson, *Proc. 1991 IEEE Particle Accelerator Conference, IEEE Conf. Record 91CH3038-7*, L. Lizama and J. Chew, Eds. New York: IEEE, p. 555.
- [145] J. Smolin, T. Katsouleas, C. Joshi, J. Davis, and C. Pellegrini, *Bullet. Amer. Phys. Soc.*, vol. 35, p. 2103, 1990.
- [146] B. N. Breizman, P. Z. Chebotaev, I. A. Koop, A. M. Kudryavstev, V. M. Panasyuk, Y. M. Shatunov, A. N. Skrinsky, and F. A. Tsel'nik, *Proc. 8th Int. Conf. High-Power Particle Beams*, B. N. Breizman and B. A. Knyazev, Eds. Piscataway, NJ: World Scientific, 1993, p. 272.
- [147] E. S. Weibel, *Phys. Rev. Lett.*, vol. 2, p. 83, 1959.
- [148] D. Whittum, "Transverse two-stream instability of a beam with a Bennett profile," *Phys. Rev. E*, submitted 1994.
- [149] D. H. Whittum, W. H. Sharp, S. S. Yu, M. Lampe, and G. Joyce, *Phys. Rev. Lett.*, vol. 67, pp. 991–994, 1991; M. Lampe, G. Joyce, S. P. Slinker, and D. H. Whittum, *Phys. Fluids B*, vol. 5, pp. 1888–1901, 1993.
- [150] J. Krall, private communication, 1995.
- [151] H. L. Buchanan, "Electron beam propagation in the ion-focused regime," *Phys. Fluids*, vol. 30, pp. 221–227, 1987.
- [152] D. Chernin, *Particle Accel.*, vol. 24, p. 29, 1988.
- [153] C. Siders, private communication, 1995.
- [154] A. M. Weiner, "Femtosecond optical pulse shaping and processing," submitted to *Progr. Quantum Electron.*
- [155] D. Pinkos, J. Squier, D. Schumacher, P. Bucksbaum, B. Kohler, V. V. Yakovlev, and K. R. Wilson, "Production of programmable amplified shaped pulses in femtosecond lasers," in *Ultrafast Phenomena IX, Springer Series in Chemical Physics*, vol. 60, P. F. Barbara, W. A. Knox, G. A. Mourou, and A. A. Zewail, Eds. Berlin: Springer-Verlag, 1994, pp. 180–182.
- [156] A. G. Litvak, *Zh. Eksp. Teor. Fiz.*, vol. 57, p. 629, 1969; *Sov. Phys. JETP*, vol. 30, p. 344, 1969.

- [157] C. Max, J. Arons, and A. B. Langdon, "Self-modulation and self-focusing of electromagnetic waves in plasmas," *Phys. Rev. Lett.*, vol. 33, pp. 209–212, 1974.
- [158] G. Schmidt and W. Horton, "Self-focusing of laser beams in the beat-wave accelerator," *Comments Plasma Phys. Controlled Fusion*, vol. 9, pp. 85–90, 1985.
- [159] P. Sprangle, C. M. Tang, and E. Esarey, "Relativistic self-focusing of short-pulse radiation beams in plasmas," *IEEE Trans. Plasma Sci.*, vol. PS-15, pp. 145–153, 1987.
- [160] G. Z. Sun, E. Ott, Y. C. Lee, and P. Guzdar, "Self-focusing of short intense pulses in plasmas," *Phys. Fluids*, vol. 30, pp. 526–532, 1987.
- [161] T. Kurki-Suonio, P. J. Morrison, and T. Tajima, "Self-focusing of an optical beam in a plasma," *Phys. Rev. A*, vol. 40, pp. 3230–3239, 1989.
- [162] A. Ting, P. Sprangle, and E. Esarey, "Simulation of short intense laser pulse propagation in the laser wakefield accelerator," in *Proc. AIP Conf. Advanced Accelerator Concepts*, vol. 193, C. Joshi, Ed. New York: Amer. Inst. Phys., 1989, pp. 398–407.
- [163] A. B. Borisov, A. V. Borovskiy, V. V. Korobkin, A. M. Prokhorov, C. K. Rhodes, and O. B. Shiryaev, "Stabilization of relativistic self-focusing of intense subpicosecond ultraviolet pulses in plasmas," *Phys. Rev. Lett.*, vol. 65, pp. 1753–1756, 1990.
- [164] P. Sprangle, A. Zigler, and E. Esarey, "Elimination of laser prepulse by relativistic guiding in a plasma," *J. Appl. Phys.*, vol. 58, pp. 346–348, 1991.
- [165] A. B. Borisov, A. V. Borovskiy, O. B. Shiryaev, V. V. Korobkin, A. M. Prokhorov, J. C. Solem, T. S. Luk, K. Boyer, and C. K. Rhodes, "Relativistic and charge-displacement self-channeling of intense ultrashort laser pulses in plasmas," *Phys. Rev. A*, vol. 45, pp. 5830–5845, 1992.
- [166] L. A. Abramyan, A. G. Litvak, V. A. Mironov, and A. M. Sergeev, "Self-focusing and relativistic waveguiding of an ultrashort laser pulse in a plasma," *Zh. Eksp. Teor. Fiz.*, vol. 102, pp. 1816–1824, 1992; *Sov. Phys. JETP*, vol. 75, pp. 978–982, 1992.
- [167] X. L. Chen and R. N. Sudan, "Necessary and sufficient conditions for self-focusing of short ultraintense laser pulse in underdense plasma," *Phys. Rev. Lett.*, vol. 70, pp. 2082–2085, 1993.
- [168] ———, "Two-dimensional self-focusing of short intense laser pulse in underdense plasma," *Phys. Fluids B*, vol. 5, pp. 1336–1348, 1993.
- [169] H. S. Brandi, C. Manus, G. Mainfray, T. Lehner, and G. Bonnau, "Relativistic and ponderomotive self-focusing of a laser beam in a radially inhomogeneous plasma I: Paraxial approximation," *Phys. Fluids B*, vol. 5, pp. 3539–3550, 1993.
- [170] G. Bonnau, H. S. Brandi, C. Manus, G. Mainfray, and T. Lehner, "Relativistic and ponderomotive self-focusing of a laser beam in a radially inhomogeneous plasma II: Beyond the paraxial approximation," *Phys. Plasmas*, vol. 1, pp. 968–989, 1994.
- [171] P. Gibbon, P. Monot, T. Auguste, and G. Mainfray, "Measurable signatures of relativistic self-focusing in underdense plasmas," *Phys. Plasmas*, vol. 2, pp. 1305–1310, 1995.
- [172] A. B. Borisov, A. V. Borovskiy, V. V. Korobkin, A. M. Prokhorov, O. B. Shiryaev, X. M. Shi, T. S. Luk, A. McPherson, J. C. Solem, K. Boyer, and C. K. Rhodes, "Observation of relativistic and charge-displacement self-channeling of intense subpicosecond ultraviolet (248 nm) radiation in plasmas," *Phys. Rev. Lett.*, vol. 68, pp. 2309–2312, 1992.
- [173] A. B. Borisov, X. Shi, V. B. Karpov, V. V. Korobkin, J. C. Solem, O. B. Shiryaev, A. McPherson, K. Boyer, and C. K. Rhodes, "Stable self-channeling of intense ultraviolet pulses in underdense plasma, producing channels exceeding 100 Rayleigh lengths," *J. Opt. Soc. Amer. B*, vol. 11, pp. 1941–1947, 1994.
- [174] P. Monot, T. Auguste, P. Gibbon, F. Jakober, G. Mainfray, A. Dulieu, M. Louis-Jacquet, G. Malka, and J. L. Miquel, "Experimental demonstration of relativistic self-channeling of a multiterawatt laser pulse in an underdense plasma," *Phys. Rev. Lett.*, vol. 74, pp. 2953–2957, 1995.
- [175] C. G. Durfee, III and H. M. Milchberg, "Light pipe for high intensity laser pulses," *Phys. Rev. Lett.*, vol. 71, pp. 2409–2411, 1993.
- [176] C. G. Durfee, III, J. Lynch, and H. M. Milchberg, "Development of a plasma waveguide for high-intensity laser pulses," *Phys. Rev. E*, vol. 51, pp. 2368–2389, 1995.
- [177] P. E. Young, M. E. Foord, J. H. Hammer, W. L. Kruer, M. Tabak, and S. C. Wilks, "Time-dependent channel formation in a laser-produced plasma," *Phys. Rev. Lett.*, vol. 75, pp. 1082–1085, 1995.
- [178] A. Zigler, Y. Ehrlich, C. Cohen, J. Krall, and P. Sprangle, "Optical guiding of high intensity laser pulses in a long plasma channel formed by a slow capillary discharge," *J. Opt. Soc. Amer. B*, 1996; A. Zigler, private communication, 1996.
- [179] T. M. Antonsen, Jr. and P. Mora, "Leaky channel stabilization of intense laser pulses in tenuous plasmas," *Phys. Rev. Lett.*, vol. 74, pp. 4440–4443, 1995.
- [180] G. Shvets and J. S. Wurtele, "Instabilities of short-pulse laser propagation through plasma channels," *Phys. Rev. Lett.*, vol. 73, pp. 3540–3543, 1994.
- [181] P. Sprangle, J. Krall, and E. Esarey, "Hose-modulation instability of intense laser pulses in plasmas," *Phys. Rev. Lett.*, vol. 73, pp. 3544–3547, 1994.
- [182] G. Shvets, private communication, 1995.
- [183] X. Liu and D. Umstadter, "Self-focusing of intense subpicosecond laser pulses in a low pressure gas," in *Shortwavelength V: Physics with Intense Laser Pulses*, vol. 17, M. D. Perry and P. B. Corkum, Eds. Washington, D.C.: Opt. Soc. Amer., 1993, pp. 45–49.
- [184] A. Braun, G. Korn, X. Liu, D. Du, J. Squier, and G. Mourou, "Self-channeling of high-peak-power femtosecond laser pulses in air," *Opt. Lett.*, vol. 20, pp. 73–75, 1995.
- [185] P. Sprangle, E. Esarey, and J. Krall, "Self-guiding and stability of optical beams in gases undergoing ionization," *Phys. Rev. E*, submitted, 1996; "Laser driven electron acceleration in vacuum, gases, and plasmas," *Phys. Plasmas*, vol. 3, May 1996.
- [186] J. F. Drake, P. K. Kaw, Y. C. Lee, G. Schmidt, C. S. Liu, and M. N. Rosenbluth, "Parametric instabilities of electromagnetic waves in plasmas," *Phys. Fluids*, vol. 17, pp. 778–785, 1974.
- [187] W. M. Manheimer and E. Ott, "Parametric instabilities induced by the coupling of high- and low-frequency plasma modes," *Phys. Fluids*, vol. 17, pp. 1413–1421, 1974.
- [188] D. W. Forslund, J. M. Kindel, and E. L. Lindman, "Theory of stimulated scattering processes in laser-irradiated plasmas," *Phys. Fluids*, vol. 18, pp. 1002–1016, 1975.
- [189] D. W. Forslund, J. M. Kindel, W. B. Mori, C. Joshi, and J. M. Dawson, "Two-dimensional simulations of single-frequency and beat-wave laser-plasma heating," *Phys. Rev. Lett.*, vol. 54, pp. 558–561, 1985.
- [190] P. Bertrand, A. Ghizzo, T. W. Johnston, M. Shoucri, E. Fijalkow, and M. R. Feix, "A nonperiodic Euler–Vlasov code for the numerical simulation of laser-plasma beat-wave acceleration and Raman scattering," *Phys. Fluids B*, vol. 2, pp. 1028–1037, 1990.
- [191] V. K. Tripathi and C. S. Liu, "Raman backscattering in laser wakefield and beat-wave accelerators," *Phys. Fluids B*, vol. 3, pp. 468–470, 1991.
- [192] P. Sprangle and E. Esarey, "Stimulated backscattered harmonic generation from intense laser interactions with beams and plasmas," *Phys. Rev. Lett.*, vol. 67, pp. 2021–2024, 1991.
- [193] E. Esarey and P. Sprangle, "Generation of stimulated backscattered harmonic radiation from intense laser interactions with beams and plasmas," *Phys. Rev. A*, vol. 45, pp. 5872–5882, 1992.
- [194] C. J. McKinstry and R. Bingham, "Stimulated Raman forward scattering and the relativistic modulational instability of light waves in rarefied plasma," *Phys. Fluids B*, vol. 4, pp. 2626–2633, 1992.
- [195] S. C. Wilks, W. L. Kruer, K. Estabrook, and A. B. Langdon, "Theory and simulation of stimulated Raman scatter at near-forward angles," *Phys. Fluids B*, vol. 4, pp. 2794–2800, 1992.
- [196] C. B. Darrow, C. Coverdale, M. D. Perry, W. B. Mori, C. Clayton, K. Marsh, and C. Joshi, "Strongly coupled stimulated Raman backscatter from subpicosecond laser-plasma interactions," *Phys. Rev. Lett.*, vol. 69, pp. 442–445, 1992.
- [197] P. Mounaix and D. Pesme, "Space and time behavior of backscattering instabilities in the modified decay regime," *Phys. Plasmas*, vol. 1, pp. 2579–2590, 1994; Ph. Mounaix, D. Pesme, W. Rozmus, and M. Casanova, Eds., "Space and time behavior of parametric instabilities for a finite pump wave duration in a bounded plasma," *Phys. Fluids B*, vol. 5, pp. 3304–3318, 1993.
- [198] A. S. Sakharov and V. I. Kirsanov, "Theory of Raman scattering for a short ultrastrong laser pulse in a rarefied plasma," *Phys. Rev. E*, vol. 49, pp. 3274–3282, 1994.
- [199] P. Bertrand, A. Ghizzo, S. J. Karttunen, T. J. H. Pattikangas, R. R. E. Salomaa, and M. Shoucri, "Generation of ultrafast electrons by simultaneous stimulated Raman backward and forward scattering," *Phys. Rev. E*, vol. 49, pp. 5656–5659, 1994.
- [200] S. C. Wilks, W. L. Kruer, E. A. Williams, P. Amendt, and D. C. Eder, "Stimulated Raman backscatter in ultraintense, short pulse laser-plasma interactions," *Phys. Plasmas*, vol. 2, pp. 274–279, 1995.
- [201] C. Rousseaux, G. Malka, J. L. Miquel, F. Amiranoff, S. D. Baton, and P. Mounaix, "Experimental validation of the linear theory of stimulated Raman scattering driven by a 500-fs laser pulse in a pre-formed underdense plasma," *Phys. Rev. Lett.*, vol. 74, pp. 4655–4658, 1995.
- [202] K. M. Krushelnick, A. Ting, A. Fisher, C. Manka, H. R. Burris, and E. Esarey, "Second harmonic generation of stimulated Raman scattered light in underdense plasmas," *Phys. Rev. Lett.*, vol. 75, pp. 3681–3684, 1995.

- [203] A. Ting, K. M. Krushelnick, A Fisher, C. Manka, and H. R. Burris, "Extreme broadening of stimulated Raman scattered light from high intensity laser plasma interactions," NRL Rep. NRL/MR/6790-95-7667, 1995.



**Eric Esarey** was born in Wyandotte, MI on September 12, 1960. He received the B.S. degree in nuclear engineering from the University of Michigan, Ann Arbor, in 1981 and the Ph.D. degree in plasma physics from the Massachusetts Institute of Technology, Cambridge, in 1986.

From 1986 to 1988, he was employed by Berkeley Scholars, Inc., and Berkeley Research Associates, Inc. Since 1988, he has been a Research Physicist in the Beam Physics Branch of the Plasma Physics Division at the U.S. Naval Research Laboratory. He has published over 50 technical articles and letters in refereed scientific journals. His research has concentrated on the areas of advanced accelerators, advanced radiation sources, intense laser interactions with beams and plasmas, nonlinear optics, and free electron lasers.

**Phillip Sprangle** (M'90-SM'92), photograph and biography not available at the time of publication.

**Johathan Krall**, photograph and biography not available at the time of publication.

**Antonio Ting**, photograph and biography not available at the time of publication.